Nanostructures and Metallophthalocyanines: Applications in Microbial Fuel Cells

A thesis submitted in fulfillment of the requirements for the degree of

MASTERS IN SCIENCE

of

RHODES UNIVERSITY

by

SEAN EDWARDS

December 2010

ABSTRACT

Microbial fuel cells (MFCs) are a promising form of alternative energy capable of harnessing the potential energy stores in organic waste. The oxygen reduction reaction (ORR) forms an integral role in the generation of electricity in MFCs however it is also a potential obstacle in enhancing the performance of MFCs. Platinum, a commonly used catalyst for the ORR, is expensive and rare. Significant research has been conducted into developing alternative catalysts. Metallophthalocyanines (MPc) have garnered attention for use as catalysts. Iron phthalocyanine (FePc) has been shown to have catalytic activity towards the reduction of oxygen. Coupling of the catalyst to nanostructured carbon materials, such as multi-walled carbon nanotubes, has been observed to have several advantages as nanostructures have a high surface-to-volume ratio. In this study, we have attempted to assess the suitability of FePc, both its bulk and nanostructured form, as an oxygen reduction catalyst and acid functionalized multi-walled carbon nanotubes for use as a catalyst support using electrochemical techniques such as cyclic voltammetry and electrochemical impedance spectroscopy. We showed, for the first time, the catalytic nature of nanostructured FePc towards the ORR. Applying the data obtained from the electrochemical analyses, electrodes were modified using FePc and MWCNTs and applied to an *Enterobacter cloacae*-based MFC. Several operational parameters of the MFC, such as temperature and ionic strength, were optimized during the course of the study. We showed that optimized FePc:MWCNT-modified electrodes compared favourably to platinum-based electrodes in terms of power densities obtained in a microbial fuel cell.

ACKNOWLEDGEMENTS

I would like to extend my deepest gratitude towards the following persons:

- Prof. Janice Limson, my supervisor, for her invaluable guidance and patience and allowing me the freedom to choose this project.
- My family for the sacrifices they have made to ensure that I got the opportunity to study further after school.
- The members of the Biosensor Research Group particularly Mr. Ronen Fogel and Mr. Shane Flanagan for their constant motivation, critique, and guidance.
- To Rhodes University and the members of the Department of Biochemistry, Microbiology and Biotechnology for their assistance and support.
- Prof. Tebello Nyokong for her assistance and support
- DST/MINTEK Nanotechnology Innovation Centre which without whose funding this dissertation would not have been made possible.
- Ms. Leanne Cooper, for her constant motivation and never ending support.
- To my digsmates, Ms. Shan Ambrose, Ms. Hailey Johnson, Ms. Lara Sciscio, and Mr Matthys Kroon, for making this a great year and for listenening to my presentations despite having no knowledge of the topic.

1 Contents

LIST OF ABBREVIATIONS

A	Amperes
BEAMR	Bioelectrochemically assisted microbial reactor
BR	Britton-Robinson
C_{dl}	Double layer capacitance
CNTs	Carbon nanotubes
COD	Chemical oxygen demand
CoPc	Cobalt phthalocyanine
CTAB	Hexadecyl trimethyl ammonium bromide
CV	Cyclic voltammetry
DMAc	Dimethyl acetamide
DMF	N'N - dimethyl formamide
DMFC	Direct Methanol fuel cell
e^-	electron
F	Faraday
FePc	Iron Phthalocyanine
GCE	Glassy carbon electrode
HOMO	Highest occupied molecular orbital
HOPG	Highly orientated pyrolytic graphite
IS	Ionic strength
KBr	Potassium bromide
KCl	Potassium chloride
LUMO	Lowest unoccupied molecular orbital
M	Molar
MFC	Microbial fuel cell
Mn	Manganese
MPc	Metallophthalocyanine
MWCNTs	Multiwalled carbon nanotubes
NMP	Dimethyl pyrrolidone
OD	Optical density
ORR	Oxygen reduction reaction
PEM	Proton exchange membrane
ppm	parts per million
Pt	Platinum
Q	Constant Phase element
R	Resistance
RCM	Reinforced clostridial medium
R_{ct}	Charge transfer resistance
Redox	Reduction/Oxidation
R_s	Solution resistance
SWCNTs	Single walled carbon nanotubes
T	Tangent hyperbolic diffusion
UV/Vis	Ultraviolet/Visible
V	Volts
v/v	volume/volume
W	Watts
Z_w	Warburg Impedance

LIST OF FIGURES

LIST OF TABLES

Chapter 1: Introduction

1.1 The need for alternative energy

In the current global environment, energy demand is greatly outstripping energy supply leading to shortages of energy reserves (Matson and Carasso, 1999). The majority of countries of the world are still heavily reliant on fossil fuels such as coal and crude oil to meet their energy demands (Matson and Carasso, 1999; Tan *et al.*, 2008). The growing demand for fossil fuels is primarily a factor of developing nations requiring increasingly larger amounts of energy to support their expanding economies and to improve the standard of living available to all people (Rout *et al.*, 2008). Not only are the energy reserves being depleted in the process, the environmental consequences of using these energy sources are coming to the fore, most notably the increase in carbon emissions from the burning of fossil fuels (Matson and Carasso, 1999; Tan *et al.*, 2008). Carbon emissions, linked to the burning of fossil fuels, have dramatically increased over the past 30 years leading to strain on the natural environment (Matson and Carasso, 1999; Tan *et al.*, 2008).

Carbon dioxide (CO_2) is the predominant greenhouse gas, and 70-75% of all CO_2 emissions are due to combustion of fossil fuels (Hoel and Kverndokk, 1996). As can be seen in Figure 1.1, the bulk of electricity generated around the world is from fossil fuels which include coal and petroleum. Utilization of these fossil fuels has been linked to increased greenhouse gases (Zecca and Chiari, 2010; Rout *et al.*, 2008). Add to that the fact that coal and oil reserves are finite and the fact that the world's population is ever expanding, the pressure on these reserves is on the increase (Zecca and Chiari, 2010). Nuclear power may be considered a clean source of power however there is still a need to dispose of the radioactive waste generated from the reactors (Curtiss et al, 1996). Up until now, there has been no viable means to do so (Curtiss *et al*., 1996). The risks involved with using nuclear power also make it an uneasy alternative to fossil fuels (Curtiss *et al.*, 1996). Electricity generation from renewable energy sources, including

solar and wind power, makes up only 3 % of the global production (Figure 1.1). A shift from focusing on the traditional energy sources to finding new alternative "green" energy resources (environmentally friendly energy) is on the rise especially in developed countries (Bullen *et al.*, 2006).

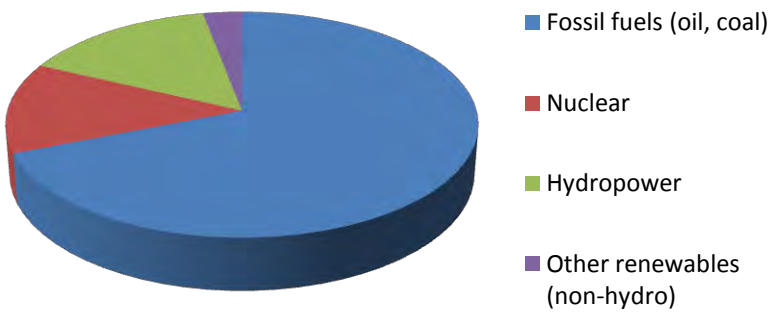

Figure 1-1. Global electricity generation as of 2008 (adapted from Internet Reference 1)

Active research is being conducted into alternative energy sources (Tan *et al.*, 2008) and one of the technologies at the forefront are fuel cells which are environmentally friendly and a pollutant-free energy source (Bullen *et al.*, 2006).

1.2 Defining fuel cells

Fuel cells have the potential to make a lasting impact in the energy sector without the added risks of fossil fuels (Davis and Higson, 2007). The research into fuel cells, particularly biofuel cells, is relatively new compared to other established fields of science (Davis and Higson, 2007). As such, there is still much to learn about fuel cells and there are many areas of fuel cell technology that need to be studied to unlock the full potential of this technology (Davis and Higson, 2007; Bullen *et al.*, 2006).

Fuel cells generate electrical energy by the conversion of chemical energy via electrochemical reactions (Logan, 2008). Fuel cells work by using relatively simple chemical reactions in which a fuel such as hydrogen gas is converted to energy (in the form of electricity) and water is produced as a by-product (Bullen *et al.*, 2006). Fuel cells can be divided into chemical fuel cells and biological-based fuel cells. The latter includes microbial fuel cells (MFC) and enzymatic fuel cells (EFC), depending on the type of biocatalyst used (Bullen *et al.*, 2006). Chemical fuel cells include hydrogen fuel cells, direct methanol fuel cells (DMFC), alkaline fuel cells and proton exchange membrane (PEM) cells (Bullen *et al.*, 2006).

The most common type of fuel cell is the hydrogen fuel cell depicted in Figure 1.2 and it is from here where biological fuel cells (biofuel cells) are derived (Logan, 2008). A fuel cell consists of two working electrodes, namely the cathode and anode, submerged in an electrolytic solution and separated by a semi-permeable PEM (Logan, 2008). While several permutations exist, a common setup is one where the anode is submerged in the fuel source while the cathode is submerged in a buffer of suitable ionic strength (Logan, 2008; Liu *et al.*, 2006).

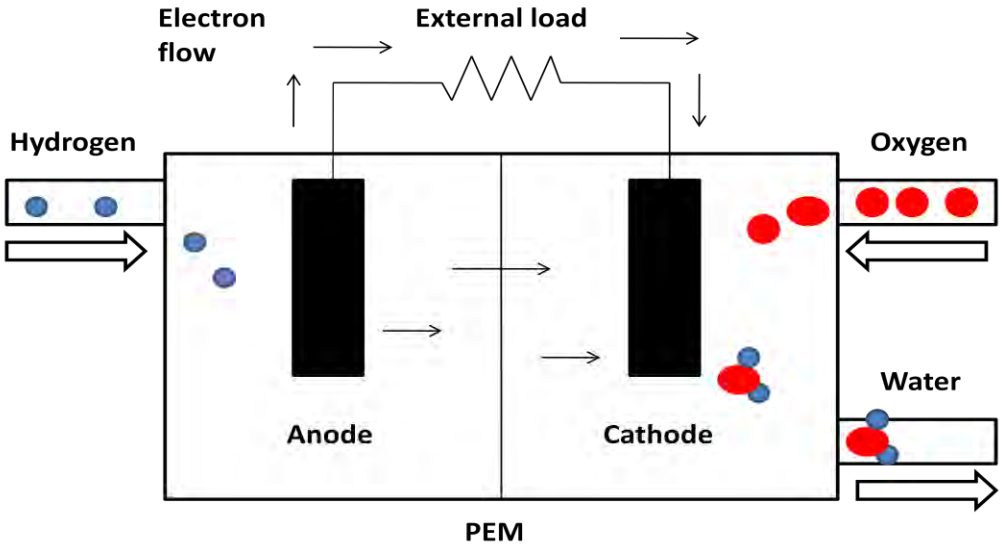

Figure 1-2. A schematic diagram of a fuel cell (adapted from Internet Reference 2). Hydrogen (blue) is oxidized at the anode; protons flow through the PEM while electrons flow through the external circuit to the cathode. Oxygen (red) is reduced at the cathode producing water.

For MFCs, the anodic compartment must often be purged with nitrogen to maintain anoxic conditions except when aerobic bacteria are used (Davis and Higson, 2007; Lui *et al.*, 2006). The generation of electricity from the fuel cell involves an oxidative reaction at the anode and a reductive reaction at the cathode as can be seen in Figure 1.2 (Bullen *et al.*, 2006). Oxidation of a fuel at the anode releases electrons which move through an external circuit to the cathode (Bullen *et al.*, 2006). The PEM separating the anodic and cathodic compartment allows protons to cross and move towards the cathode thereby balancing the charge in the cell (Bullen *et al.*, 2006). The flow of electrons through the external circuit results in the generation of electricity (Kim *et al.*, 2006).

The catalyst used in a fuel cell is a critical component responsible for driving the redox reaction that eventually produces electricity (Bullen *et al.*, 2006). It is of importance as it determines, along with other factors, the efficiency of the system output (Davis and Higson, 2007). The majority of catalytic materials used in fuel cells are derived from various metals and are used to enhance the rates of the half reactions that comprise the fuel cell (Lui *et al.*, 2006). The most common electrocatalyst is based upon solid platinum, often in the form of platinum mesh or platinum-embedded carbon (Kim *et al.*, 2006). When this platinum electrocatalyst is in contact with one of the electrodes in a fuel cell, it increases the rate of oxygen reduction to water (Kim *et al.*, 2006).

When a fuel cell operates by either utilizing a primary fuel such as hydrogen gas or organic waste to generate a secondary fuel which is then used for electricity generation, the cell is termed a secondary fuel cell (Davis and Higson, 2007). In the case of biofuel cells, primary or direct biofuel cells directly utilize biocatalysts such as whole cells or enzymes in redox reactions to generate electricity (Kim *et al.*, 2006). Secondary or indirect biofuel cells utilize biocatalysts, such as bacterial cells, for the production of simple fuels such as hydrogen or methane gas from more complex organic molecules such as starch (Kim *et al.*, 2006). The biocatalysts are immobilized on the electrode surface and when the fuel is in contact with the electrode surface, the biocatalyst oxidizes the fuel releasing electrons and protons (Kim *et al.*, 2006).

Platinum is commonly used at the cathode as a catalyst for the reduction of oxygen (Logan, 2008).

MFCs are biological fuel cells that make use of microorganisms to synthesize a secondary fuel from a primary fuel such as organic waste (Logan, 2008). Many bacterial strains have been used in MFCs including *Geobacter sulferreducens, Shewanella oneidensis,* and *Clostridium butyricum* (Park *et al.*, 2001; Logan and Regan, 2006; Biffinger *et al.*, 2007). *Enterobacter cloacae*, a facultative anaerobic bacterium, has been shown to metabolically produce hydrogen and therefore has the potential for use in MFCs however its use in MFCs has been limited (Kumar and Das, 2001; Nambiar *et al.*, 2009). It is the bacteria that supply the MFC with the fuel it requires to generate electricity. Nutrients supplied to the bacteria, ranging from glucose to domestic wastewater, in the anodic compartment are continually metabolized by the bacterial cells generating the secondary fuel (often hydrogen) that is then oxidized at the electrode to produce the electrons and protons that are crucial to power generation (Bullen *et al*, 2006).

MFCs operate like any other fuel cell, with the presence of an anode and cathode separated by a PEM however the architecture of MFCs has become an important research area on its own (Logan, 2008). MFCs are not just limited to the standard two-chambered design; single-chambered MFCs have become more popular as the design offers many advantages over the standard design such as decreasing the internal resistance of the MFC (Oh and Logan, 2005; Sun *et al.*, 2009). Despite the advantages offered by single-chambered MFCs, the two-chambered design is still favoured in the laboratory due to their simplicity and they exhibit higher coulombic efficiencies (Sun *et al*., 2009).

The power densities generated by MFCs is low in relation to chemical fuel cells thereby limiting their applications however MFCs have found use in remediation of wastewaters (Liu and Logan, 2004; Logan, 2008). Several studies have looked into the utilization of MFCs to remediate several types of wastewaters and in the process generating electricity (Oh and Logan, 2005; Feng *et al.*, 2008; Venkata Mohan et al., 2008). The coupling of wastewater remediation to

electricity generation is a growing field of research. Wen *et al*. (2009) achieved a power output of 264 $mW.m^{-2}$ using brewery wastewater while Min *et al.* (2005) achieved power densities of 45 $mW.m^{-2}$ in a two-chambered MFC and 261 $mW.m^{-2}$ in a single-chambered MFC using swine wastewater as a feedstock. The power densities where achieved while still maintaining a chemical oxygen demand (COD) removal of 40 % (Wen et al., 2009). Power outputs of MFCs using defined substrates such as lactate or glucose is often lower relative to power production from wastewater ranging from 0.3 to 49 $mW.m^{-2}$ (Liu and Logan, 2004).

1.2.1 Problems associated with fuel cells

Biofuel cells bring with them a different set of problems relative to chemical fuel cells especially in terms of cost and power generation (Bullen *et al.*, 2006; Davis and Higson, 2007). For any fuel cell the power output, P_{cell} (equation below) is likely to be the bottom line determining its value:

$$P_{cell} = E_{cell} \times I \quad \text{(Bullen } et\ al.,\ 2006\text{)}.$$

Where P_{cell} is the power output of the cell, E_{cell} is the cell potential (in volts), I is the measured current (in Amperes). Power density is the measure of power generation (current and voltage) per surface area of electrode and is determined by the level of catalyst loading on the electrode surface (Cheng *et al.*, 2006). The major obstacle in the way of fuel cell commercialization is the power output (Bullen *et al.*, 2006; Cheng *et al.*, 2006). The critical challenges faced in optimizing fuel cell performance involve low power densities as a result of low catalyst loading on the electrodes; short lifespan for biofuel cells due to difficulties in immobilizing the catalyst on to the electrode; and inefficient electron conduction between the catalysts and the electrodes (Cheng *et al.*, 2006). Research into solutions for increasing the power density of fuel cells has focused on the improvement of the electrodes in terms of the materials employed in their construction, the type of catalysts used and immobilization strategies for immobilizing catalysts on the surface of electrodes in order to increase catalyst loading (Cheng *et al.*, 2006).

Finding an ideal material from which to construct electrodes is essential in solving the problem of poor catalyst loading and hence low power outputs (Cheng *et al.,* 2006). Reducing the required catalyst loading when using platinum however may have an advantage in that it may decrease the costs involved (Bullen *et al.*, 2006). Conductive materials have also been examined as electron transfer mediators thereby shuttling electrons from the catalyst to the electrode surface (Bullen *et al.*, 2006). Some research focus has thus been centred on carbon nanotubes (as detailed further) as well as conductive polymers as they may serve more than one purpose namely as electron mediators, as suitable materials for the immobilization of catalysts on the electrode and finally in high surface area to volume ratio in the case of carbon nanotubes, to increase surface loading (Bullen *et al.*, 2006).

1.2.2 Current trends in fuel cell research

Significant research has focused on the development of biofuel cells that use microbial or enzymatic biocatalysts, however chemical fuel cells lead the way in terms of power output and stability currently (Lu and Reddy, 2007). One of the means to obtain higher levels of power from fuel cells is to increase the catalytic activity of catalysts towards the oxygen reduction reaction (ORR) at the cathode of the fuel cell (Lu and Reddy, 2003). Research into new, improved catalysts for the ORR has branched into two paths: the first one has focused on developing platinum-based alloys through heat-treatment and chemical means as platinum is considered the most suited catalytic material for oxygen reduction (Wang, 2005). Developing platinum alloys can decrease the amount of platinum required therefore decreasing the costs involved (Lu and Reddy, 2003).

The second path has focused on the development of non-noble metal catalysts for oxygen reduction, in particular metal porphyrins and phthalocyanines (Lu and Reddy 2003; Zhang *et al.*, 2008). In addition, some new carbon nanomaterials with special physicochemical properties, such as ordered porous carbons, graphite fibers, C_{60} fullerene clusters and carbon nanotubes (CNTs), have been studied as supports for ORR electro-catalysts (Zheng *et al.*, 2008). These are

discussed further in the ensuing sections. Nanostructures are beneficial for use as either electrocatalysts or catalyst supports as they possess a much larger surface to volume ration than bulk materials (Wildgoose *et al.*, 2006). The reactivity of materials can be greatly enhanced when the material is at a nanoscale as a decrease in size of the material leads to an increase in the active surface area (Antolini, 2008). CNTs were shown to have higher ORR activities when used as electro-catalyst support rather than traditional carbon materials such as graphite (Zheng *et al.*, 2008). Nevertheless, the CNTs have weak interactions with the supported metals, which restrict further improvement of the ORR activity (Zheng *et al.*, 2008).

1.3 Electrocatalysis in fuel cells

Platinum is a precious transition metal with high resistance to oxidation and corrosion and is also one of the rarest elements found in Earth's crust with an average abundance of approximately 0.005 ppm whereas an element like iron has an abundance of approximately 41 000 ppm (Ravindra *et al.,* 2004; Glaister and Mudd, 2010). South Africa provides over 80 % of the world's platinum (Glaister and Mudd, 2010; Ravindra *et al.,* 2004). Only about 30 tons of the metal is mined per year whereas a metal such as gold generates yields of about 2 800 tons per year (Glaister and Mudd, 2010). Not only is platinum rare, it is also costly with the price per ounce topping $ 1600 as of 2010. Platinum and its compounds have found use in various fields ranging from use as laboratory equipment, dentistry equipment, jewelry, electrical contacts and electrodes, and for use in catalytic converters (Glaister and Mudd, 2010; Ravindra *et al.,* 2004). Its use as an electrode material in fuel cells has garnered significant attention due to its ability to catalyze the reduction of oxygen. The ORR is an important reaction in the functioning of both chemical and biological fuel cells and platinum has proven to be the ideal catalyst for the reaction in terms of catalytic ability and corrosion resistance (Logan, 2008). However due its rarity and cost, there has been a shift towards alternative catalytic materials for use in fuel cells.

1.3.1 Metallophthalocyanines as alternative electrocatalysts

Metallophthalocyanines (MPc) are synthetic aromatic coordination compounds that have a planar structure and consist of a phthalocyanine macrocycle coordinated to a transition metal such as iron, cobalt or manganese (Figure 1.3) (Parra *et al.,* 2004; Zhao *et al.*, 2005). MPcs are versatile, have high catalytic activity towards many molecules, and low cost of raw materials (Shahrokian et al, 2009). They exhibit rich electrochemical behaviour and their properties may be varied by changing the metal ion centre or by altering the peripheral substituents present on the MPc (Parra *et al.*, 2004). There are many examples in nature demonstrating the interesting ability of macrocyclic organic N4-complexes to catalyze redox reactions involving molecules such as O_2, H_2, and N_2 (Okunola et al, 2008). These include reactions found in enzymatic systems such as sulphite reductase, nitrate reductase, cytochrome *c* oxidase, blue copper oxidases, pseudocatalase, photosystem II, nitrogenase and hydrogenase (Okunola et al, 2008). In each case, the enzyme contains one or more metal atoms at the active site and in many cases the enzyme may also include active peripheral metal sites (Okunola et al, 2008). N4-macrocyclic complexes containing first row transition metals have also been extensively applied for electrocatalytic redox reactions (Okunola et al, 2008). Of these macrocycles, complexes of cobalt and iron have been mostly applied as reduction electrocatalysts, especially for oxygen reduction. (Okunola et al, 2008).

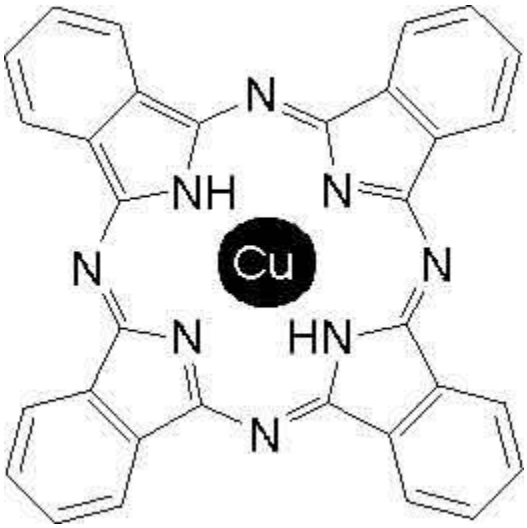

Figure 1-3. Phthalocyanine ring coupled to copper (Internet Reference 3)

The interest in MPcs has arisen due to their redox behaviour and the fact that nearly any metallic and some non-metallic elements may be used in the central cavity of the MPc (Zhang *et al.*, 2008). The metal centre can undergo a series of oxidative and reductive electron transfer processes centered on the metal center or phthalocyanine ring making them versatile tools for electron relay reactions that activate redox processes (Lever, 1999; Matemadombo *et al.*, 2007). The metal centre (M), which is key to the redox behaviour shown, undergoes oxidation and reduction related with (M^{3+}/M^{2+}) and (M^{2+}/M^{+}) while the phthalocyanine ring can be sequentially reduced at least four times (Lever, 1999; Yilmaz *et al.*, 2007). MPcs are also easily modified through the addition of ring substitutions, without losing their chemical stability (Zhang *et al.*, 2008). By adding charged substituents such as carboxyl or sulphonated groups, the problem of MPcs being poorly soluble in most organic solvents can be overcome (Yilmaz *et al.,* 2007; Ceyhan *et al.*, 2006). Water-soluble MPcs have tended to be preferred and have been shown to be promising materials as electro-catalysts (Yilmaz *et al.*, 2007; Ceyhan *et al.*, 2006). Non-aqueous MPcs however offer benefits with regards to immobilization in that the MPcs will not readily leach off the electrode surface into solution.

Metal phthalocyanines (Figure 1.3) and porphyrins (biological analogues of MPcs) have been shown to be good oxygen-reduction catalysts, and reportedly may be comparable in efficiency to platinum-based catalysts for the reduction of oxygen (Zhao *et al.*, 2005; Sun *et al.*, 2001). MPcs have been shown to catalyze many other reactions such as hydrogen peroxide reduction and cysteine reduction among others (Ceyhan *et al.,* 2006; Fogel *et al.*, 2007; Yilmaz *et al.,* 2007).

MPcs have several advantages over transition metal catalysts in that they can be synthesized from any metal or metalloid element; they are susceptible to several modifications through the addition of substituents and modification of the ring system, and MPcs have the ability to add or remove many electrons and still retain their structure and stability allowing for reversible redox reactions (Lever, 1999). The performance of the MPc electrodes however has been shown to decrease with a change in pH levels and decreasing buffer concentrations (Hao Yu *et*

al., 2007). This could be problematic in biofuel cells as they are susceptible to changes in pH and ionic strength of buffers (Liu *et al.*, 2006). Both cobalt phthalocyanine (CoPc) and iron phthalocyanine (FePc) electrodes were tested and they both showed oxygen-reducing activity similar to that of platinum-based electrodes (Sun *et al.*, 2001; Zhao *et al.*, 2005; Cheng *et al.* 2006; Hao Yu *et al.*, 2007).

Iron (II) phthalocyanine (FePc) has been reported to be one of the most promising metal-chelates as catalysts for the oxygen reduction reaction under acidic conditions (Harnisch et al, 2009). FePc has been used as cathode material for MFCs (Hao Yu et al, 2007). The ability of FePc to lower the overpotential is of particular importance in fuel cells as the reduction of oxygen occurs at high overpotentials and is therefore energetically demanding (Biffinger *et al.*, 2007). Nanostructured FePc has recently been shown to enhance electron transfer kinetics, and enhance catalytic responses for the detection of thiocyanate and nitrite (Mamuru and Ozoemena, 2009). There is however no available literature on using nano FePc for the reduction of oxygen. It is plausible that nano FePc, based on evidence from the bulk form of FePc, could prove advantageous for ORR. Synthesis of nano FePc involves using the surfactant, hexadecyl trimethyl ammonium bromide (CTAB), which assists in the breaking of the intramolecular forces between FePc molecules changing them from their crystallite form to a nanostructured amorphous form (Mamuru and Ozoemena, 2009).

The proposed reaction mechanism for the reduction of oxygen on non-precious metal catalysts suggests that the metal–N4 moiety that is bound to the carbon support plays a crucial role in the oxygen reduction reaction (Subramanain et al, 2009). Oxygen reduction generally proceeds through parallel two- and four-electron reaction pathways, which can be expressed as in Figure 1.4. (Hao Yu et al, 2009):

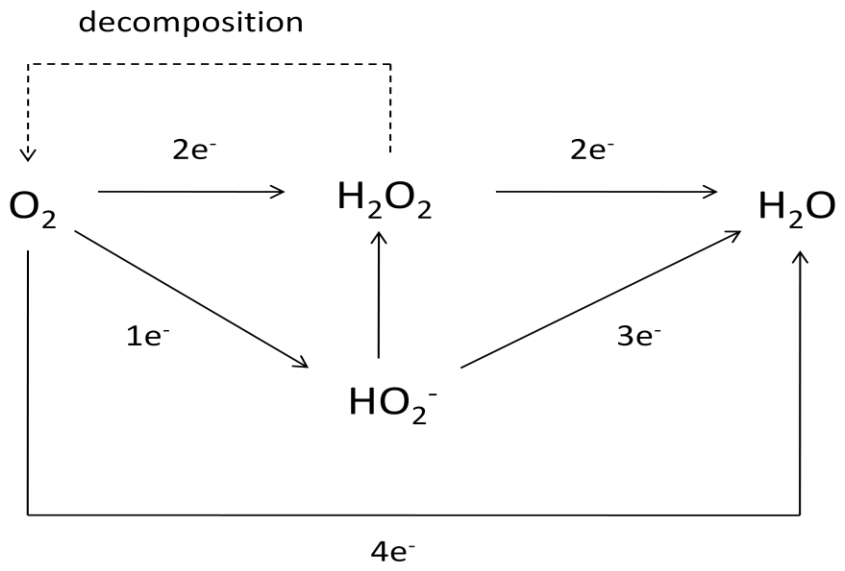

Figure 1-4. The reduction of oxygen showing the 4 e- reduction pathway as well as alternative 1 e^-, 2 e^-, and 3 e^- reduction pathways (adapted from Baker et al., 2008).

It has been reported that FePc has the ability to promote direct $4e^-$ oxygen reduction to water, while CoPc promotes O_2 reduction to H_2O_2 by a 2 e^- pathway (Hao Yu *et al.*, 2007). The 4 e^- pathway is more desirable as the 2 e^- pathway produces hydrogen peroxide which can damage the electrode structure (Hao Yu *et al.*, 2007). Extensive studies on metal macrocycles for oxygen reduction have been carried out in either strongly acidic or alkaline solutions however it has been reported that FePc is efficient at reducing oxygen at neutral pH (Van der Putten *et al.*, 1987; Van den Brink *et al.*, 1984; Maldonado and Stevenson, 2004; Hao Yu *et al*., 2009). FePc has shown highly selective catalytic activity for oxygen reduction in *the* presence of methanol and carbon monoxide (CO) in direct methanol fuel cells (DMFC) and hydrogen fuel cells (Hao Yu *et al.*, 2007). The chemical stability of FePc in acidic conditions is low due to the demetalisation of the macrocycle rings, however, the stablility in neutral and alkaline media is much higher which suggests their application in MFCs and other biological fuel cells operating at neutral pH will be more feasible than in DMFCs and hydrogen fuel cells (Hao Yu *et al.*, 2009).

Coupling of catalysts such as platinum nanoparticles with carbon nanostructures has shown to be promising in increasing the power outputs of fuel cells however not much work has been

done using nanostructured hybrids in biofuel cells (Hao Yu *et al.*, 2007; Zhao *et al.*, 2005). Nanostructured hybrids have shown great promise for use in biosensors as they increase the catalytic response and exhibit faster electron transfer kinetics (Agboola *et al.*, 2008). Advances made with hybrids in biosensors can be applied to electrode development for MFCs. Okunola *et al.* (2008) conducted electrochemical analyses of various porphyrins (Fe, Mn, Co) combined with MWCNTs for the reduction of oxygen and found the nanostructured hybrids were favourable for use. According to these authors, the incorporation of MWCNTs improved conductivity of the immobilized layer.

1.3.2 Application of Nanomaterials in fuel cells

The extraordinary nature and unique mechanical, electronic, thermal and chemical properties of carbon nanotubes have attracted considerable interest in potential applications such as advanced composite materials, nano-electronic devices, electrochemical capacitors for energy storage and hydrogen-storage (Kunadian *et al.* 2009). Carbon nanotubes have been shown to possess great potential for use in fuel cell catalysis (Hacker *et al.*, 2005; Salimi *et al.*, 2005). The use of nanomaterials has enjoyed significant attention for use in fuel cells for electro-catalysis and the synthesis of electrodes. Nanomaterials that have been tested include metal nanoparticles, nanofibres and nanotubes (Kim *et al.*, 2006). Nanomaterials offer many advantages over more traditional materials such as increasing the catalytic surface area at which electrocatalysis occurs as nanoparticles have been shown to have a large surface area per unit mass (Kim *et al.*, 2006; Qiao *et al.*, 2007). The increased surface area allows for greater catalyst loading and improves immobilization of the catalyst resulting in improved power densities and greater stability over time thereby addressing key problems faced in fuel cell design (Kim *et al.*, 2006; Qiao *et al.*, 2007).

The use of nanostructured carbon in fuel cell applications has perhaps generated the most interest with their use in the construction of modified electrodes (Stolarczyk *et al.*, 2008). Electrodes consisting of carbon-based nanomaterials provide good conducting properties and

ease of modification through functionalization (Stolarczyk *et al.*, 2008). Carbon nanostructured electrodes may be further modified using MPcs as they can adsorb strongly onto carbon-based electrode materials (through π-π orbital overlapping) at monolayer levels allowing for the synthesis of hybrid CNT-MPc materials for electrocatalytic purposes as has been shown for biosensor applications (Silva *et al.*, 2007; Kakade and Pillai, 2008).

1.3.2.1 Carbon Nanotubes

1.3.2.1.1 Properties of Carbon Nanotubes

Carbon nanotubes (CNTs) are made from hexagonal graphene sheets and are a porous nanostructure material with unique electrical and structural properties that make them attractive for electro-catalysis (Hacker *et al.*, 2005; Salimi *et al.*, 2005; Vaisman et al, 2006). CNT forms include as either single-walled (Figure 1.5) or multi-walled. Multi wall carbon nanotubes (MWCNT) consist of two or more seamless graphene cylinders concentrically arranged whereas single walled carbon nanotubes consist of one sheet only (Vaisman et al, 2006). They possess small dimensions, ultra-strong mechanical properties, chemical stability and high electrical conductivity (Salimi *et al.*, 2005; Silva *et al.*, 2007; Wen *et al.*, 2007).

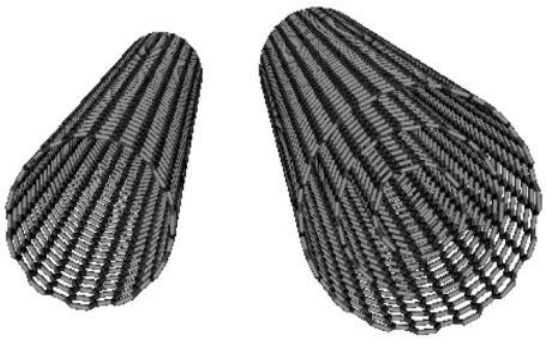

Figure 1-5. Comparison of single-walled (SWNT) and multi-walled (MWNT) nanotubes (Internet Reference 4)

Each carbon atom in graphene is connected evenly to three other carbon atoms at a bond angle of 120° in the xy plane resulting in sp^2 hybridization (Vaisman et al, 2006). A weak π bond is present in the z axis (Vaisman et al, 2006). The sp^2 hybridization forms the hexagonal lattice of a sheet of graphite (Vaisman et al, 2006). The p_z orbital is responsible for van der Waal's interactions (Vaisman et al, 2006). The free electrons present in the pz orbital are free to move within this cloud and become delocalized (Vaisman et al, 2006). This is the primary reason why graphite and therefore CNTs can conduct electricity, whereas diamond, in which sp^3 hybridization occurs, behaves as an insulator (Vaisman et al, 2006). Delocalized π-electrons of carbon nanotubes can also be utilized to promote adsorption of various moieties on the CNT surface via π–π stacking interactions (Vaisman et al, 2006).

Futhermore, nanotubes have been shown to exhibit superconductive properties under very specific conditions i.e. their electrical resistance is reported to be zero (Qiao *et al.*, 2007). The carbon–carbon sp^2 bond present in CNTs is one of the strongest in nature making carbon nanotubes one of the most rigid and strongest materials ever synthesized (Vaisman *et al.*, 2006).

1.3.2.1.2 Electrochemistry of Carbon Nanotubes

Nanotubes exhibit subtle electronic behaviour that is associated with the potential shift (decreasing of overpotentials) and the reaction rate enhancement toward various electroactive substrates (Silva *et al.*, 2007). These electronic properties also enable nanotubes to promote the electron-transfer of redox reactions (Wen *et al.*, 2007; Schilling and Bron, 2008). Recent research tends to suggest that the electrochemical reactivity of nanotubes is only resident in edge-plane sites, defects occurring at the ends or along the tube axis, or in metal impurities such as residual iron or iron oxide nanoparticles remaining from production of the CNTs via chemical vapour deposition (Wildgoose *et al.*, 2006; Silva *et al.*, 2007; Batchelor-McAuley *et al.*, 2008).

CNTs are themselves electrochemically inert (Gong *et al.*, 2005). The methods used for preparing CNTs introduce impurities such as metal catalysts like iron, amorphous carbon and carbon nanoparticles which would give the CNTs electrochemical activity (Prehn *at al.* 2008; Gong *et al.*, 2005). It is for this reason that purification is required (Gong *et al.*, 2005). Pretreatment with acid acts to shorten the nanotubes and introduce side defects (Gong *et al.,* 2005). This partial oxidization of the CNTs introduces functional oxygenated groups at the open ends and defects along the sidewall (Gong *et al.*, 2005). It is these edge plane defects that have been proposed to impart electrochemical activity to the CNTs (Wildgoose *et al*., 2006; Banks and Compton).

CNTs have two "kinds" of carbon atoms that are essential to its electrochemical properties: those at tube ends and those at the sidewall of tubes (Batchelor-McAuley *et al.*, 2008). Electrochemically both behave differently. Those at the tube ends behave like the edge plane of highly orientated pyrolytic graphite (HOPG) and possess favourable electrochemical properties whereas those at the sidewall resemble the basal plane of HOPG and exhibit slow electron transfer kinetics (Gong *et al.*, 2005). The electrochemical properties of CNTs have been attributed to the edge-like plane of CNTs (Banks and Compton, 2005; Gong *et al.*, 2005; Wildgoose *et al*., 2006). MWCNT conduction is mainly due to the outer shell which is usually much larger than SWCNTs. Therefore, MWCNTs should in theory have a relatively high electrical conductivity (Prehn *et al.,* 2008).

1.3.2.1.3 Use of carbon nanotubes for modification of electrodes

Although nanotubes show great promise for various applications, pristine CNTs tend to have poor solubility in most organic and aqueous solutions and difficulty in processing as thin films in solvents, as well as the attachment of metals, which has hampered certain aspects of research into their use (Guo and Li, 2006; Casagrande *et al.*, 2008). The nano-scale dimensions of CNT presents a problem with their dispersion since as the surface area of a particle increases, so does the attractive forces between the aggregates (Vaisman *et al.*, 2006). CNTs will then tend to

aggregate together in most aqueous and organic solutions due to the van der Waal's forces existing between the tubes (Gong *et al.*, 2005). Pretreatment and functionalization increases the solubility of the CNTs and has led to advancements in carbon nanotubes utilization (Kakade and Pillai, 2008; Casagrande *et al.*, 2008).

Two common practices for dispersal of carbon nanotubes include mechanical dispersion methods and chemical dispersion methods (Vaisman *et al.,* 2006). Mechanical dispersal methods such as ultrasonication and high shear mixing are often used as they can separate nanotubes from each other, but can also fragment the nanotubes. Chemical dispersal methods used include surface functionalization of CNT to improve their chemical compatibility with the target medium (solvent or polymer solution/melt), which can lead to a reduction in their tendency to agglomerate (Vaisman *et al.,* 2006). CNTs can be functionalized quite easily through chemical oxidation by either using strong acids (nitric acid and sulphuric acid) which acts by adding functional groups (carboxyl moieties) onto the edge plane of the nanotubes and it is these functional groups that can facilitate strong bonding with either electrode surfaces or metals (Kakade and Pillai, 2008; Vaisman *et al.*, 2006). Aggressive chemical functionalization, such as the use of neat acids at high temperatures, can introduce structural defects resulting in inferior properties for the tubes (Vaisman *et al.*, 2006).

Functionalization of carbon nanotubes may be either covalent or non-covalent (Kakade and Pillai, 2008; Guo and Li, 2006). Non-covalent functionalization involves the wrapping of CNTs with conjugated polymers and small organic polymers while covalent functionalization involves the modification of the convex surfaces of CNTs by aliphatic molecules, organic functional molecules and atom transfer radical polymerization of vinyl monomers (Guo and Li, 2006). Non-covalent treatment of CNTs is particularly attractive because it presents the possibility of adsorbing various groups onto the CNT surface without disturbing the π system of the graphene sheets (Vaisman *et al.*, 2006). Non-covalent surface treatment through the use of surfactants or polymers has been widely used to prepare solutions of dispersed nanotubes (Vaisman *et al.*, 2006). CNTs have been shown to exhibit a sufficient solubility only in a limited number of

solvents, namely, DMF, dimethyl acetamide (DMAc) and dimethyl pyrrolidone (NMP) (Vaisman *et al.*, 2006).

Films of CNTs have been prepared through dispersion in polymers such as Nafion™ and Teflon, This is practical for electrochemical applications, however it is not ideal for fundamental electrochemical studies as random dispersal onto the electrode surface without an organized orientation limits determination of the contributions of the ends and the sidewall of the nanotubes to the electrochemical properties of the CNTs (Gong *et al.*, 2005).

1.4 Electrode modification for fuel cell applications

Drawing on the advantages that metallophthalocyanines and nanomaterials offer to electrocatalysis, electrodes modified using these materials for use in fuel cells (Parra *et al.*, 2004). The modification of carbon electrodes with nanomaterials such as carbon nanotubes and other catalytic materials like MPcs has been studied extensively for improving oxygen reduction with examples of catalysts being used including metallophthalocyanine films, carbon nanotubes and fullerenes with the aim of applying this to fuel cells (Duarte *et al.,* 2008). Electrodes may be modified by simple adsorption of the catalyst to the electrode surface (Duarte *et al.*, 2008). This relies on π-π interactions between the electrode surface and the catalyst (Duarte *et al.*, 2008). The simplicity of the method however may have its drawbacks as these catalytic films may be easily leached off the electrode surface thereby drastically reducing the lifespan of the electrode (Duarte *et al.*, 2008). Modification of electrodes via electropolymerization has been shown to be a more efficient method as it creates films that are more stable due to their compactness and the reproducibility of the process is greater than other processes (Duarte *et al.*, 2008). Self-assembly of thin catalytic films has been tested and shown to be simple and versatile for the preparation of ultrathin multilayer films (Duarte *et al.*, 2008). Several methods of multilayer film construction have been developed including electrostatic assembly (relies on electrostatic interactions between two oppositely charged layers), hydrogen-bonding interactions and covalent assembly (Duarte *et al.*, 2008).

1.4.1 Immobilization of catalysts and electrocatalyst supports

An important aspect of improving the efficiency of fuel cells is to increase its operating life span. This may be done by improving the design of electrodes, especially when it comes to the immobilization of catalytic material (Bullen *et al.*, 2006)**.** For the electrochemical testing of catalysts used in fuel cells, a simple approach is ideal and this may be done through simple deposition of MPcs onto an electrode (Tau and Nyokong, 2007). MPcs adsorb onto glassy carbon electrodes based on the π-π interactions between the electrode and the phthalocyanine macrocycle (Tau and Nyokong, 2007). Another traditional means for MPc immobilization is the preloading of the MPc species onto a mesoporous material such as carbon black particles followed by coating of the composite material onto the electrode (Zhang *et al.*, 2007). This method has a drawback in that the electrode has a short lifespan and decreases considerably in efficiency with time (Zhang *et al.*, 2007).

To overcome this problem, alternative strategies for immobilization of catalysts have been researched including the incorporation of MPcs into a film of conducting polymers (Zhang *et al.*, 2008). Polypyrrole and Nafion® have been commonly used due to their high robustness, conductivity, and high electrochemical stability in various aqueous environments (Zhang *et al.*, 2007). The polymer films may easily be formed through electrochemical polymerization (Yilmaz *et al.,* 2007). Nafion™ is a sulfonated tetrafluorethylene copolymer and is considered an ionomer as it has ionic properties (Zhou *et al.,* 2008). Nafion's unique ionic properties are a result of incorporating perfluorovinyl ether groups terminated with sulfonate groups onto a tetrafluoroethylene (Teflon®) backbone (Zhou *et al.*, 2008). Nafion has received a considerable amount of attention as a proton conducter for proton exchange membrane (PEM) fuel cells because of its excellent thermal and mechanical stability (Zhou *et al.*, 2008). It has been widely used to immobilize and disperse electrocatalysts onto electrode surfaces (Gong et al, 2005). It has been shown to be useful in preparing CNT-based electrodes due to its capability in confining the CNTs to the electrode surface and solubilizing the CNTs in solution (Gong et al,

2005). Nafion is an insulating polymer however CNTs make up for this due to their own high conductance. Non-covalent attachment of the polymer to the CNTs does not disrupt the electronic and structural properties of the CNTs (Gong et al, 2005).

Chitosan, a biological polymer, has attracted attention for use in the modification of electrodes (Zhao *et al.*, 2008). Chitosan is one of the most studied natural biopolymers for the fabrication of biosensors, coatings and scaffolds for biomedical applications due to the advanced properties of the material, such as antimicrobial activity, corrosion resistance and biocompatibility (Casagrande et al, 2008). Chitosan is a natural polymer and is biodegradable and biocompatible which presents opportunities for use in biologically-based fuel cells (Yi *et al.*, 2005). Few biological polymers have such a high content of primary amines, and these amines confer important functional properties to chitosan that can be exploited for biofabrication purposes (Yi *et al*., 2005). Together with favourable chelating and film forming ability, chitosan has been used to stabilize metal nanoparticles to form chitosan-nanoparticle nanocomposites (Zhao *et al.*, 2008).

Triton X-100 is a nonionic surfactant comprising hydrophilic polyethylene oxide groups and hydrocarbon lipophilic or hydrophobic groups (Janczuk *et al.*, 1995; Li *et al.*, 2004). It is commonly used as a detergent in molecular biology, to permeabilize eukaryotic cells, as well as for the dispersion of carbon materials for soft composite materials (Janczuk *et al.*, 1995; Li *et al.*, 2004). There is however no literature showing its use in biological fuel cells for dispersion of catalysts on the electrode surface.

1.5 Techniques used to develop nanostructured surfaces

1.5.1 Cyclic voltammetry

Cyclic voltammetry (CV) is a potentiostatic technique that involves the application of an excitation signal to intentionally disturb a system from equilibrium (Wang, 1994). The current

generated from the analyte being investigated allows the attainment of the important information about the analyte as the current is proportional to the concentration of the analyte (Kissinger and Heineman, 1996).

CV works by scanning the potential of the working electrode linearly from an initial potential to a switch potential, from which the voltage is then scanned back to the starting potential (Kissinger and Heineman, 1996). The change in current obtained from the forward and reverse scan is recorded as a function of the change in potential. During the potential scan, the analyte will be oxidized or reduced depending on its reduction/oxidation (redox) properties (Kissinger and Heineman, 1996). Analytes will have redox properties unique to them and this will therefore allow for identification of the analyte based on these properties.

A typical CV representative of a reversible redox couple can be seen in Figure 1.6. The analyte, R, is oxidized to O and O is then reduced to regenerate R in the return scan in a reversible redox process. CV will be initiated at a potential in which no redox reactions will occur so that the reduced form of the analyte is maintained throughout the bulk solution and electrode-solution interface. The potential is increased linearly (in the direction of the arrow) resulting in the oxidation of R to generate O, the oxidized form of the redox couple. During the oxidation of R, the anodic peak current increases until the surface concentration of R is depleted through its conversion to O. As the potential is increase sufficiently positive of the redox potential, any R that reaches the electrode surface (through diffusion) is instantaneously oxidized to O. This indicates that the concentration of R is essentially zero at the switch potential. In the reverse scan of the redox couple, O is reduced to regenerate R resulting in the generation of a cathodic current.

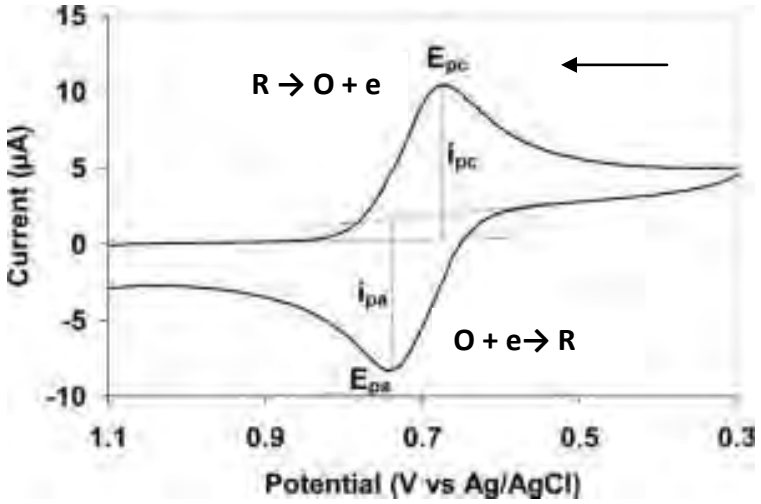

Figure 1-6. A typical cyclic voltammogram showing Ipa, the anodic current obtained from oxidation, and Ipc, the cathodic peak current obtained from reduction (adapted from Kissinger and Heineman, 1996)

1.5.2 Raman spectroscopy

Raman spectroscopy is a spectroscopic technique that is used to study vibrational, rotational and other low frequency modes in a system. It is based on the scattering of incident light by the interaction of electromagnetic waves with the molecular structure of a particular material. The scattered light is characteristic to the chemical bonds present within the molecule, therefore the information obtained from Raman spectroscopy is used to identify the chemical structure of the molecule of interest. It has been widely used to characterize thin films (Mashazi *et al.*, 2007), biological tissues (Manoharan *et al.*, 1996), pharmaceuticals (Wartewig and Neubert, 2005) and nanomaterials (Wang et al, 2008; Tantang *et al.*, 2009).

On interaction with the molecule of interest, the electromagnetic wave is redirected which results in the scattering of light (Gouadec and Colomban, 2007). There is a transfer of energy to the electron cloud of the molecule as a result of the collision of the electromagnetic wave with the molecule in question. The molecule is excited from a ground energy state to a virtual energy state as a result of this energy transfer which is expressed as a distortion in the

distribution of the electron cloud (Gouadec and Colomban, 2007). The energy level of the virtual state is greater than the quantum energy states of the molecule, resulting in the molecule relaxing to a lower energy state through the emission of excess energy which takes the form of scattered light. Depending on the relaxation energy state, the frequency of emission follows Rayleigh, Stokes Raman or anti-Stokes Raman scattering (Gouadec and Colomban, 2007).

1.5.3 Electrochemical Impedance Spectroscopy

Impedance spectroscopy is an electrochemical technique that is based on the concept of electrical resistance (Coster *et al.*, 1996). Electrical resistance is the ability of a circuit element to resist the flow of electrical current and it is defined by Ohm's law in terms of the ratio between voltage E and current I (Coster *et al.*, 1996). The principal of electrical resistance is limited to only one circuit element which is the ideal resistor. An ideal resistor has several simplifying properties:

- It follows Ohm's Law at all current and voltage levels.
- Its resistance value is independent of frequency.
- AC current and voltage signals through a resistor are in phase with each other.

In real world applications however circuit elements exhibit much more complex behavior which cannot be explained by the simple concept of resistance. Impedance, just like resistance, is a measure of the ability of a circuit to resist the flow of electrical current. Impedance however is not limited by the simplifying properties that resistance is limited by (Coster *et al.*, 1996).

Measuring the impedance of an electrochemical system requires the application of a small alternating (a.c.) current of known frequency, ω, and small amplitude, i_0, to the system and then measuring the amplitude, V_o, and the phase difference, Φ, of the electrical potential that develops across it (Coster *et al.*, 1996). The excitation signal, expressed as a function of time, has the form:

$$E(t) = E_\Phi \cos(\omega t)$$

E(t) is the potential at time t_r, while E_Φ is the amplitude of the signal and ω is the radial frequency (Mansfeld, 1990). The relationship between radial frequency ω and frequency f is expressed as:

$$\omega = 2\pi f$$

In a linear system, the response signal I(t) is shifted in phase (ωt – Φ) and has a different amplitude, I_Φ (Mansfeld, 1990):

$$I(t) = I_\Phi \cos(\omega t - \Phi)$$

An expression that is analogous to Ohm's law is then derived which allows for the calculation of the impedance of a system (Mansfeld, 1990):

$$Z = \frac{E(t)}{I(t)} = \frac{E_\Phi \cos(\omega t)}{I_\Phi \cos(\omega t - \Phi)} = Z_0 \frac{\cos(\omega t)}{\cos(\omega t - \Phi)}$$

Impedance, Z, is represented by real and imaginary components which describe the resistance and reactance respectively and can be represented by appropriate electrical circuit elements in series (Coster et al, 1996). The electrochemical response contains valuable information both on interfacial structures present at the electrode surface as well as the dynamics of interfacial processes (Ragoisha and Bondarenko, 2005).

1.6 Aims and Objectives

The aim of this thesis was to examine the role of nano and bulk FePc as catalysts for the reduction of oxygen in MFCs while using nanostructured materials for enhancement of the electrode surface area. Nano FePc, synthesized from bulk FePc, has yet to be investigated for its application as a catalyst for the reduction of oxygen. Immobilization of iron phthalocyanine and multi-walled carbon nanotubes was investigated for their potential to improve the oxygen reduction reaction at the cathode of a MFC. Hybrid systems in which MPcs have been coupled to MWCNTs have yet to be fully investigated for use in MFCs however various studies showing the electrochemical properties of these hybrid surfaces indicate they have great potential for catalysis in MFCs. The key objectives of the study were broken down as follows:

Chapter 2 discusses the experimental procedures that are to be used.

Chapter 3 examines the potential of bulk and nano FePc to catalyze the reduction of oxygen.

Chapter 4 examines the use of MWCNTs for enhancement of oxygen reduction as well as serving as a support for FePc immobilization in a hybrid system.

Chapter 5 examines the performance and optimization of MPc and MWCNT modified electrodes in terms of power densities generated in a MFC.

2 Chapter 2: Methodology

2.1 General Reagents

Milli-Q water was used for the preparation of all reagents as well as for the rinsing of all glassware. All glassware used was rinsed with 5 % nitric acid and milli-Q water prior to use. Multi-walled carbon nanotubes (diameter = 110 nm – 170 nm, length = 5 – 9 µm; >90% purity) were purchased from Sigma-Aldrich as was Iron (II) metallophthalocyanine. N-N-dimethylformamide (DMF) was used to suspend all functionalized MWCNTS (Merck Chemicals). Nitric acid (55 %) and sulphuric acid (98 %) purchased from Merck Chemicals was used for functionalizing MWCNTs. Bare carbon paper, platinum-embedded carbon paper sheets and Nafion™ 117 (N117) (185 µm and 1100 equivalent weight (EW)) proton exchange membrane were a gift from the Johnson Matthey group, UK.

2.1.1 Functionalization of multi-walled carbon nanotubes

Crude MWCNTs (25 mg) were added to a mixture of 10 ml 55% nitric acid aqueous solution and 30 ml 98% sulphuric acid. The mixture was sonicated for 8 hours. Sodium hydroxide (200 ml, 0.2 M) was then added to the mixture which was then allowed to settle overnight. The top layer of acidic solution was siphoned off and the settled MWCNTs were resuspended in milliQ water. The MWCNTs were centrifuged initially at 12,500 rpm for 20 min using a JA-14 rotor on an Avanti J-E centrifuge (Beckman Coulter, United States of America) and then centrifuged further at 10 000 rpm for 10 min. This wash step was repeated until the pH of the supernatant was neutral. The MWCNTs were then dried in an oven at 70°C. The functionalized MWCNTs were suspended in DMF only when required.

2.1.2 Synthesis of nano iron (II) phthalocyanine

Nano FePc particles were synthesized as described previously by Mamuru and Ozoemena (2009) with a slight modification. Briefly, 0.15 g FePc was dissolved in 5 ml of 98 % concentrated sulphuric acid. The solution was then added dropwise into a vigorously stirred 300 mL aqueous solution containing 0.45 g hexadecyltrimethyl ammonium-bromide (CTAB) ($C_{16}H_{33}N(CH_3)_3Br$) (Sigma-Aldrich). Protection of the nano FePc in a CTAB environment ensures much better dispersal of FePc avoiding aggregation which can negatively impact on the catalytic activity of FePc (Mamuru and Ozoemena, 2009). The resulting solution was then centrifuged at 12000 rpm for 15 min using a JA-20 rotor on an Avanti J-E centrifuge (Beckman Coulter, United States of America). The obtained precipitate was washed repeatedly with water until neutral. It was then dried to obtain the nano FePc powder.

2.1.3 Characterization of bulk FePc and nano FePc

Raman spectroscopy was carried out using a Bruker RAM II FT-Raman spectrometer with an excitation Nd:YAG laser (1064 nm). Both bulk and nano FePc were mixed with oven-dried potassium bromide. The mixture of FePc and KBr was compressed into a pellet. The spectra were recorded in the Stokes branch of the spectrum between 400 cm^{-1} and 1600 cm^{-1}.

UV/Visible spectroscopy was performed using a Powerwave plate reader, Bio-tek Instruments, Inc. (USA). The data was analyzed using KC Junior software (Bio-tek Instruments). Suspensions of nano FePc and bulk FePc (concentration 0.5 mg/ml) were prepared in absolute ethanol. Aliquots of each solution were added to wells of a flat-bottom 96-well microtiter plate (polystyrene) (Greiner Bio-one, Germany). Absolute ethanol was used as the negative control to zero the spectrometer.

2.2 Electrochemical procedures

Electrochemical analyses were performed using a Potentiostat/Galvanostat 30 (PGSTAT 30) from Autolab. The data was analysed using General Purpose Electrochemical System version 4.9 (GPES) software (Eco Chemie B.V.). A standard three-cell system was utilized for all electrochemical work. Glassy carbon stalk electrodes (Bioanalytical Systems, USA), a platinum stalk working electrode and reference electrodes (stored in 3 M KCl saturated with NaCl) (Ag/AgCl vs. 0.225 V) were purchased from Bioanalytical Systems, USA. A glassy carbon stalk electrode (GCE) with a diameter of 3 mm was used for all electrochemical work. Platinum wire was utilized as a counter electrode. All electrochemical tests were performed using a 40 mM Britton-Robinson (BR) buffer which was prepared by mixing equimolar solutions of orthophosphoric acid, glacial acetic acid and boric acid (all from Merck Chemicals). BR buffer was chosen as the supporting electrolyte as it has been shown to be a useful model buffer for conducting wide pH range studies. The pH of the buffer was adjusted accordingly using 0.2 M sodium hydroxide. pH measurements were done using a WTW pH 330i pH meter (Germany), coupled to a Sentix 41 pH electrode.

Aqueous solutions were degassed with nitrogen gas (instrument grade, Afrox) by purging for 10 min prior to use.

The GCE was polished thoroughly before each scan with a slurry of aluminium oxide (>10 microns, 99.7% metals from Sigma-Aldrich) on a Buehler felt pad (BASi). The GCE was then sonicated in absolute ethanol for 1 minute to remove any residual aluminum oxide and then rinsed in distilled water.

All glassware was thoroughly cleansed with warm soapy water and rinsed with milliQ water. The electrochemical cells were rinsed with 5 % nitric acid, and then rinsed with milliQ water prior to use.

2.2.1 Modification of Electrode surfaces

The dip-dry method, relying on physical adsorption to the electrode surface, was used to modify a GCE with FePc, MWCNTs and a mix of FePc and MWCNTs. Both bulk and nano FePc of varying concentrations (1 mg/ml, 2.5 mg/ml and 5 mg/ml) were dispersed in absolute ethanol and then sonicated for 1 hour. The dispersal in ethanol and sonication limited aggregation of the FePc molecules. This was followed by depositing 10 µl of FePc onto the electrode surface and then allowing it to dry at 60°C for 10 min in a PL001 laboratory oven (Prolab Instruments, Switzerland). The same procedure was carried out for MWCNTs; however the MWCNTs were dispersed in DMF. For modification of a GCE with a hybrid mix of FePc and MWCNTs, a solution of FePc and MWCNTs was prepared in a ratio of 3:1. This mixture was left to stand for 30 min before use to allow for interaction of FePc with the MWCNTs. A GCE was then modified as before.

2.2.2 Examination of the effect of modified surfaces on the reduction of oxygen at a GCE

The effect of the modification of a GCE with FePc, MWCNTs, and hybrid FePc:MWCNTs for the reduction of oxygen was investigated using cyclic voltammetry (CV). No electrochemical pretreatment was carried out prior to CV. An equilibration time of 3 seconds and a step potential of 0.0137 V were used for all electrochemical analyses. The scan rate was varied from 25 mV to 200 mV. A GCE was modified as discussed in section 2.2.1 with either FePc, MWCNTs or FePc:MWCNTs. 40 mM BR buffer was used as the electrolyte. CV of the modified surfaces was conducted initially in the absence of oxygen to confirm the immobilization of FePc, MWCNTs and FePc:MWCNTs. CV was then conducted in the presence of oxygen to determine the current and potential responses of the modified surfaces towards oxygen reduction. Comparisons were made with the current and potential responses obtained from studies at an unmodified GCE. The current and potential response was recorded after baseline correction of the reduction peaks using GPES software.

2.2.3 Examination of the effect of pH on oxygen reduction at an unmodified and modified GCE

The effect of the modification of a GCE with FePc, MWCNTs, and hybrid FePc:MWCNTs for the reduction of oxygen across a range of pH levels was investigated using cyclic voltammetry (CV) as described before in (2.2.2). CV of the modified surfaces was conducted in BR buffer of pH 2, pH 3, pH 4, pH 5, pH 6, pH 6, pH 7 and pH 8. Comparisons were made with the current and potential responses obtained at an unmodified GCE. The current and potential response was recorded after baseline correction of the reduction peaks using GPES software (Eco Chemie).

2.2.4 Impedance Spectroscopy

Impedance spectroscopy was performed using a Potentiostat/Galvanostat 30 (PGSTAT 30) with a FRA module from Autolab. Nova 1.6 (Eco Chemie) software was used to analyze the data. CV was performed for each electrode modification using the redox probe in order to determine the $E_{1/2}$ of the reaction at the electrode. An equimolar solution of 10 mM potassium ferricyanide ($K_4Fe(CN)_6$) and 10 mM potassium ferrocyanide ($K_3Fe(CN)_6$) (as redox probes) was prepared in 0.25 M phosphate buffer at pH 7 for use as the redox probe. All electrodes used were polished with aluminum oxide paste on a polishing pad. Electrochemical impedance spectroscopy experiments were recorded in the frequency range between 10 kHz and 100 mHz with an amplitude 5mV sinusoidal modulation centred at $E_{1/2}$.

2.3 Microbial fuel cell

2.3.1 Bacterial Growth Conditions

Enterobacter cloacae, strain 16657, was obtained as a vacuum dried culture from DSMZ (Deutsche Sammlung von Mokroorganismen und Zellkulturen Gmbh). The bacterium was grown anaerobically in Reinforced Clostridial Medium (RCM) (Fluka Analytical) which comprised meat extract (10 g/l), peptone (5 g/l), yeast extract (3 g/l), D(+)-glucose (5 g/l), starch (1 g/l), sodium

chloride (5 g/L), sodium acetate (3 g/l), L-cysteine hydrochloride (0.5 g/l), and agar (0.5 g/l). L-cysteine hydrochloride served as an oxygen scavenger. Cells were grown at 30°C in a controlled environment room.

Growth curves, in which the optical density was measured using a spectrophotometer at 600 nm (OD_{600}), were carried out over a period of 24 hours to determine the time it takes for the bacteria to reach log phase. The required mass of RCM was dissolved in milliQ water and this mixture was then autoclaved at 121°C for 15 min. Aliquots of 5 ml were poured into sterilized test tubes using sterile technique. Each test tube was inoculated with 5 µl. The test tubes were incubated at 30°C on a shaking incubator at 120 rpm for 24 hours. OD_{600} was measured every hour using a Powerwave UV/Vis spectrophotometer (using 96 multi-well plates) using KC junior software. Uninoculated RCM was used to blank the spectrophotometer. Sampling and recording of the OD was done in triplicate.

2.3.2 Gram stain of *Enterobacter cloacae*

A gram stain of a log phase culture of *E.cloacae* was performed according to the following protocol. A 20 ul aliquot of log phase culture was deposited onto a clean glass slide which was then passed through a flame to heat-fix the culture onto the slide. The bacterium was then stained with crystal violet for 30 seconds; the stain was rinsed off with water. The bacterium was then stained with iodine for 30 seconds; the iodine was rinsed off using water. After rinsing the bacterium with absolute ethanol until all visible dye was removed, the bacterium was counterstained with safranine for 1 minute. The safranine (obtained from technical staff) was rinsed off with water and then the slide was dried at room temperature. A cover slip was placed over the slide, and then the bacterial cells were visualized under a Nikon YS100 light microscope.

2.3.3 Glycerol stocks

To avoid contaminating the original culture of *E.cloacae*, glycerol stocks of the bacterium were prepared. A log phase culture of the bacterium was grown up from the original culture, and then 500 ul of the log phase culture was mixed with an 80 % solution of glycerol (prepared from 100% stock). The stocks were stored at -20°C until needed.

2.3.4 Microbial fuel cell electrode modification

Iron (II) phthalocyanine and MWCNTs were prepared as before for electrochemical analyses. The carbon paper electrodes were modified using a simple dip-dry method that relied on physical adsorption of the electrocatalysts onto the carbon paper. A 200 µl aliquot of FePc, MWCNTs or FePc:MWCNTs was deposited onto the electrode which was then dried in an oven at 70°C for 10 min.

2.3.5 Use of Polymers for Immobilization of FePc and MWCNTs

Chitosan, Nafion™ and Triton X-100 were investigated for potential use as an immobilization and dispersing agent for MPcs and MWCNTs on the electrode surface. A 1 mg/ml solution of chitosan (sourced from crab shells; ≥ 75% acetylation; Sigma-Aldrich) was prepared by dissolving an appropriate amount in 5% acetic acid. The mixture was sonicated for 30 min to allow for complete dissolution of the chitosan. A 1 % (v/v) solution of Triton X-100 was prepared from a stock solution. A 1 % (v/v) solution of Nafion™ was prepared from a stock of Nafion™. The solution was sonicated for 30 min. FePc was then mixed with the polymer in a 1:1 ratio. The same procedure was followed for MWCNTs and FePc:MWCNT mixtures. The nanotubes immobilized on the electrodes without dispersant were suspended in dimethyl formamide (DMF). Nanotubes have been shown to have good solubility in DMF (Vaisman *et al.*, 2006). Each solution of nanotubes was sonicated for a few min prior to immobilization onto the

electrode surface. According to Vaisman *et al.* (2006), sonicating the functionalized MWCNTs in DMF would be lead to sufficient dispersal. Immobilization was conducted as before (2.2.1).

2.3.6 Preparation of Nafion N117 membrane

The Nafion 117 membrane (Johnson Matthey Technology Centre, UK) was cut into circles with a diameter of 2 cm. The membrane was then boiled in 3 % hydrogen peroxide for 1 hour and then rinsed in milliQ water. This served to clean the membrane and therefore remove any unwanted impurities. The membrane was then boiled in 0.2 M sulphuric acid, which served to sulphonate the membrane, for 1 hour and then thoroughly rinsed in milliQ water. The cleaned membrane was stored in sterilized milliQ water until needed.

2.3.7 Microbial fuel cell design and operation

A two-chambered H-type MFC was constructed using 250 ml Schott bottles connected by a glass bridge clamped together (as shown below). The chambers were separated with a cation selective membrane (Nafion 117). The electrodes were carbon paper sheets (Johnson Matthey Technology Centre, UK) with an area of 4 cm^2. The electrodes were connected to the external resistor using crocodile clips. A fixed external resistance (680 Ω) was used to complete the circuit. All apparatus and media used were autoclaved prior to use. The anode chamber was filled with 150 ml RCM while the cathode chamber was filled with 0.25 M sodium phosphate buffer which had been spiked with 10 % hydrogen peroxide prior to use in order to increase the dissolved oxygen concentration. The MFC was assembled under sterile conditions ensuring aseptic technique was followed. The anode chamber was inoculated with 100 µl of log phase *E.cloacae* and then sealed. The voltage of the system was measured every 30 min using a multimeter (DT803B Digital Multimeter). The current generated was calculated using the equation $I = V/R$ while the power was calculated using the equation $P = IV$ where I is the current in amperes and V is the voltage in volts. The power density was calculated using the equation (Logan, 2008):

$$P_{elec} = \frac{E^2_{MFC}}{A_{elec}R_{ext}}$$

where E is the voltage in volts, A is the electrode surface area in m^2, and R is the external resistance in ohms.

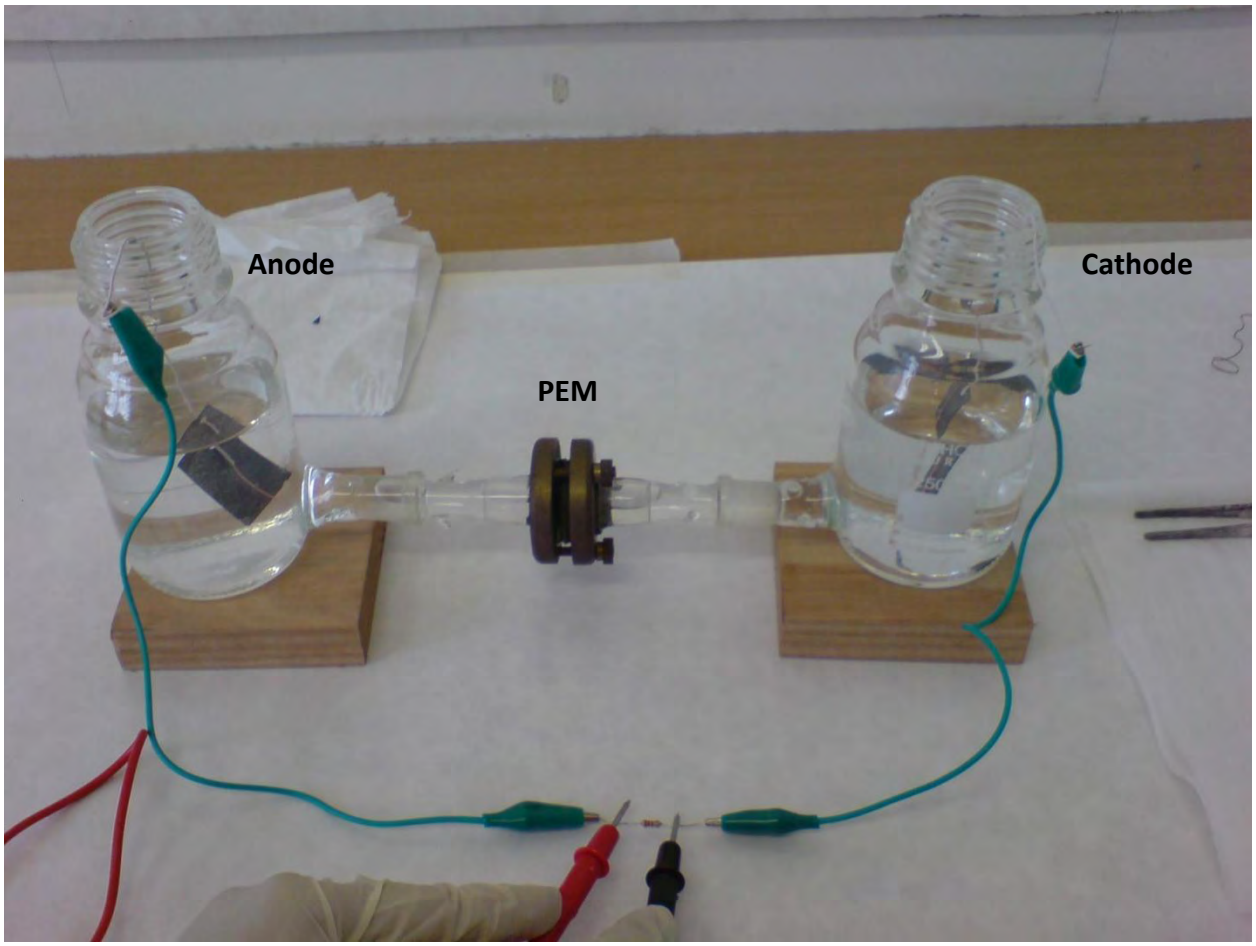

Figure 2-1: Laboratory scale H-type fuel cell design

2.3.7.1 Optimization of microbial fuel cell

All MFCs operated in this study made use of RCM as the growth medium in the anodic compartment.

Temperature: MFCs were set up as in section 2.3.7. The temperature of a controlled environment (CE) rooms were set at 25°C and at 35°C. MFCs were operated in the CE rooms for 10 hours, with the voltage being recorded as per before.

Agitation: MFCs were set up as before (section 2.3.7). The anodic compartment of each MFC was placed onto a magnetic stirrer and a sterilized stirrer bar was placed into the anodic compartments. The anode chamber of each MFC was then stirred at 100 rpm for the entire time of operation. Voltage was recorded as before.

Ionic strength: MFCs were set as before (section 2.3.7). Sodium chloride (Merck) was added to the growth medium to be used in the anodic compartment in concentrations of 100 mM, 200 mM and 300 mM. The MFC was set up as before and operated for 10 hours. Voltage was recorded as before.

2.3.8 Statistical analysis of Data

All experimental work was performed in triplicate and the mean value was calculated. The standard deviation for each set of values was determined using Microsoft Excel. To determine whether there was significance between data points, a student's T-test was performed using Microsoft Excel.

3 Chapter 3: Electrochemical reduction of oxygen at unmodified and Iron phthalocyanine modified surfaces

3.1 Electrochemical reduction of oxygen

The oxygen reduction reaction (ORR) serves an important role in biosensors and more importantly, fuel cells (Sun *et al.*, 1999). There is no definitive agreement on the mechanism involved for the ORR however it was shown earlier that oxygen can be reduced either via a 4 electron reduction or via a 2 electron reduction that involves hydrogen peroxide as a reaction intermediate (Hao Yu et al, 2009). Taylor and Humffray (1975) suggested the following mechanism for ORR at a GCE:

$$O_2 + e^- \leftrightarrow O_2^-{}_{ads.\ \text{before migration}}$$

$$O_2^-{}_{ads.\ \text{before migration}} \leftrightarrow O_2^-{}_{ads.\ \text{after migration}}$$

$$2O_2^-{}_{ads.} + H_2O \rightarrow O_2 + HO_2^- + OH^-$$

The mechanism involved the migration of oxygen to the electrode surface followed by the adsorption (ads.) of oxygen to the electrode surface whereby oxygen was reduced. Zhang *et al.* (1984) later proposed a similar, but more detailed, mechanism that also involved the adsorption of oxygen to the electrode surface whereby oxygen was reduced to several intermediates:

$$O_{2ads} + e^- \rightarrow [O_2^-{}_{ads.}]$$

$$[O_2^-{}_{ads.}] \rightarrow \{O_2^-{}_{ads.}\}$$

$$\{O_2^-{}_{ads.}\} + HOH \rightarrow HO_{2ads} + OH^-$$

$$HO_{2ads} + e^- \rightarrow HO_2^-{}_{ads}$$

$$HO_2^-{}_{ads} \rightarrow HO_2^-{}_{aq}$$

The electroreduction of oxygen on carbon surfaces such as glassy carbon (GC) or highly orientated pyrolytic graphite (HOPG) is much slower than on metals such as platinum or gold

(Yang and McCreery, 2000), precipitating the need for electrode modification with catalytic materials. The choice of electrode material greatly influences the electrochemical reduction of oxygen as does the solution medium used. FePc has been to shown catalyze the reduction of oxygen via a 4 electron reduction (Baker *et al.*, 2008). FePc provides a cheaper alternative and its application for use in MFCs is examined here.

3.1.1 The oxygen reduction reaction at a bare glassy carbon electrode

Oxygen reduction at a bare GCE occurs between a potential of -0.5 V and -0.8 V depending on pH (Figure 3.1). It is a non-reversible reduction, as can be seen by the absence of a return anodic peak. This is consistent with literature (Maldonado and Stevenson, 2004). To confirm the identity of the peak, a degassed solution showed no peaks attributable to dissolved oxygen at a bare GCE (Figure 3.1).

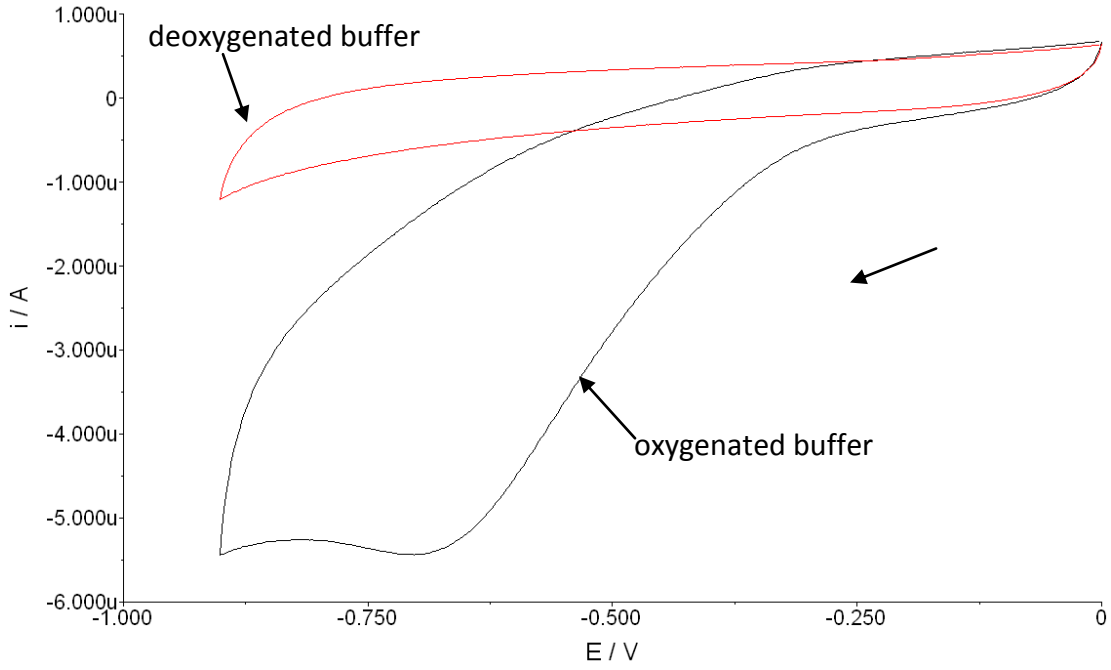

Figure 3-1. The reduction of oxygen at a bare GCE in oxygenated buffer and deoxygenated buffer. Electrolyte: 40 mM Britton-Robinson buffer, pH 7. Scan rate = 200 mV/s.

Figure 3.2 A and B shows the effect of pH on oxygen reduction at a bare GCE between pH 2 and pH 8. It can be seen that there is a shift in the peak towards more negative potentials with decreasing acidity (Figure 3.2 A).

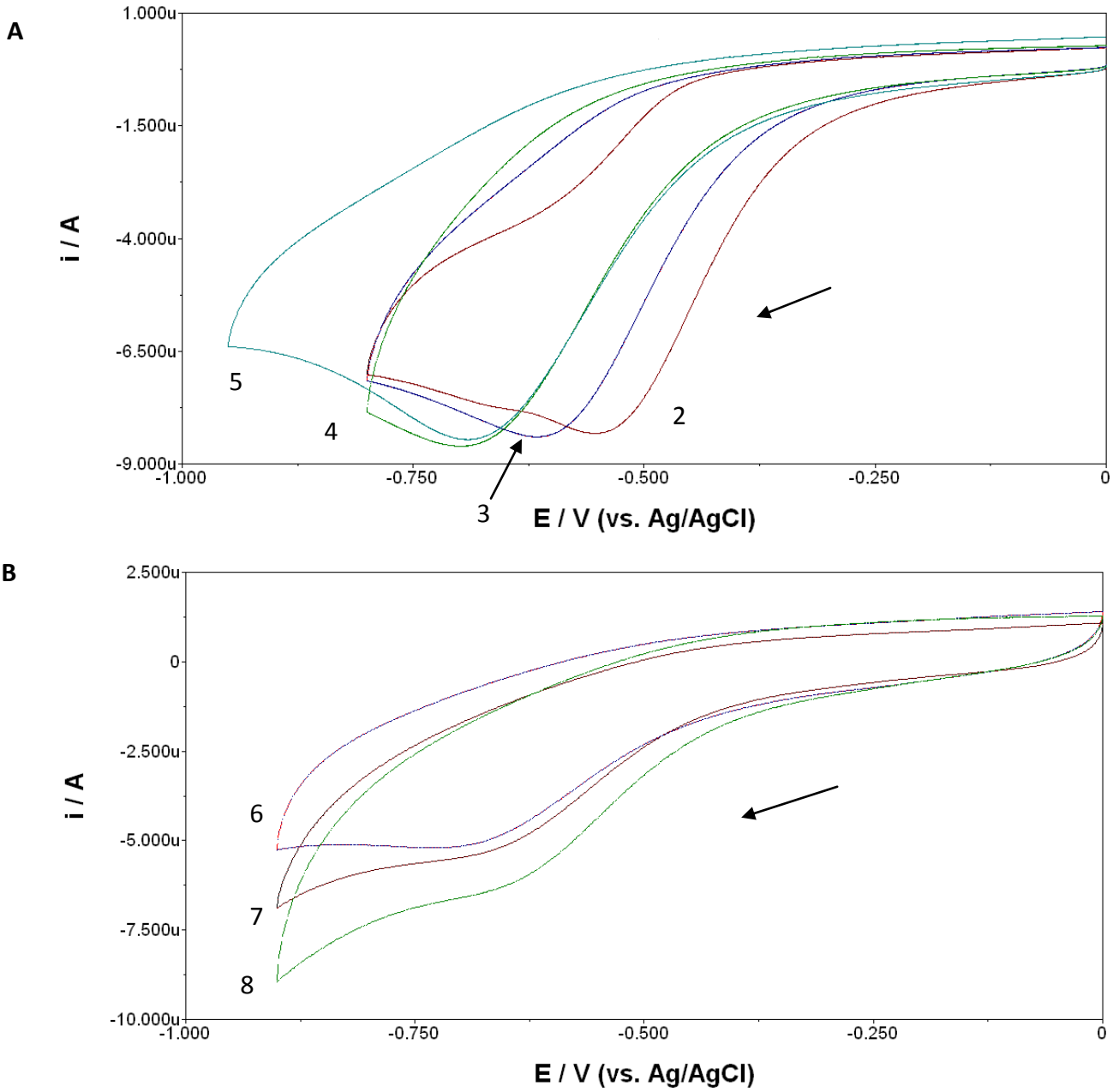

Figure 3-2. The reduction of oxygen at a bare GCE A) pH 2 to 5 and B) pH 6 to 8. Electrolyte: 40 mM Britton-Robinson buffer. Scan rate = 200 mV/s. The numbers denote the pH.

The shift in reduction potential is more apparent at lower pH values (Figure 3.2B). This can be more clearly seen in Figure 3.3, in which the reduction potentials for oxygen reduction at a bare GCE from pH 2 to pH 8 was compared to the current responses obtained. The current response presented was determined after baseline correction. This was repeated for all modified surfaces.

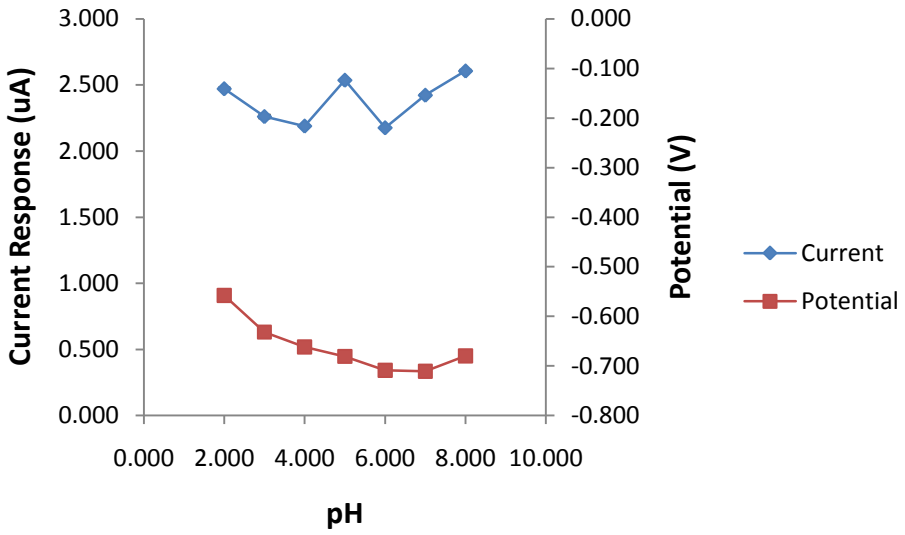

Figure 3-3. Current and Potential response of oxygen reduction at a bare GCE from pH 2 to pH 8. Error bars show standard deviation from mean (Error bars are not visible due to low deviation). n = 3

At pH 2, reduction occurs at -558 mV whereas at pH 8, reduction occurs at -680 mV. This is a shift of 122 mV from pH 2 to pH 8, approximately 17 mV per pH unit. The slope of potential versus pH (calculated from the linear region from pH 3 to 6) is 25.7 mV/pH unit. A value of ~ 30 mV/pH unit indicates a 2 e^- and 1 H^+ transfer. From the plot of peak potential against the logarithmic of scan rate, a Tafel slope of 232.8 mV/decade was determined for pH 2 while that of pH 7 was calculated to be 207.2 mV/decade (Appendix 1). Using the the Randles-Sevcik equation for a diffusion controlled irreversible redox reaction, the number of electrons involved in the reduction of oxygen was calculated (Bard, 1980):

$$Ip = 2.98 \times 10^5 \, n \, (\alpha \, n_a)^{1/2} \, A \, D^{1/2} \, C \, v^{1/2}$$

Where Ip represents the peak current (in amperes), n the total number of electrons transferred, α the transfer coefficient ,n_a the number of electrons transferred during the rate limiting step, A the electrode surface area (in cm^2), D the diffusion coefficient (in $cm^2.s^{-1}$), C the concentration of oxygen (in $mol.cm^{-3}$) and v the scan rate (in $V.s^{-1}$). At pH 3, *n* was equal to 1.0 while at pH 7, *n* was equal to 1.7. This suggests that at neutral pH, the reduction of oxygen at a bare GCE involves possibly two electrons whereas at acidic pH, the reduction occurs via a 1 electron reduction. Yang and McCreery (2000) showed that at a bare GCE across a pH range, an overall $2e^-$ reduction at high pH values (pH 7 and higher) was expected resulting in the formation of H_2O_2 or HO_2^-, while at low pH values, the ORR was sluggish and likely to follow a 1 e^- reduction.

The current response for oxygen reduction is greatest at pH 8 and with no observable linear trend with the peak at pH 5 and pH 8 (Figure 3.3). This is similar to Zhang and Yang (2007) where no trend was observed from pH 2 to pH 8, the highest being observed at pH 6. The proposed mechanism for oxygen reduction from literature shows that the adsorption of O_2^- is a critical step. Early mechanisms suggested for the ORR at a GCE by Taylor and Humffray (1975) and then later adapted by Zhang *et al.* (1984) shows the first step is that of molecular oxygen adsorbing to the electrode surface.

Pretreatment of the electrode by polishing with alumina serves to remove impurities and thereby expose “fresh” carbon and it can also introduce a limited number of oxygen-containing functional groups to the electrode surface (Sljukic *et al.*, 2005). The pretreatment therefore increases the number of potential active sites present at the electrode surface. As mentioned, these functional groups can act as mediators in proton transfer between the electrode surface and electroactive species in solution. The electrode was thoroughly polished between each set of scans at different pH levels. Any potential differences in the degree of polishing could potentially have a direct effect on the electrochemical behavior of the electrode. The lack of a desirable trend in the changes of current response could therefore be related to the pretreatment of the electrode.

3.2 Characterization of nano FePc

3.2.1 UV/Visible spectroscopy

It was proposed in this thesis that the reduction of oxygen could be enhanced through the use of nanostructured FePc. The synthesis of nano FePc from bulk FePc was discussed in chapter 2. The synthesized nano FePc, as well as the bulk FePc from which it was synthesized, was characterized using UV/Vis spectroscopy and Raman Spectroscopy. The main principle of the synthesis of nano FePc is simply the breaking of the intramolecular forces and protection of the species in a CTAB environment (Mamuru and Ozoemena, 2009). CTAB is a surfactant which aids the dispersal of FePc. Figure 3.4 shows the UV/Visible spectrum of nano FePc and bulk FePc.

A

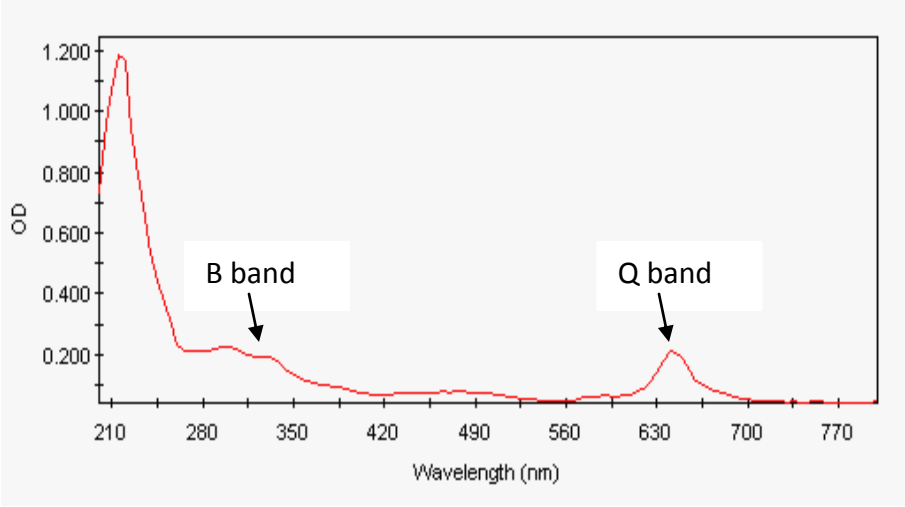

B

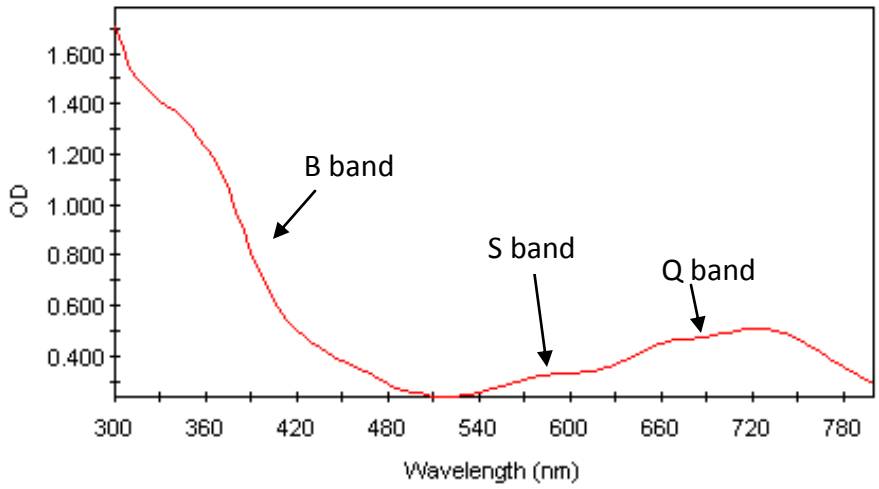

Figure 3-4. Absorption spectra of A) nano FePc and B) bulk FePc.

The absorption spectra of both bulk FePc and nano FePc (Figure 3.4) exhibit the characteristic peaks seen with FePc however it is not entirely clear how different the absorption spectra of bulk FePc and nano FePc will be as there is very little known literature on the absorption spectrum of nano MPcs. The Q band of FePc is generally present at a wavelength of 652 nm, the S band is seen at 596 nm and the B (Soret) band is seen at 330 nm (Zanguina et al, 2002). The Soret band is associated with metal-to-ligand charge transfers (Terzian and Benlian, 1990; Baker *et al*., 2009). The Q band is associated with π-π* transition, which involves transition of excited electrons from the HOMO (highest occupied molecular orbital) level to the LUMO (lowest

unoccupied molecular orbital) level (Leznoff and Lever, 1993). The Q and B bands are always seen within this range, depending on solvent used (Bayo *et al*., 1990).

Nano FePc exhibits a clearly defined Q band at approximately 640 nm and a less defined B band at approximately 320 nm (Figure 3.4A). There is no presence of an S band for nano FePc (Figure 3.4A). Bulk FePc exhibits a Q band at approximately 660 nm and a B band at approximately 340 nm while a poorly defined S band is present at approximately 590 nm (Figure 3.4B). The Q band and B band are not clearly defined for bulk FePc (Figure 3.4B). They are seen as broad peaks. This could be due to aggregation of the bulk FePc particles. It is still evident that there is a shift in the Q band and B band to a shorter wavelength for the nano FePc relative to the bulk FePc. Li et al, (2004) showed that in the presence of a surfactant, there was a shift in the Q band of nano FePc to a shorter wavelength. It was shown that this was partly due to the decrease in the size of the FePc particles and reduction of aggregation. Since a surfactant, CTAB, was used in the synthesis of nano FePc, this is expected. Nano FePc particles have been shown to be smaller than bulk FePc particles (Mamuru and Ozoemena, 2009). Therefore the shift in the Q and B band could be attributed to a decrease in particle size.

3.2.2 Raman Spectroscopy

To further characterize the nano FePc, Raman spectroscopy of both bulk and nano FePc was performed (Figure 3.5).

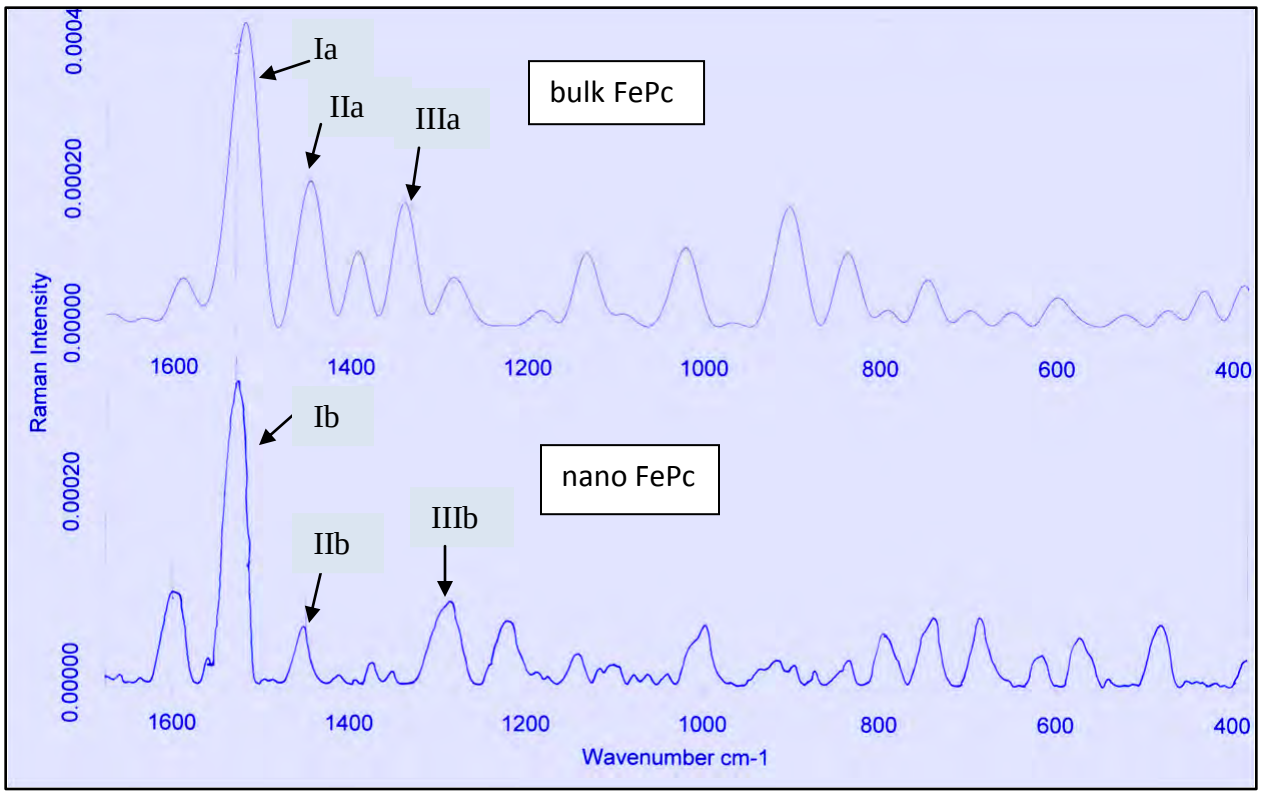

Figure 3-5. Raman spectrum of bulk FePc (top) and nano FePc (bottom)

The region from 1200 cm^{-1} to 1500 cm^{-1} relates to C-N and C-H bonds and stretching between bonds such as C-C and C-N bonds (Melendres, 1980; De Wael *et al.*, 2005; Mashazi *et al.,* 2007). With respect to the Raman spectrum of bulk FePc, the peaks labeled Ia (1520 cm^{-1}), IIa (1446 cm^{-1}) and IIIa (1340 cm^{-1}) are attributed to C=C (Peak Ia), C-N (Peak IIa), and C-H (Peak IIIa) bond formation and bond stretching as suggested by Melendres (1980). From Figure 3.4, the most noticeable difference between bulk FePc and nano FePc is the region of 1200 cm^{-1} to 1500 cm^{-1}. Using the peaks Ia, IIa and IIIa as reference points from which to compare the spectrum of nano FePc, it is apparent that the corresponding peaks for nano FePc, Peak Ib (1529 cm^{-1}), Peak IIb (1475 cm^{-1}) and Peak IIIb (1378 cm^{-1}), have shifted to shorter wavenumbers (Figure 3.4). Boone *et al* (1999) suggested that the Raman peaks and their intensities are dependent on crystalline size. The synthesis of nano FePc should lead to a decrease in the particle size of FePc. The change in peak positions observed in the Raman spectrum of nano FePc could be attributed to the decrease in the particle size. The differences in molecular structure of bulk FePc and

nano FePc are not entirely known as there is very little literature present and most of the literature on nano FePc focuses on its electrochemical behavior. As mentioned before, the synthesis of nano FePc requires that the intramolecular forces between the FePc particles are broken.

It is not known however what intramolecular forces are involved. There are π- π interactions between individual FePc particles and perhaps C-H bonds between individual particles. The greatest shift in wavenumber between nano FePc and bulk FePc was observed for peak III. Peak III was attributed to C-H bonding. C-H bonding would be the likeliest form of intramolecular bonding present in FePc. This could explain the greater shift in peak IIIb relative to the other peaks. The differences seen in the Raman spectrum of nano FePc relative to bulk FePc suggests that they are different forms of FePc.

3.3 Iron phthalocyanine as an electrocatalyst

To confirm the modification of a GCE with FePc, CV was conducted initially with a wide scan range in deoxygenated buffer. The iron centre of FePc has the ability to undergo several redox reactions related to Fe^{3+}/Fe^{2+} and Fe^{2+}/Fe^{1+} (Leznoff and Lever, 1993). The phthalocyanine ring undergoes reduction at very negative potentials (over -1000 mV) while the ring is oxidized at positive potentials close to 1000 mV (Leznoff and Lever, 1993).

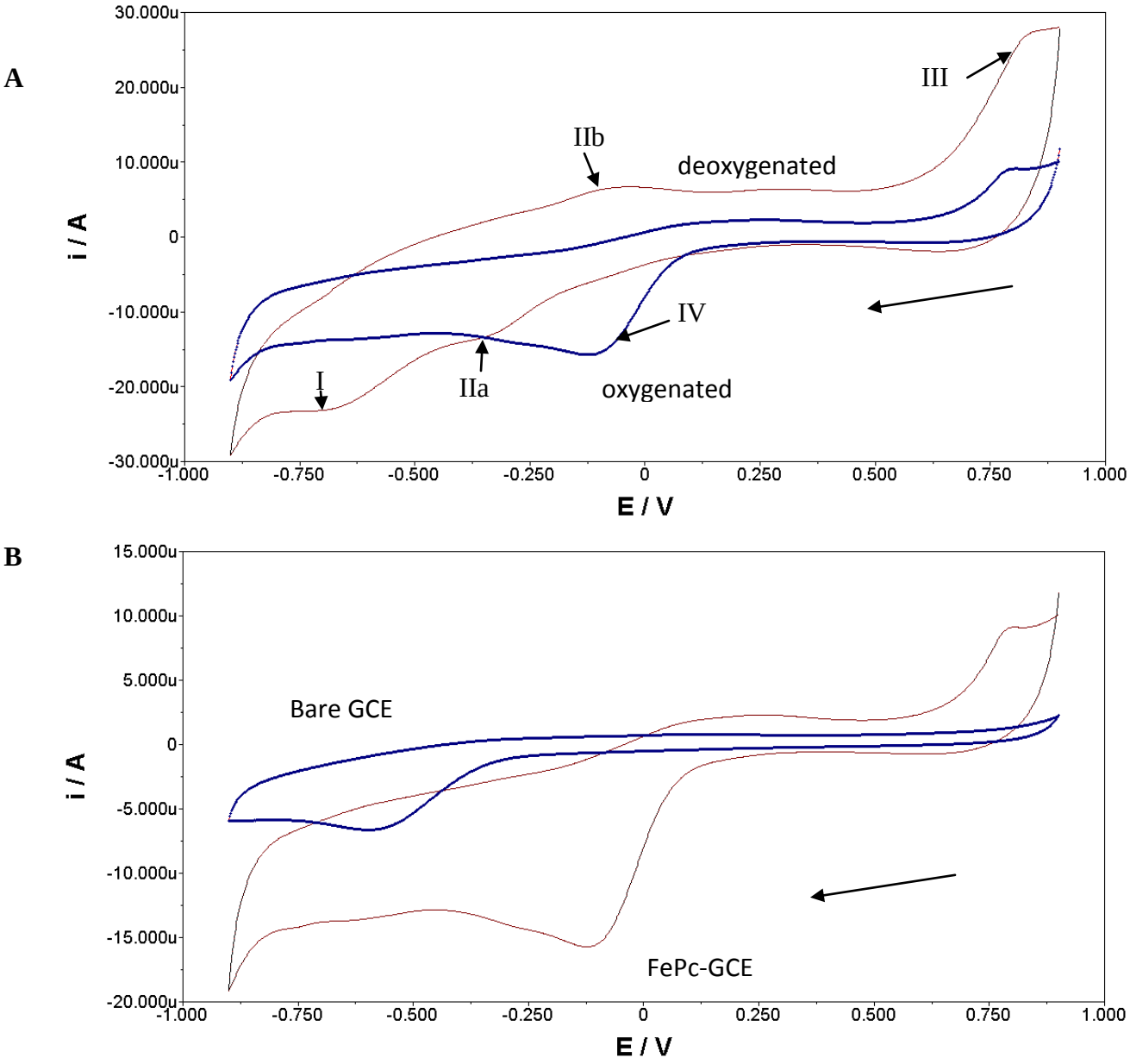

Figure 3-6. Cyclic voltammogram of an FePc-modified glassy carbon electrode. A) FePc-modified electrode in oxygenated buffer and deoxygenated buffer. Peak I = Fe(III)Pc(-2)/[Fe(II)Pc(-3)]$^{-}$; Peak IIa and b = Fe^{3+}/Fe^{2+}; Peak III = ring oxidation; Peak IV = Oxygen reduction. B) Reduction of oxygen at a FePc-modified GCE relative to a bare GCE in oxygenated buffer. 40mM Britton-Robinson Buffer. Scan rate = 200 mV.s^{-1}

The peaks labeled IIa (-300 mV) and IIb (-100 mV) can be assigned to the redox couple Fe^{3+}/Fe^{2+} (Fig 3.6A) (Leznoff and Lever, 1993). Peaks I (-700 mV) is indicative of Fe(III)Pc(-2)/[Fe(II)Pc(-3)]$^{-}$, while peak III (800 mV) is attributed to ring oxidation (El Hourch and Belcadi, 1992; Leznoff and

Lever, 1993). The peak at -100 mV (Peak IV) in Figure 3.6A at a FePc-modified GCE in the presence of oxygen is attributed to the reduction of oxygen at this surface, which is consistent with literature values for reduction of oxygen at FePc (Lever, 1999). It is shown that an FePc-modified electrode reduces oxygen at a much more positive potential than at a bare GCE (Figure 3.6B). There is a shift in reduction potential of approximately 500 mV towards more positive potentials at the FePc-modified GCE. There is also a substantial increase in the current response generated by the modified electrode relative to the bare GCE. It is evident from the initial electrochemical data that FePc is indeed catalytic towards the reduction of oxygen as seen by the shift in potential (Figure 3.6B). This catalytic behavior towards oxygen is consistent with literature reports (El Hourch and Belcadi, 1992; Hao Yu *et al.,* 2009)

The simplified mechanism for reduction of oxygen at an FePc-modified electrode proposed by Van der Putten *et al.* (1987) is as follows (Me refers to the metal centre):

$$Me^{2+} + O_2 \rightarrow Me^{3+} + O_2^-$$

$$Me^{3+} + O_2^- \xrightarrow{H^+,\ e^-} \text{products} + Me^{3+}$$

$$Me^{3+} + e^- \rightarrow Me^{2+}$$

A similar mechanism proposed by Beck (1977) indicates that oxygen present in solution adsorbs to the metal centre of the phthalocyanine much like the mechanism on a GCE. The metal centre is then oxidized from Me^{2+} to Me^{3+} (Beck, 1977). The electrons lost from the metal centre then reduce the adsorbed oxygen resulting in the formation of O_2^-. O_2^- is further reduced to either hydrogen peroxide ($2e^-$ reduction) or water ($4e^-$ reduction). The metal centre is then reduced back to its Me^{2+} state.

Van den Brink *et al.* (1984) proposed a similar, more detailed model:

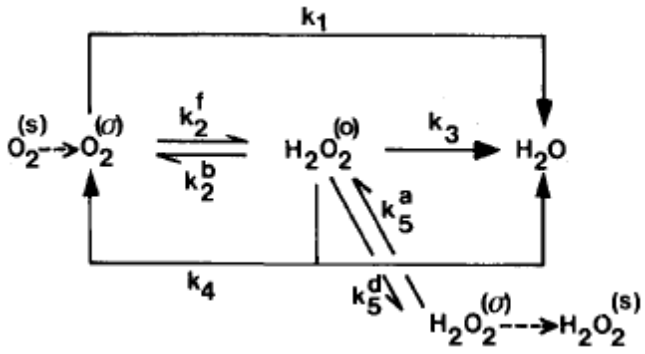

Figure 3-7: Detailed mechanism of the reduction of oxygen at the electrode surface. (s) = species in solution; (δ) = adsorbed species; k = reaction constants.

The mechanism involves the adsorption of oxygen from solution onto the electrode (as indicated by the mechanism proposed earlier), more specifically the metal centre of the phthalocyanine. The adsorbed oxygen is either reduced via a $4e^-$ reduction to produce water or it can be initially reduced via a $2e^-$ reduction to produce H_2O_2 at the electrode surface. The H_2O_2 can both desorb from the electrode surface and go into solution or it can be further reduced via another $2e^-$ reduction to produce water.

The electrochemical response of both nano FePc and bulk FePc was investigated using CV (Figure 3.8).

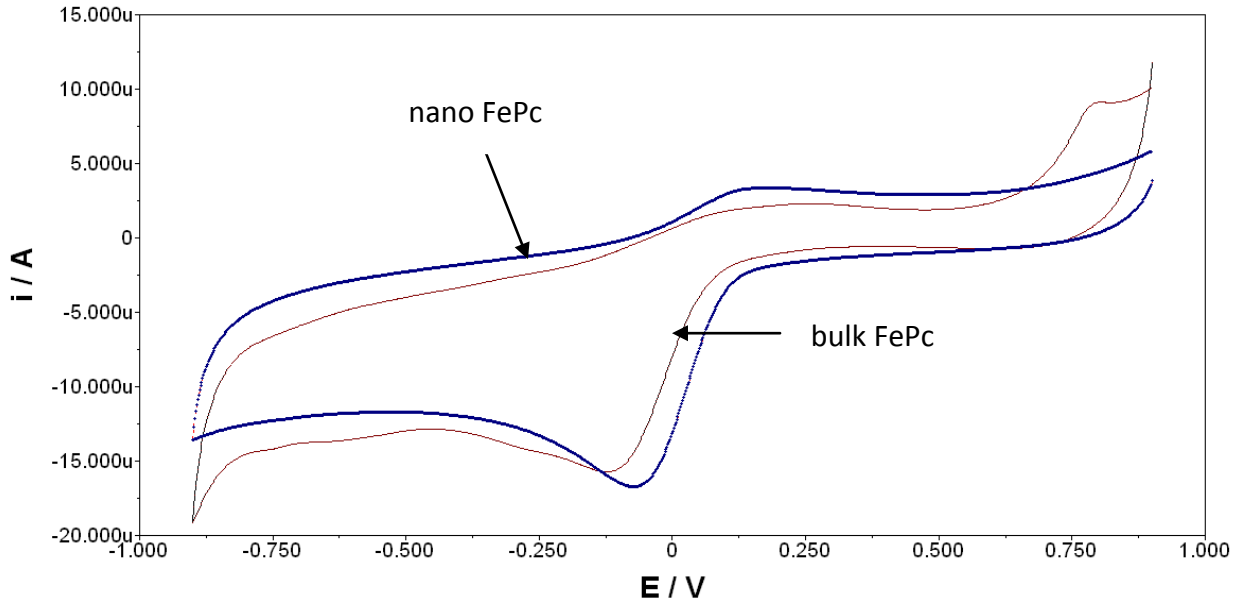

Figure 3-8. Representative CVs of nano FePc and bulk FePc in the presence of oxygen. Electrolyte = 40 mM BR buffer pH 7. Scan rate = 200 $mV.s^{-1}$.

Comparison of the CV of nano FePc and bulk FePc indicates no substantial difference in the electrochemical behavior of the two forms of FePc however further studies on the reaction kinetics of nano FePc would need to be conducted to draw any conclusions (Figure 3.8). Of prime interest in these studies is the degree to which reduced aggregation and reduction in size of bulk FePc to nano FePc lowers the reduction potential for oxygen and impacts on current response.

A comparison of the potential responses from both bulk FePc-modified electrodes and nano FePc-modified electrodes shows that both forms of FePc are catalytic towards the reduction of oxygen (Figure 3.9).

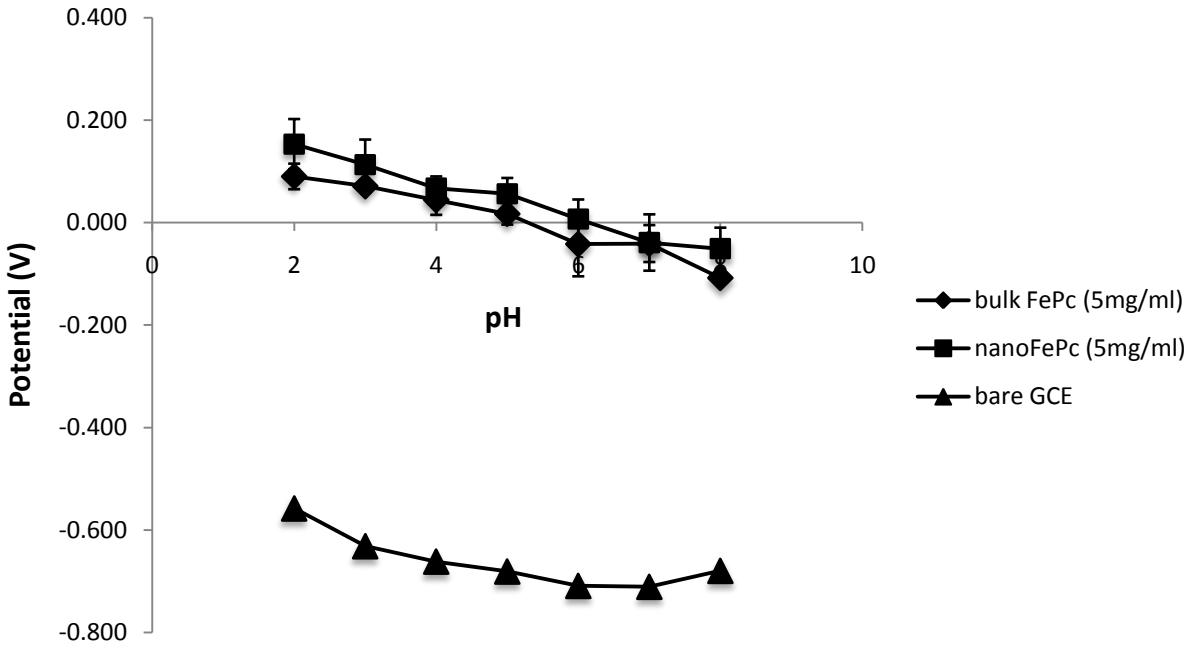

Figure 3-9. Potential response of bulk FePc vs. nano FePc. 40 mM BR buffer. Scan rate = 200 mV/s. Error bars show standard deviation from mean. n = 3

Oxygen reduction occurs at very negative potentials at a bare GCE whereas the reduction of oxygen at both bulk and nano FePc modified electrodes occurs at more positive potentials (Figure 3.9). As for oxygen reduction at a bare GCE, the ORR at FePc-GCE is pH dependent (Figure 3.9). Reduction potential is shifted to more positive potentials with increasing acidity. Bulk FePc and nano FePc show a similar trend across the pH range studied. The slopes obtained from the linear region of Figure 3.8 for nano FePc and bulk FePc are in the region of 25 mV/pH which is indicative of a $2e^-$ and $1H^+$ process. Both forms of FePc show a large shift in potential relative to a bare GCE however statistical analysis showed there was no significant difference ($p < 0.05$) at any pH value between the potentials of oxygen reduction between bulk and nano FePc (Figure 3.9).

A comparison of the current response obtained from bulk and nano FePc-modified electrodes shows that both forms of FePc greatly enhance oxygen reduction relative to a bare GCE (Figure 3.10).

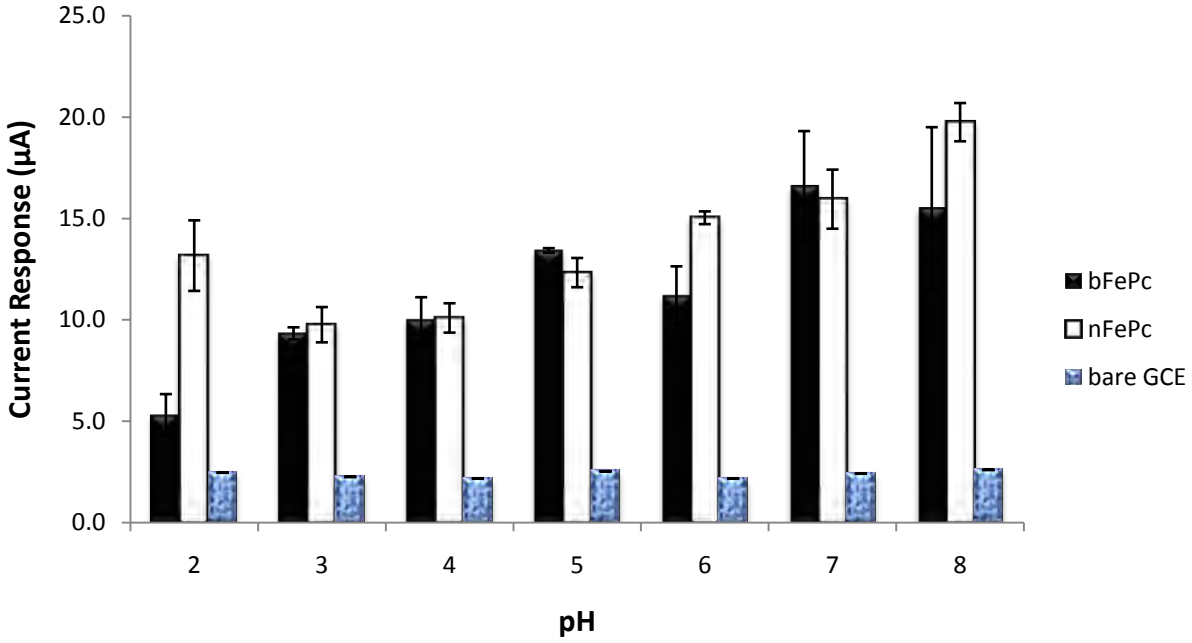

Figure 3-10. Current response of bulk FePc vs. nano FePc. Black = bulk FePc; White = nano FePc; Shaded = bare GCE. Error bars show standard deviation from mean. n = 3

Across a pH range of 2 to 8, bulk and nano FePc showed greater current response for the reduction of oxygen relative to a bare GCE (Figure 3.10). At a bare GCE the highest current response is observed at pH 5 and 8 (Figure 3.3). FePc-modified electrodes showed a different trend to a bare GCE. The general trend seen for both bulk FePc and nano FePc, was an increase in the current response with increasing alkalinity (Figure 3.8). Statistical analysis using a T-test showed there was no significant difference in current response between nano FePc and bulk FePc except at pH 2 ($p < 0.05$) (Figure 3.10) where statistically significant increases in current response was observed at the nano FePc modified GCE. Similar current responses and lowering of the potential values were observed at both surfaces. Given this, further mechanistic studies were confined to bulk FePc considering that the time-consuming production of nano FePc did not yield significantly different responses compared to bulk FePc.

The effect of varying the loading rate of both bulk FePc and nano FePc at a GCE for ORR was investigated (Figure 3.11). A suspension of the desired FePc was dispersed in absolute ethanol at varying concentrations namely 1 mg/ml, 2.5 mg/ml and 5 mg/ml.

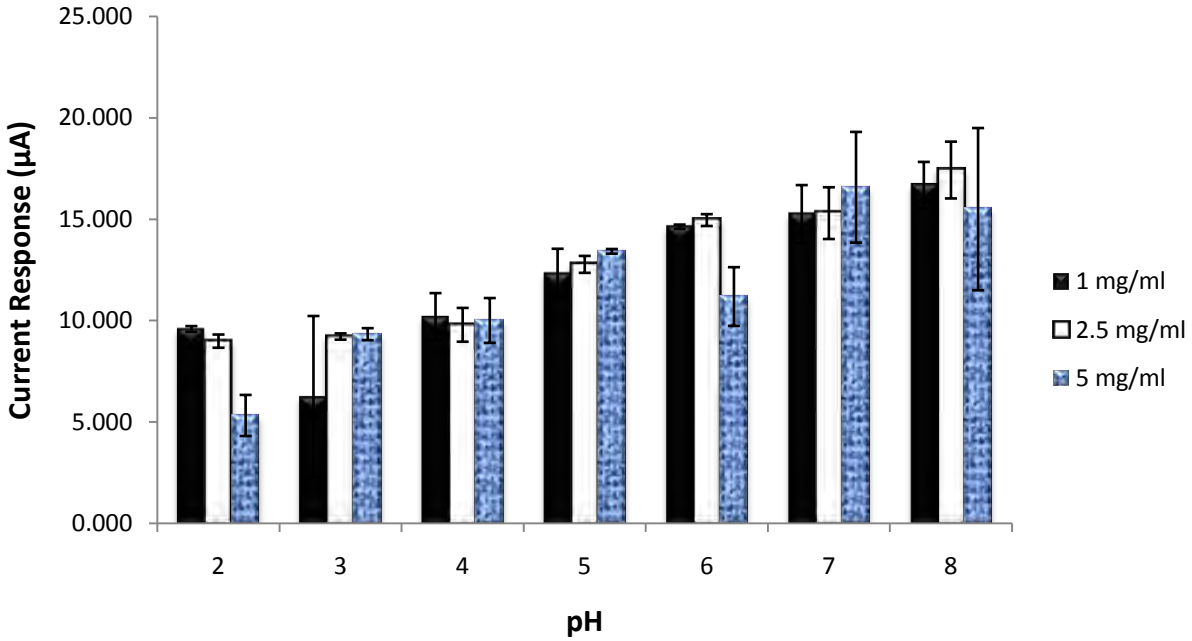

Figure 3-11. Current responses of bulk FePc at varying loading rates. Error bars show standard deviation from mean. n = 3.

The loading rates studied do not have any apparent effect on the overall current response obtained from a bulk FePc-modified GCE (Figure 3.11). All three loading rates tested gave very similar current responses across the entire pH range. It would be expected that the current response would increase with increasing loading rate. A possible explanation is that bulk FePc does tend to aggregate in solution even after dispersion under sonication. If aggregation did occur on the electrode surface, it could decrease the rate of oxygen reduction resulting in a lower and more variable current response at these loading concentrations examined.

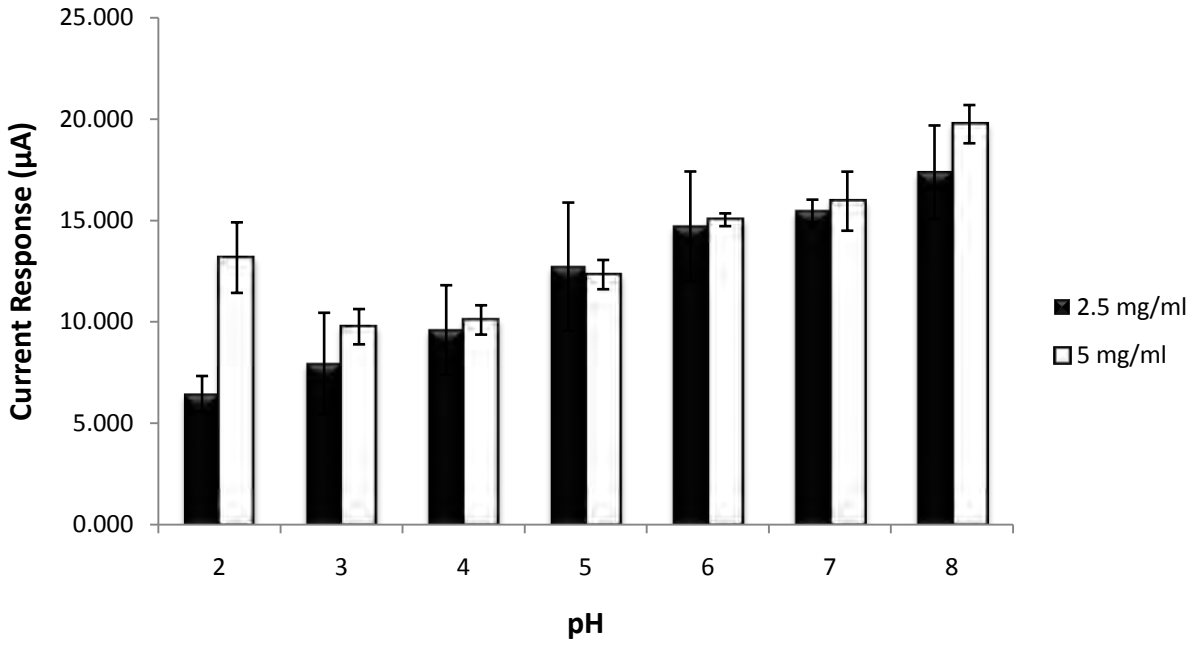

Figure 3-12. Current responses of nano FePc at varying concentrations. 1 mg/ml not shown as the current response was too low. Error bars show standard deviation from mean. n = 3

Similar to studies at bulk FePc-modified GCEs (Figure 3.12), there is no apparent effect of loading on current response for oxygen reduction. There is however an increase in deviation from the mean for the current response obtained at bulk FePc-modified electrodes (Figure 3.10), whereas the reverse is seen for nano FePc-modified GCEs (Figure 3.12).

A scan rate study of a FePc-modified GC towards the reduction of oxygen across the pH range of 2 to 8 was conducted in order to determine whether the reaction at the electrode was diffusion controlled (Figure 3.13). The scan rate first used was 25 mV/s; and then increased after each scan.

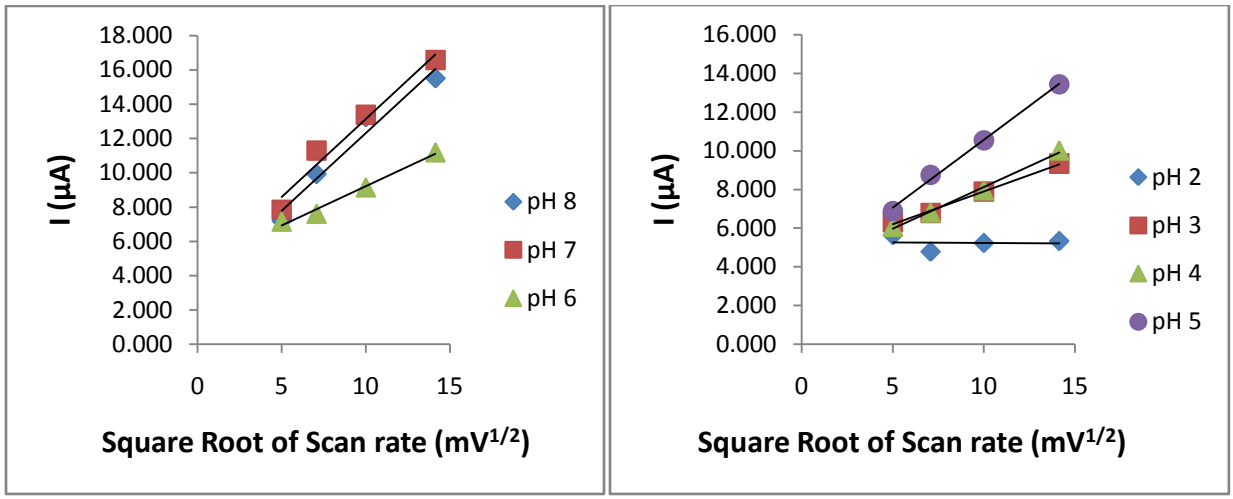

Figure 3-13. Peak current vs. square root of the scan rate for FePc-modified GCE across a pH range. Scan rates used were 25 mV, 50 mV, 100 mV and 200 mV

The oxygen reduction reaction at FePc-modified GCE shows a linear relationship between peak current and the square root of the scan rate between pH 3 and pH 8 indicating that the reaction is diffusion-controlled mass transport (Li *et al.*, 2006), with increasing diffusion coefficient under alkaline conditions.

3.4 Conclusions

Previous studies of oxygen reduction at a GC surface have shown the ORR to be sluggish. In this study, the ORR was investigated from pH 2 to pH 8. A poorly linear trend was seen for the reduction of oxygen across the pH range. This was similar to results obtained by Zhang and Yang (2008). The highest reductive currents were seen at pH 5 and pH 8 while there was a shift in the reductive potential to more negative values with increasing pH value. Tafel slope analysis gave values of n = 1 and n = 1.7 at a pH of 2 and pH 7 respectively. Literature shows that the reduction of oxygen occurs via a 2 e^- reduction at high pH values at a pretreated GC surface whereas at lower pH values, the reduction is sluggish and may often proceed via a one electron reduction (Yang and McCreery, 2000; Sljukic *et al.*, 2005). The results obtained are therefore in line with literature.

Nano FePc and bulk FePc were characterized using Raman spectroscopy and UV/Visible spectroscopy. The UV/Vis spectrum showed a shift in the Q band of nano FePc relative to bulk FePc. This was attributed to the effects of dispersal of nano FePc in a surfactant (CTAB). Li *et al.* (2004) demonstrated the effect of surfactants on the Q band and showed the presence of a surfactant could shift the Q band either to a longer or shorter wavelength. The Raman spectrum of nano FePc was shown for the first time. In comparison with bulk FePc, the Raman spectrum indicated no substantial structural modifications. There were shifts in bands in the region of 1200 cm^{-1} to 1500 cm^{-1}, the region representative of C-N and C-C bonds according to Melendres (1980). These changes suggest the formation and breaking of bonds with respect to nano FePc, which is in line with what was expected as the synthesis of nano FePc relied on the breaking of intermolecular forces present (Mamuru and Ozoemena, 2009). Differences seen in the Raman spectrum and UV/Visible spectroscopy between bulk FePc and nano FePc suggested that nano FePc had been synthesized.

Both nano FePc and bulk FePc, relative to a bare GCE, shifted the reductive potential for the ORR towards a more positive reductive potential which is in line with literature for bulk FePc. Nano FePc and bulk FePc showed similar potential responses across the pH range, in the range of -100 mV to +200 mV. There was a shift towards a more negative reductive potential with an increase in pH value for both forms of FePc relative to a bare GCE which exhibited reduction potentials in the range of -700 mV. The current responses for nano FePc and bulk FePc were much greater than that obtained from a bare GCE, with a maximum in excess of 15 µA at pH 8 (relative to 2.6 µA for a bare GCE). The difference in current response seen for bulk FePc and nano FePc however was not significantly different indicating similarity in the mechanism of oxygen reduction at nano FePc and bulk FePc surfaces. The ability of FePc to shift the reduction potential and enhance current responses indicated the catalytic nature towards oxygen reduction. The work supports previous studies for FePc enhancing the reduction of oxygen (Maldanado and Stevenson, 2004; Baranton et al., 2005; Baker et al, 2008; Hao Yu et al, 2009).

4 Chapter 4: Multiwalled carbon nanotubes as an electrocatalyst support

4.1 Electrochemical response of Multi-walled carbon nanotubes

The electrochemical response of acid functionalized MWCNTs was investigated for the reduction of oxygen upon immobilization onto a GCE. Figure 4.1 shows the CV of a MWCNT-GCE in the presence and absence of oxygen.

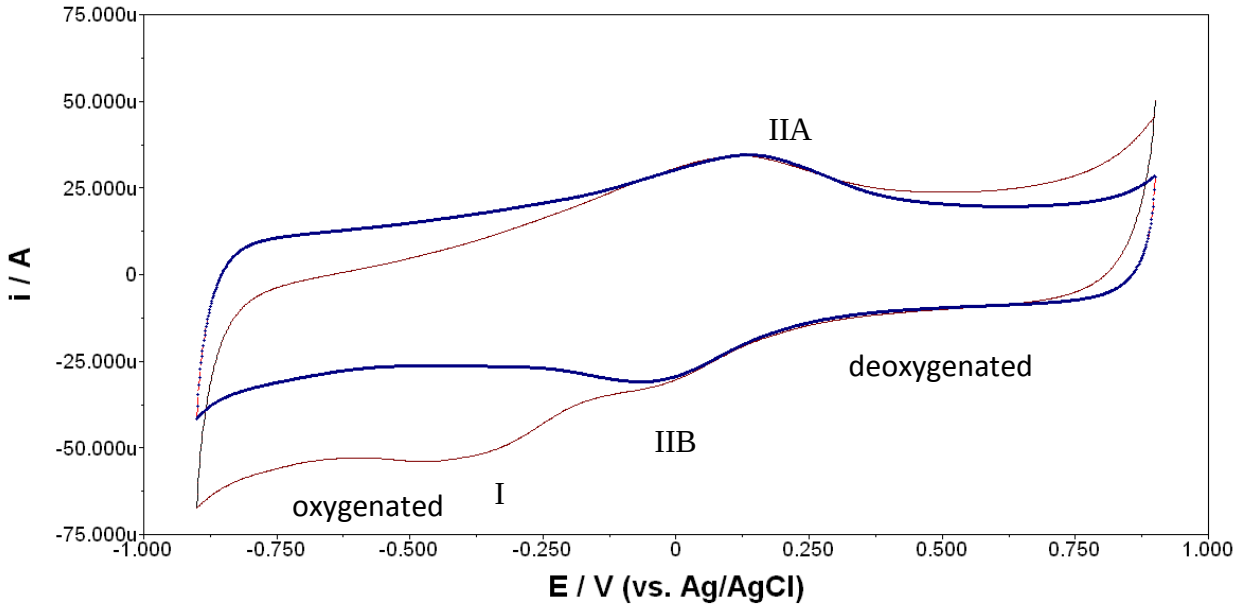

Figure 4-1. CV of the reduction of oxygen at a MWCNT-modified GCE. Peak I = Oxygen reduction; PeakIIA = Oxidation of surface; Peak IIB = Reduction of surface. The electrolyte used was 40 mM, pH 7 Britton-Robinson buffer. Scan rate: 200 mV/s.

A redox couple is observed at -70 mV (Peak IIB) and 130 mV (Peak IIA) at a MWCNT-GCE in the absence of oxygen. These peaks are visible in the CV scan in the presence of oxygen and are therefore not related to the reduction of oxygen. The redox couple can be attributed to the redox process occurring at the immobilized MWCNT layer and it provides evidence of the immobilization of MWCNTs (Li *et al.*, 2006; Kruusenberg *et al.,* 2009). Peak I (at -400 mV) shown in Figure 4.1 is only observed in oxygenated buffer. Its proximity to the potential at which

oxygen reduction occurs at a bare GCE, coupled to the fact that the peak is only visible in the presence of oxygen, suggests that this peak is that of oxygen reduction at a MWCNT-GCE.

There are two possible explanations for the redox couple: it could be impurities still present or it could be the due to the functional groups present on the MWCNTs as a result of functionalization. Li *et al.* (2006) showed the presence of a redox couple at similar potentials when immobilizing MWCNTs onto a GCE. After acid functionalization of MWCNTs, the nanotubes are cut up into smaller fragments and oxygen-containing groups (carboxyl, hydroxyl, and quinine) are added to defect sites along the length of the nanotubes as well as at the ends of the nanotubes (Banks and Compton, 2005; Li and Zhang, 2006; Wildgoose *et al*., 2006). The edge plane defects reside at the open ends of the nanotubes, and around the tube walls where one of the concentric tubes ends (Banks and Compton, 2005; Xiao *et al.,* 2009). Kruusenberg *et al.* (2009) further proposed that the surface-confined quinone-like functionalities at the edge plane sites are the main contributors, of the functional groups present, towards electroreduction of oxygen.

The potential at which the reduction occurred was compared to that of a bare GCE as a measure of the catalytic nature of MWCNTs towards oxygen reduction (Figure 4.2). Carbon nanotubes themselves are electrochemically inert and therefore not catalytic however through functionalization, catalytic moieties are added to the surface of the nanotubes as mentioned earlier (Vaisman *et al.*, 2006). The reduction of oxygen occurs at more positive potentials than that seen for a bare GCE (Figure 4.2).

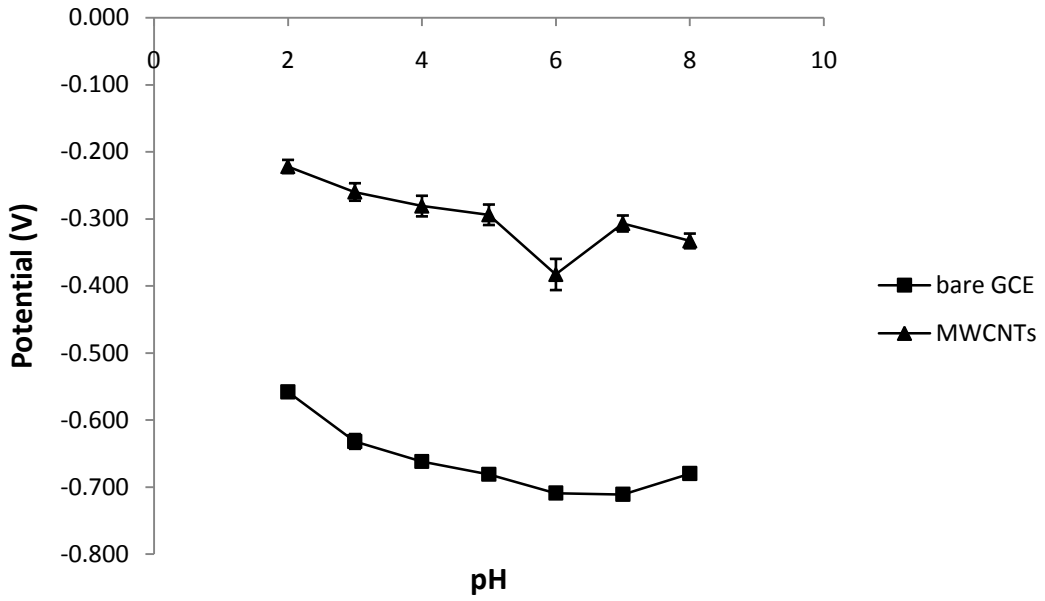

Figure 4-2. Potential response of MWCNT-GCE towards ORR across a pH range. Error bars represent standard deviation (n = 3)

The shift in potential towards more positive potentials seen for the reduction of oxygen at a MWCNT-modified electrode (Fig 4.2) suggests that the MWCNTs are catalytic towards the oxygen reduction reaction. Initially a similar trend, as seen for a bare GCE, can be seen for MWCNTs in that the potential becomes more negative with increasing alkalinity (Fig 4.2). The slope of potential versus pH for hybrid surfaces between pH 3 and 5 is 17 mV/pH unit while between pH 5 and 6 it increases to 89 mV/pH unit (indicative of a 3 electron/ 1 proton mechanism). This is in contradiction of data obtained by Kruusenberg *et al.* (2009) who showed that the electrocatalytic activity of MWCNTs, based on the reduction potential, is highest in alkaline pH due to changes in the nature of the active sites. The study done by Kruusenberg *et al*., (2009) was conducted in different buffers depending on the pH required whereas this study was conducted using only BR buffer to ensure that there was no change in the nature of the electrolyte (buffer). Kruusenberg *et al.* (2009) and Tryk *et al.* (2005) showed that there was a pH-dependence for the reduction of oxygen at CNT-modified electrodes. This was explained by the presence of quinone-type functionalities present at the electrode surface.

The effect of MWCNTs on the current response obtained for the reduction of oxygen was investigated (Figure 4.3). A MWCNT-modified GCE enhanced the current response of the reduction of oxygen relative to a bare GCE (Figure 4.3). It is evident that a MWCNT-GCE generates higher current response across a pH range of 2 to 8 relative to a bare GCE. The trend is similar to that of a bare GCE as the highest current response is seen at pH 8 (Figure 4.3). This is only true for a loading rate of 2.5 mg/ml. The effect of loading rate, using loading rates of 1 mg/ml and 2.5 mg/ml, was investigated across the pH range of pH 2 to pH 8. It was not possible to obtain reproducible results with higher loading rates as the MWCNTs tended to aggregate on the electrode surface (Streeter *et al.*, 2008). This also occurred at lower loading rates however it was less pronounced. The current response shown was recorded after base line correction.

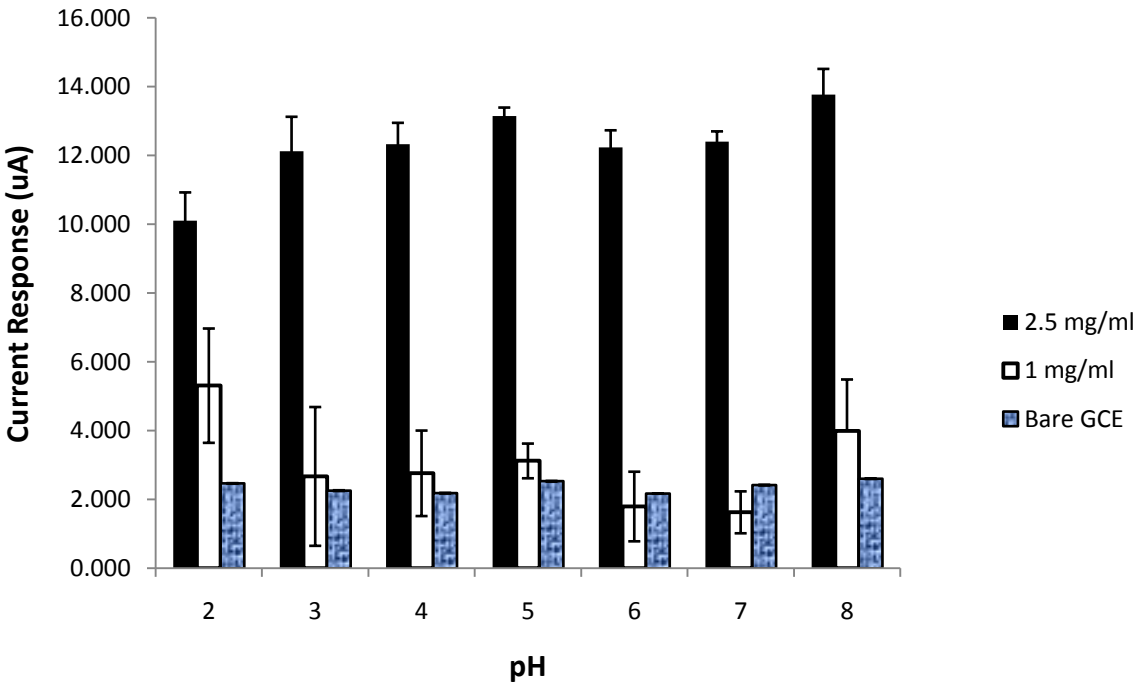

Figure 4-3. Current Response of MWCNT-GCE at different loading rates towards ORR. Error bars represent standard deviation (n = 3). Scan rate = 200 $mV.s^{-1}$

The increase in current response (Fig 4.3) seen for the reduction of oxygen at a MWCNT-modified GCE can be attributed to the increase in the surface area of the electrode and increase

in conductivity of the layer. For example, the apparent surface area of the bare GCE and MWCNT-modified GCE (at a loading rate of 1 mg/ml at pH 2) was calculated to be 0.10 cm^2 and 0.12 cm^2 respectively (Appendix 2). It could be assumed that at a higher loading rate of MWCNTs, the increase in the effective surface area of the electrode would be greater. In support of this, a higher current response is observed at a higher loading rate of 2.5 mg/ml compared to a loading rate of 1 mg/ml (Fig 4.3). At a loading rate of 2.5 mg/ml, the current response was greatly enhanced relative to a bare GCE with the highest current response at pH 5 and 8 whereas at a loading rate of 1 mg/ml, the current response is similar to that of a bare GCE (Fig 4.3).

Kruusenberg *et al.* (2009) suggests that the mechanism of oxygen reduction at a MWCNT-modified GCE follows a similar trend to that of a bare GCE. The pretreatment of a GCE leads to the formation of oxygen-containing moieties such as hydroxyl and carboxyl groups at the electrode surface. This is similar to what occurs with MWCNTs after acid pretreatment. Oxide groups in particular play a role in electron transfer between the electroactive species (oxygen) and the electrode surface at a bare GCE according to Sljukic *et al.* (2005). Assuming similar functional groups are present on the surface of MWCNTs, these functional groups can act as mediators in electron transfer between the electrode surface and electroactive species in solution. In terms of current response, the electrocatalytic nature of MWCNTs is higher at more basic pH however the reduction potential for oxygen at a MWCNT-modified surface is more positive (and therefore more catalytic) at acidic pH.

4.2 Electrochemical response of hybrid electrodes

As has been seen shown, FePc is catalytic towards the reduction of oxygen by shifting the reduction potential to a more positive potential (Chapter 3). FePc also enhanced the current response of oxygen reduction, while MWCNTs have been shown to enhance the current response of oxygen reduction at a GCE. There are several examples in literature of where electrocatalysts have been coupled to carbon nanotubes (single- and multiwalled) through

covalent and non-covalent means as the CNTs serve as an electrocatalyst support (Wu and Xu, 2007; Agboola *et al.*, 2008; Pillay and Ozoemena, 2009; Okunola *et al.*, 2008).

It was proposed that the coupling of FePc to MWCNTs could lead to further enhancements in the catalytic ability of the modified electrode towards oxygen reduction due to the fact that MWCNTs are conductive and they enhance the surface area of the electrode. Okunola *et al*. (2008) coupled metalloporphyrins to MWCNTs through electrochemical polymerization and observed enhanced activity towards oxygen reduction. MPcs would in theory interact with the MWCNTs though π-π interactions (Tau and Nyokong, 2007). The electrochemical response of a GCE modified with FePc-MWCNT was investigated for its ability to reduce oxygen (Fig 4.4).

Figure 4.4A shows the CV of a FePc:MWCNT modified GCE in the presence and absence of oxygen while Figure 4.4B compares the CV of FePc:MWCNT modified GCE to that of a bare GCE for the reduction of oxygen. The CV of the hybrid electrode in deoxygenated buffer exhibits similar characteristics to both FePc- and MWCNT modified electrodes. Peak IIA, IIB, and III observed in deoxygenated buffer are assigned to the redox process of the Fe centre. A MWCNT-modified electrode exhibited a redox couple ($E_{1/2}$ = 200 mV in acidic pH) whereas the hybrid electrode does not exhibit this in the reductive or oxidative waves at those potentials (Figure 4.4A). The peaks seen in deoxygenated buffer are less pronounced in oxygenated buffer (Figure 4.4A). Peak I, seen only in oxygenated buffer, can be attributed to the reduction of oxygen. The peak appears at -50 mV which is in the potential range of oxygen reduction at a FePc-GCE.

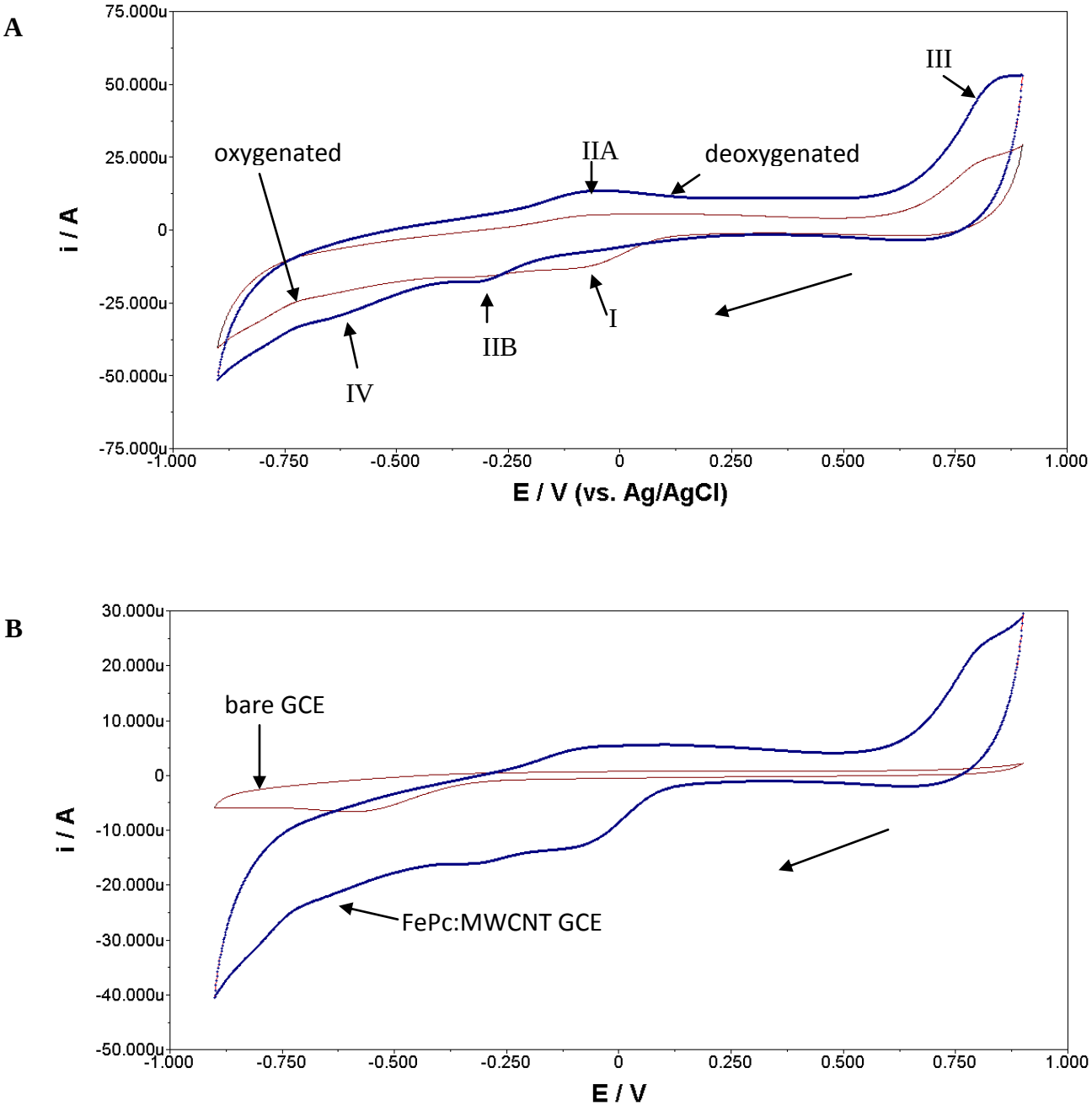

Figure 4-4. CVs of FePc:MWCNT hybrid electrodes in A) deoxygenated buffer and oxygenated buffer. Peak I = Oxygen reduction; Peak IIA = Redox of Fe centre; Peak IIB = Redox of Fe centre; Peak III = Oxidation of FePc ring; Peak IV = Redox of FePc. B) comparison of oxygen reduction at a FePc:MWCNT-GCE relative to a bare GCE. Electrolyte used was 40 mM BR buffer, pH 7. Scan rate: 200 $mV.s^{-1}$

The absence of the redox couple for MWCNTs could be due to the deposition of FePc onto the MWCNTs thereby masking the peaks. Vaisman *et al.*, (2006) and Tau and Nyokong (2007) postulated that MPcs immobilized onto MWCNTs through electrostatic π-π interactions. Figure 4.4B clearly shows the enhancement of the reduction of oxygen at a hybrid electrode relative to a bare GCE. The peak for oxygen reduction is also clearly shifted to a more positive reductive potential relative to a bare GCE (Figure 4.4B) A FePc:MWCNT hybrid electrode showed a significant shift in the potential, greater than that at MWCNT-modified GCE and comparable to that of FePc alone, at which oxygen is reduced (Fig 4.5).

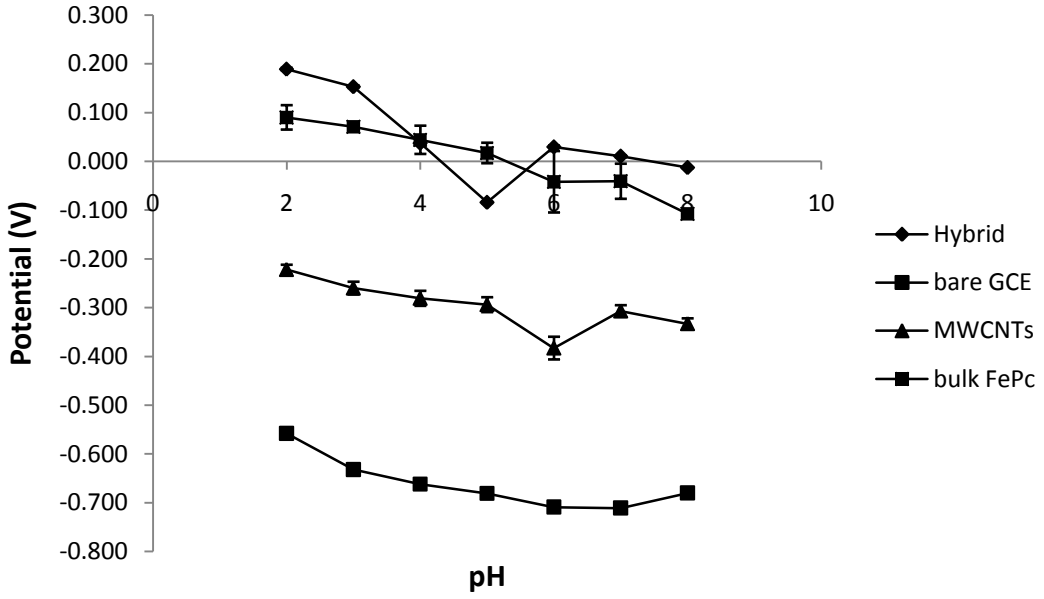

Figure 4-5. Potential response of modified surfaces relative a bare GCE. Error bars represent standard deviation (n = 3)

There is a general trend seen for the reduction of oxygen at the modified surfaces relative to a bare GCE at different pH values. The potential shifts towards a more negative potential with an increase in the alkalinity. The slope of potential vs. pH is similar for bare and FePc modified electrodes shown in Figure 4.5 (25 mV/pH) indicating similar mechanisms for ORR (2 e^- and 1 H^+). The slope for the hybrid surface and MWCNT surface however shows differences from bare and FePc-modified surfaces. From pH 3 to 5, the slope for the hybrid surface is 118 mV/pH

while for MWCNT-modified surface from pH 5 to pH 6 is 89 mV/pH unit. This indicates that at these pH values, the mechanism for ORR could be different.

Figure 4.6 examines the enhancement in current response for the reduction of oxygen offered by hybrid electrodes relative to FePc and MWCNTs alone. The hybrid surface showed much higher current responses relative to all other modified surfaces.

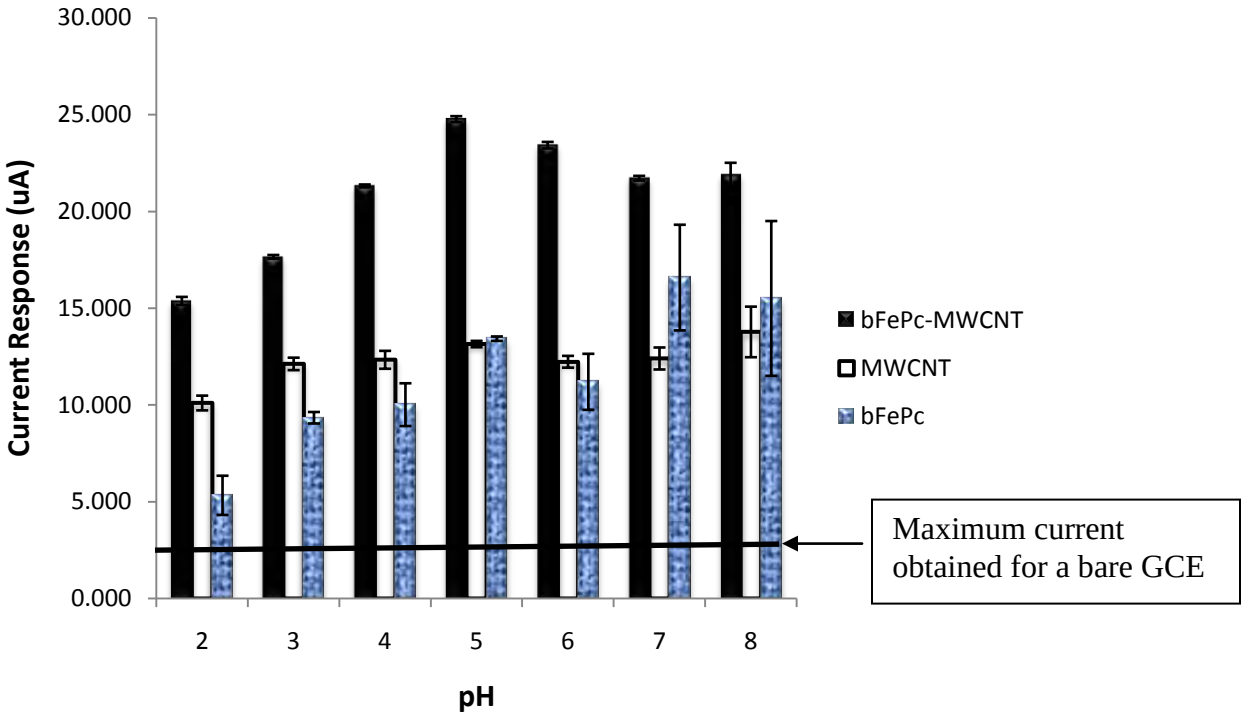

Figure 4-6. Current response of hybrid electrodes relative to bulk FePc (bFePc) and MWCNT (2.5 mg/ml) modified surfaces. Error bars represent standard deviation (n = 3). The black line represents the maximum current response obtained for a bare GCE.

Okunola *et al.* (2008) found similar results when combining several types of MPcs with MWCNTs for reduction of oxygen. FePc in combination with MWCNTs greatly enhances the current response relative to utilizing either FePc or MWCNTs alone across the entire pH range. Whereas the potential shift for the reduction of oxygen at a hybrid electrode could be attributed primarily to the catalytic action of FePc, the enhancement of the current would seem to be more a function of the role of MWCNTs. The MWCNTs greatly increases the electrode

surface area available for electrocatalyst loading leading to an enhancement of the catalytic nature of FePc. The maximum reduction current obtained from FePc was enhanced through the use of MWCNTs as a catalyst support. It is unclear of the role each component (FePc and MWCNTs) plays in the catalysis of oxygen reduction when combined. It can be assumed that the reduction of oxygen occurs primarily at FePc however MWCNTs did show catalytic behavior towards the reduction of oxygen thereby further enhancing the catalytic nature of the hybrid surface. Of particular interest in these studies is that a clear trend in the change in current is observed compared to other surfaces examined with a peak at pH 5. There is also a decrease in variability with a lower error relative to FePc-modified surfaces and MWCNT-modified surfaces. This could be attributed to decreased aggregation of FePc and MWCNTs in a hybrid structure.

4.3 Impedance Spectroscopy of modified surfaces

4.3.1 FePc-modified electrodes

CV of bare GCE and FePc-GCE was performed using the redox probe $[Fe(CN)_6]^{3-}/[Fe(CN)_6]^{4-}$] in order to determine the $E_{1/2}$ for the redox reaction at a bare GCE and FePc-GCE,. It was at this potential that impedance was conducted. The $E_{1/2}$ for the bare GCE was 0.125 V while for FePc-GCE it was 0.172 V (Figure 4.7).

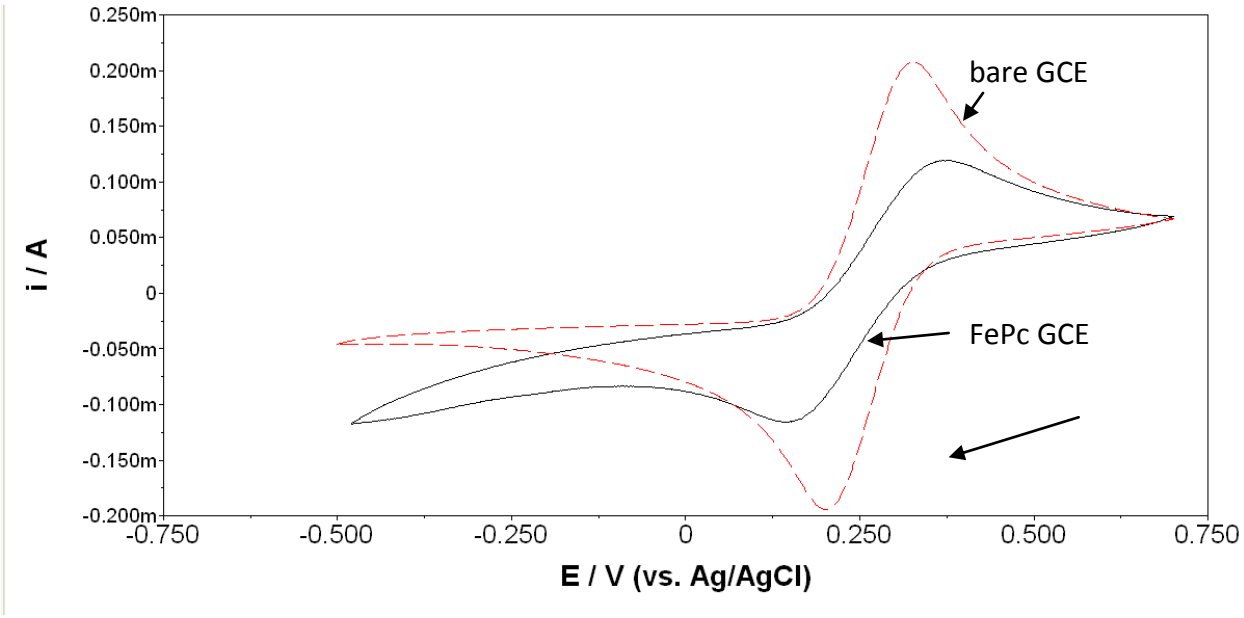

Figure 4-7. Cyclic voltammogram of bare GCE (dotted line) and FePc-GCE (solid line) in equimolar solution of 10 mM Ferricyanide and 10 mM Ferrocyanide redox probe. Scan rate = 100 $mV.s^{-1}$

The possible processes that could be involved at the electrode surface of the FePc-GCE according to Hao Yu *et al.* (2009) include:

(1) Diffusion of O_2 through the electrolyte to the reaction site.

(2) Adsorption or heterogeneous surface reaction of the oxygen, together with oxygen diffusion.

(3) Charge transfer.

(4) Diffusion of reduction products into the bulk electrolyte.

The Kramers–Kronig test was performed to establish if the impedance spectrum measured could be fitted to equivalent circuits. All the fitted values shown in Table 4.1 were obtained after several iterations. The circuit used for the bare GCE and FePc-GCE was as follows:

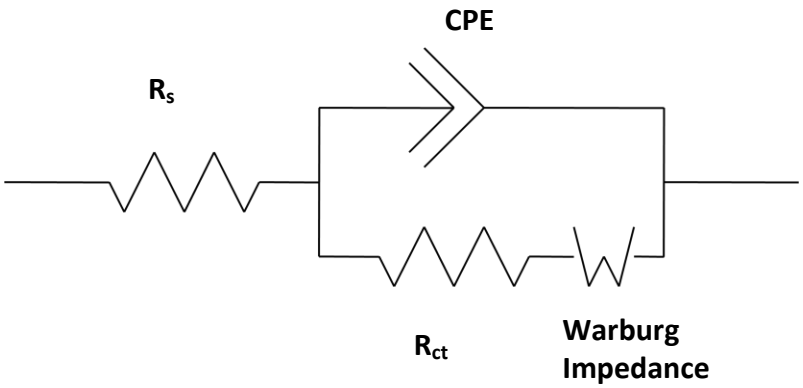

The circuit chosen to fit the data for a bare GCE as well as FePc-modified electrodes contained R_s (solution resistance), CPE (constant phase element), R_{ct} (charge transfer resistance) and Z_W (Warburg resistance). R_s accounts for the resistance offered by the working solution. The Warburg impedance is associated with the domain of mass transport control arising from the diffusion of ions to and from the electrode solution interface (Mamuru and Ozoemena, 2009). The CPE is associated with double layer charge and the adsorption of ions to the electrode surface due to the non-homogeneous surface of the electrode. It is also associated with the non-homogeneity arising from the surface roughness of the electrode as well as the non-homogeneous semi-infinite diffusion of the redox probe to the electrode surface. The R_{ct}, which is related to reaction kinetics, accounts for the resistance of electron transfer at the electrode/solution interface. The impedance of a bare GCE and FePc-GCE was represented in the form of Nyquist and Bode plots (Figure 4.8).

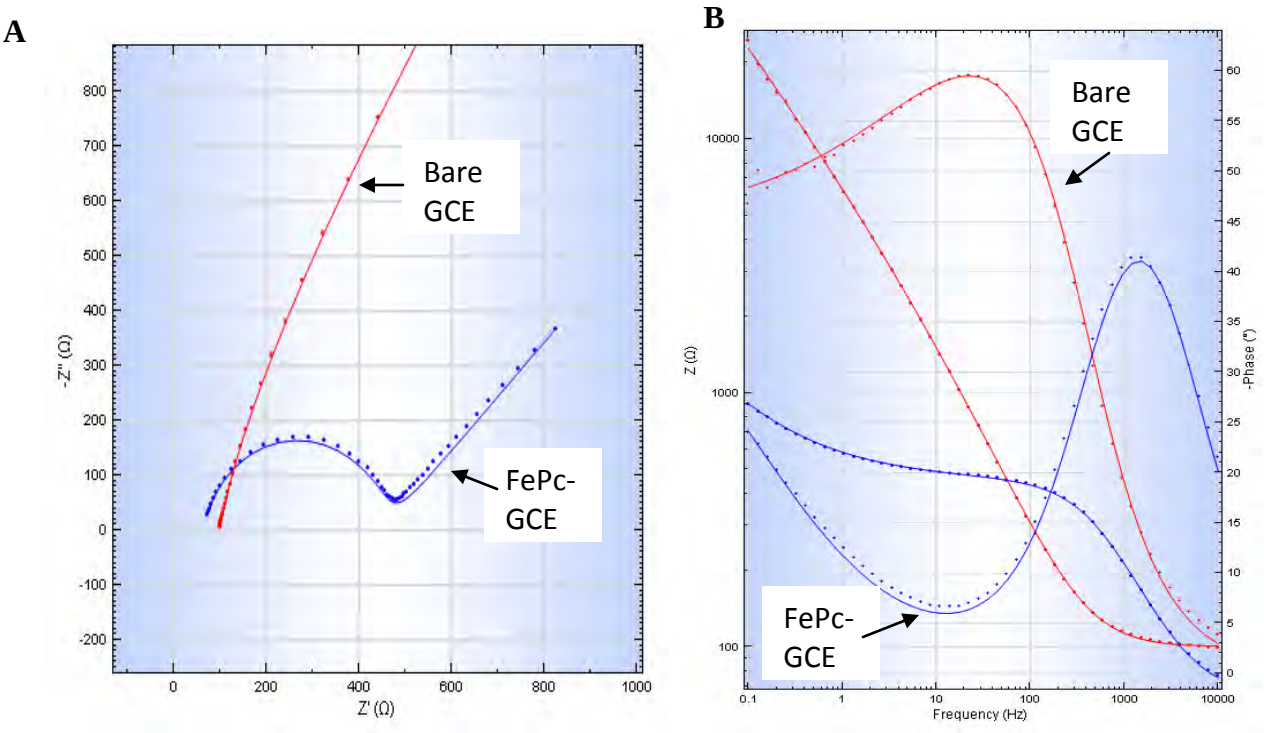

Figure 4-8. Electrochemical Impedance spectroscopy of bare GCE and FePc. A) Nyquist plot of bare GCE and FePc-GCE. B) Bode plot of bare GCE and FePc-GCE. Solid lines show the fitted data.

The data obtained for the bare GCE and FePc-GCE were fitted using the chosen circuit (Table 4.1)

Table 4-1. Fitted data obtained for impedance spectroscopy of bare GCE and FePc-GCE. The values represent the mean. mean ± standard deviation. n = 3.

	Bare GCE	FePc-GCE
R_s	89.467 Ω (±0.804)	63.867 Ω (±1.239)
R_{ct}	5.915 Ω (± 3.3)	275.3 Ω (±0.571)
W	51.2 µMho (±0.863)	2.327 mMho (±1.196)
Q	6.720 µMho (±3.435)	2.563 µMho (±4.631)
n	0.909 (±0.0004)	0.884 (±0.005)

An *n* value of zero corresponds to a pure resistor; an *n* value of 1 corresponds to a pure capacitor. (Mamuru and Ozoemena, 2009). The Nyquist plot of bare GCE and FePc-GCE (Figure

4.8 A) can be divided into two frequency regions: the kinetically controlled (high frequency) region where the semi-circle is observed and the diffusion controlled (low frequency) region where the Warburg line is observed. The semi-circle in the region of high frequency is ascribed to the charge (electron and proton) exchange at the carbon/electrolyte interface. The straight line at low frequencies can be expressed by adopting a Warburg diffusion element for the semi-infinite diffusion of the analyte at the carbon/electrolyte interface (Wu and Xu, 2007). If the diameter of the high frequency semicircle is significantly enlarged by the surface deposition of an electrocatalyst such as FePc, this indicates an increased resistance of the flow of charge through the FeP-GCE (Li *et al.,* 2008). The diameter of the semi-circle observed in Figure 4.8A corresponds to the charge transfer resistance (R_{ct}) of the FePc-GCE. The larger the semi-circle, the slower the charge or electron transfer will be. FePc has a bulky ring system which to some extent leads to slow electron transfer resulting in a larger R_{ct}. The MPc ring system therefore introduces a slight barrier to the flow of charge relative to a bare GCE. This is evident from the fitted values (Table 4.1).

A semi-circle in the high frequency region and a straight line at a slope of nearly 45° in the low frequency region as seen for FePc-GCE (Figure 4.8A) are typical of porous film coated on metals in an asymmetric metal/film/electrolyte configuration. A bare GCE (Figure 4.8A) exhibits a near straight line at high frequencies. It can be deduced that there is very little charge transfer resistance at the electrode surface. It exhibits a semi-infinite diffusive character. The fitted values (Table 4.1) show that the bare GCE is indeed more capacitive than FePc-GCE as it has an *n* value is closer to 1. This is also reflected by the larger increase in phase shift observed at lower frequencies of the Bode plot. The increase in Rct of the FePc-GCE relative to a bare GCE also serves to confirm electrode modification.

For Bode-phase angle plots, if the phase angle is less than 90° then the modified electrode is permeable to ions from solution (Matemadombo and Nyokong, 2007; Mamuru and Ozoemena, 2009).

Bode plots for the bare GCE and FePc-GCE (Figure 4.8B) clearly shows that the phase angle throughout the frequency range scanned is less than 90°. FePc exhibits a lower phase shift relative to a bare GCE (Figure 4.8 due to a lower double layer capacitance due to less charge storage at the electrode surface from either easier charge transfer or a reduced charge difference between the electrode surface and electron dense FePc layer as compared to the high charge difference between the electrode surface and the ions in solution.B). A reduction in overall impedance between the bare GCE and FePc GCE does show an increase in the ability of the FePc layer to transfer charge/electrons. It can be concluded that the FePc layer is either permeable to solution ions or catalytic (i.e. improve electron or charge transfer). Permeability of the immobilized layer is ideal as it would allow for the diffusion of ions from the active site of FePc to the electrode surface. With the addition of an increase in surface area relative to the BGCE, the FePc GCE surface allows for an increase in oxygen reduction.

4.3.2 MWCNT-modified electrodes

Cyclic voltammetry of a MWCNT-modified GCE using a ferricyanide/ferrocyanide redox probe was conducted (Figure 4.9). The $E_{1/2}$ for the bare GCE was 0.125 V while for MWCNT-GCE it was 0.133 V (Figure 4.9).

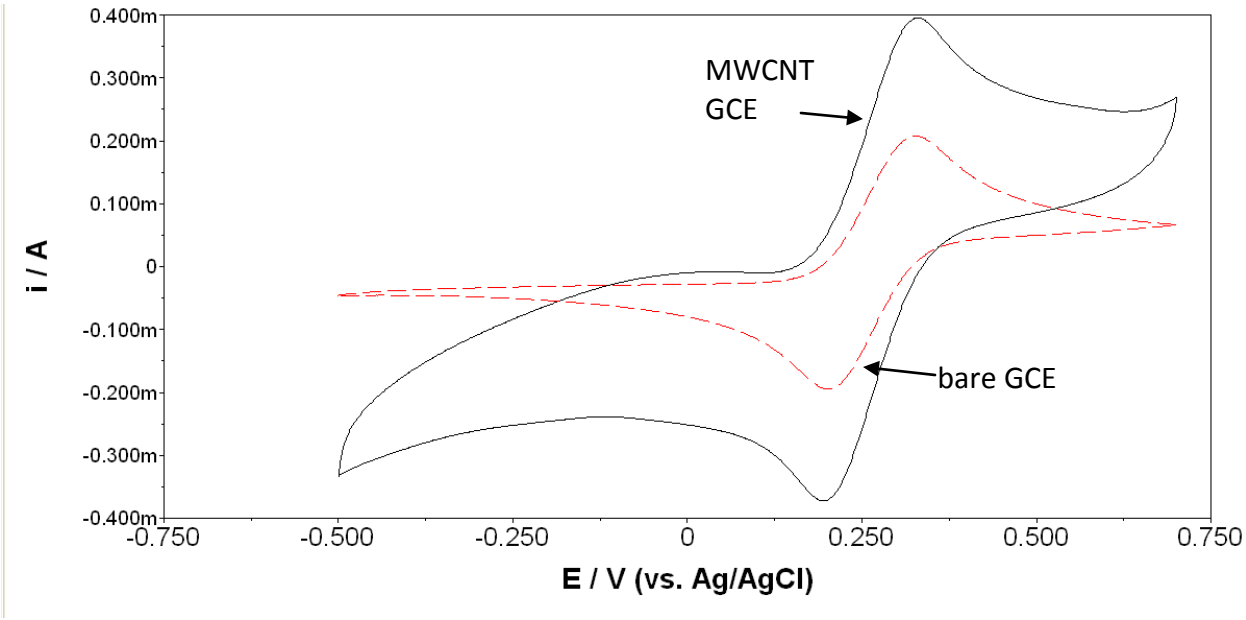

Figure 4-9. Cyclic voltammogram of bare GCE (red dotted line) and MWCNT-GCE (solid black line) in equimolar solution of 10 mM Ferricyanide and 10 mM Ferrocyanide redox probe. Scan rate = 100 $mV.s^{-1}$

The peak separation observed was similar for a bare GCE and a MWCNT-modified GCE, however the current response seen for MWCNT-GCE was higher. This suggests there is a greater surface area for the redox reaction to occur.

The Kramers–Kronig test was performed to establish if the impedance spectrum measured could be fitted to equivalent circuits. All the fitted values shown in Table 4.2 were obtained after several iterations.

The circuit used for the bare GCE and MWCNT-GCE was as follows:

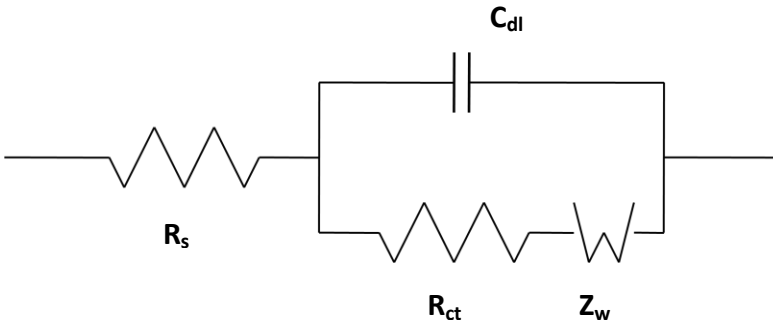

The circuit chosen to fit the data a MWCNT-modified electrode contained R_s (solution resistance), C (double layer capacitance), R_{ct} (charge transfer resistance) and W (Warburg impedance). The double layer capacitance takes into account the increased electroactive surface area afforded by MWCNTs which then leads to an increase in the number of electrolyte ions attracted to the electrode surface forming a capacitive layer (Emmenegger *et al.*, 2003).

The impedance of MWCNTs was represented in the form of a Nyquist plot and a Bode plot (Figure 4.10). A bare GCE exhibits a near straight line at high frequencies (Figure 4.10A). It can be deduced that there is very little charge transfer resistance at the electrode surface. It exhibits a semi-infinite diffusive character. A MWCNT-GCE also exhibits a near straight line at high frequencies and it can be assumed that it also displays very little charge transfer resistance at the electrode surface (Figure 4.10A).

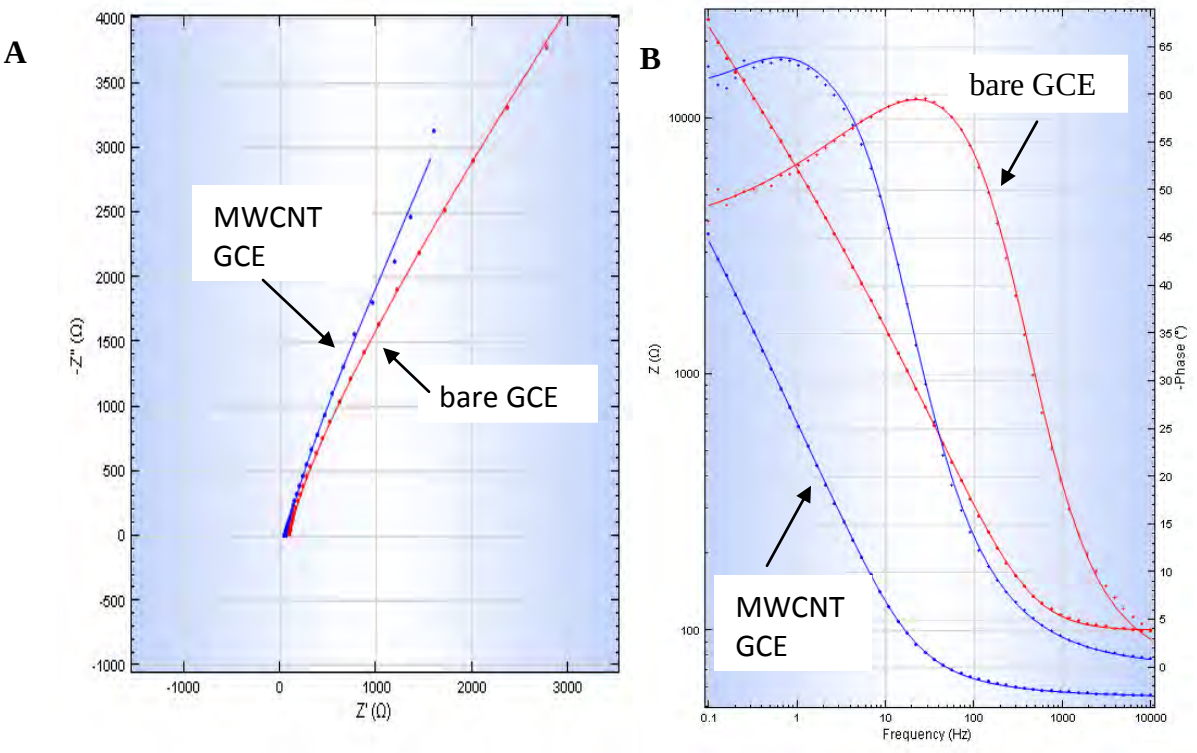

Figure 4-10. Electrochemical Impedance spectroscopy of bare GCE and MWCNTs. A) Nyquist plot of bare GCE and MWCNT-GCE. B) Bode plot of bare GCE and MWCNT-GCE. Solid line shows the fitted data

A MWCNT-modified GCE exhibits a higher Warburg impedance value and a much lower charge transfer resistance (R_{ct}) than a bare GCE (Table 4.2). The data obtained for MWCNTs indicates that there is a much faster diffusion rate of solvated ions at the electrode/electrolyte interface for a MWCNT-modified GCE than for a bare GCE. This would be expected for a GCE modified with a film of MWCNTs as they are porous and highly conductive (Wildgoose *et al.*, 2006).

Table 4-2. Fitted data obtained for impedance spectroscopy of bare GCE and MWCNT-GCE. The values presented are the mean values. Mean ± standard deviation. n = 3.

Parameter	Bare GCE	MWCNT
R_s	89.467 Ω (±0.804)	55.726 Ω (±0.59 Ω)
R_{ct}	5.915 Ω (± 3.3)	3.76 µΩ (±1.30E-06 µΩ)
W	51.2 µMho (±0.863)	328.9 µMho (±122.71 µMho)
Q/C	6.720 µMho (±3.435)	192.0 µF (±1.89E-06)
n	0.909 (±0.0004)	1

Bode plots for the bare GCE and MWCNT-GCE (Figure 4.10B) clearly shows that the phase angle throughout the frequency range scanned is less than 90° meaning there is a current leakage through the MWCNT layer. MWCNTs exhibit a marginally greater phase shift relative to a bare GCE (Figure 4.10B). The capacitance (the ability of a body to hold charge) measured for a MWCNT-modified GCE was much greater than that of a bare GCE indicating that the MWCNT layer was more capacitive than a bare GCE.

4.3.3 Impedance spectroscopy of Hybrid electrodes

The $E_{1/2}$ for the bare GCE was 0.125 V while for a FePc:MWCNT-GCE it was 0.180 V (Figure 4.11). As seen for a FePc-modified GCE, the hybrid electrode is not catalytic towards the redox probe as the peak separation is greater than that of a bare GCE.

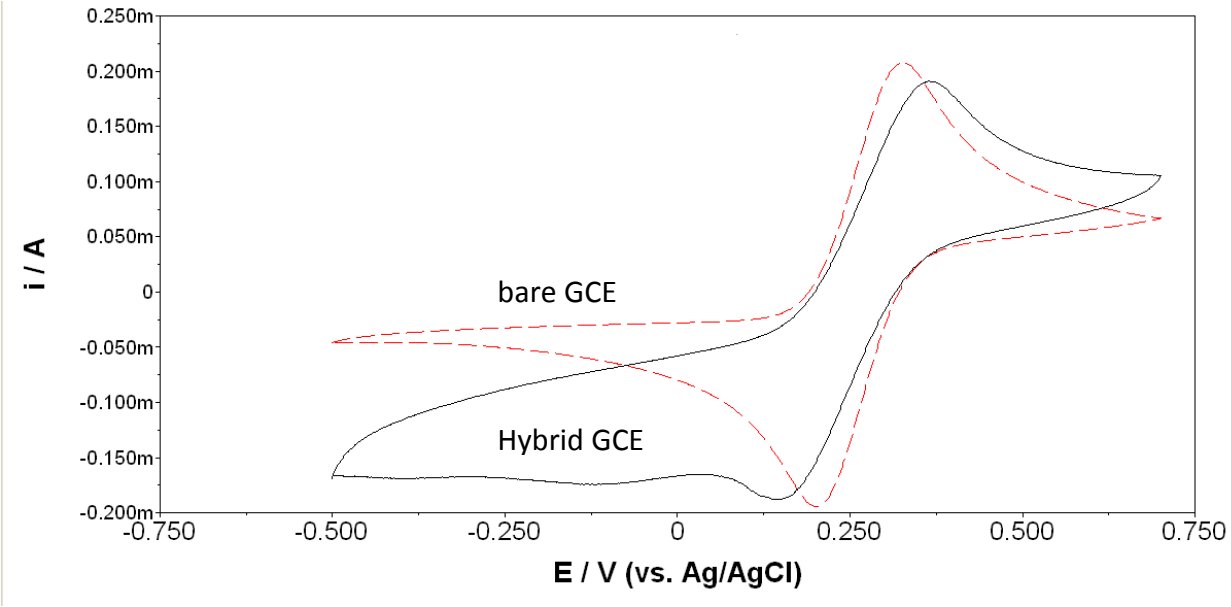

Figure 4-11. Cyclic voltammogram of bare GCE (dotted line) and FePc:MWCNT-GCE (black line) in equimolar solution of 10 mM Ferricyanide and 10 mM Ferrocyanide redox probe. Scan rate = 100 $mV.s^{-1}$

The peak separation for the hybrid electrode was similar to that of a FePc-GCE (0.172 V), however the current response seen for the hybrid electrode was higher than at a FePc-GCE. This suggests there is a greater surface area exposed due to the incorporation of the MWCNTs. The Kramers–Kronig test was first performed to establish if the impedance spectrum measured could be fitted to equivalent circuits. All the fitted values shown in Table 4.3 were obtained after several iterations.

The circuit chosen to fit the data for a bare GCE as well as MWCNT-modified electrodes contained R_s (solution resistance), CPE (constant phase element), R_{ct} (charge transfer

resistance) and Z_W (Warburg resistance). Each immobilized layer (FePc and MWCNTs) is accounted for with its own R_{ct} and capacitance.

The circuit used to fit impedance data of a hybrid GCE is as follows:

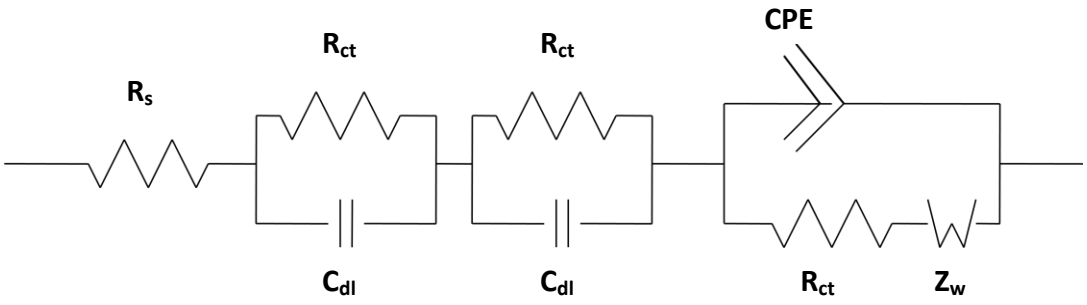

The Nyquist plot obtained for the hybrid electrode shows two small semi-circles in the high frequency (kinetically controlled) region while in the low frequency region (diffusion controlled); a straight line at approximately 45° can be seen (Figure 4.12A). The straight line in the low frequency region is explained by adopting a Warburg diffusion element. The semi-circles seen at high frequencies are a function of the charge transfer resistance of each layer immobilized at the electrode surface.

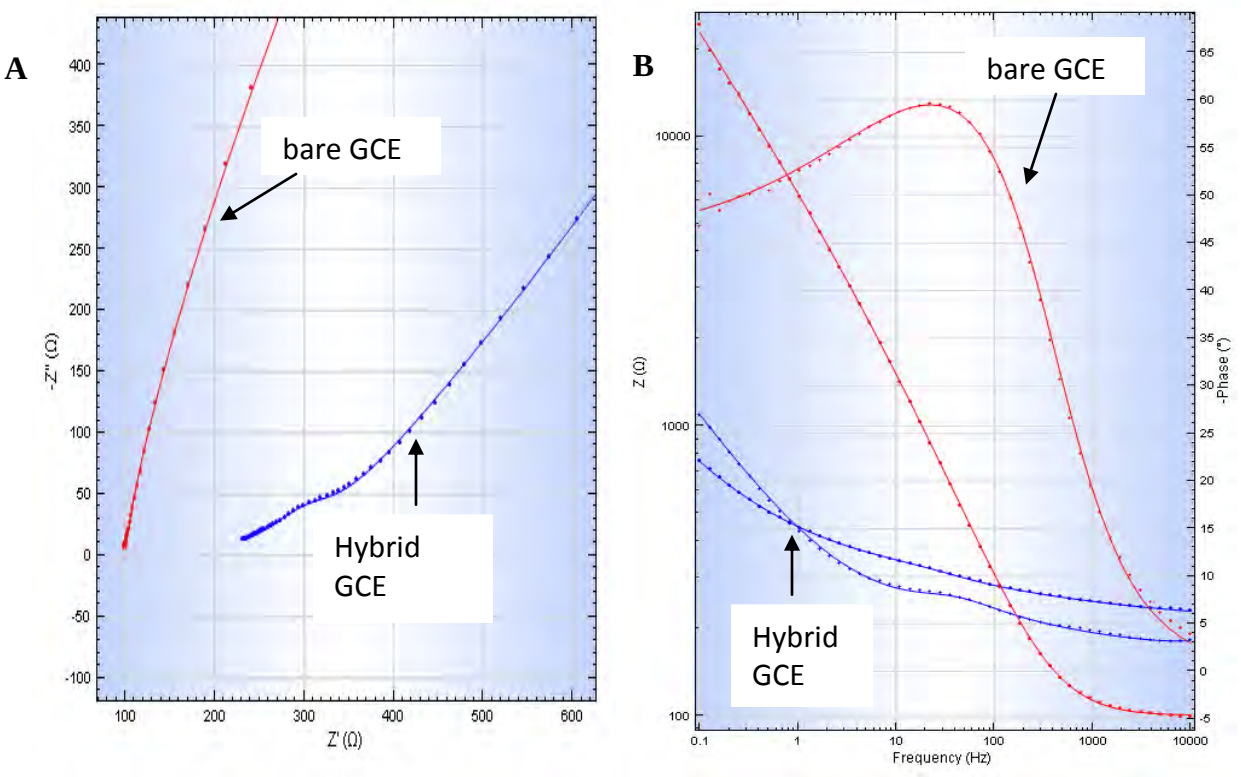

Figure 4-12. Electrochemical Impedance spectroscopy of bare GCE and FePc:MWCNTs. A) Nyquist plot of bare GCE and FePc:MWCNT-GCE. B) Bode plot of bare GCE and MWCNT-GCE. Solid line shows the fitted data.

The circuit that gave the best fit suggests two distinct layers represented by FePc (RC1) and MWCNTs (RC2) which were both immobilized onto the electrode surface. Each layer has its own R_{ct} and capacitance. There is no literature explaining the electrochemical impedance response of FePc coupled to MWCNTs. The processes involved at the electrode/electrolyte interface are therefore not clear. It could be assumed that there is adsorption of the electroactive species to the FePc layer; this is preceeded by the diffusion of ions through the conductive layer of MWCNTs to the electrode surface.

The FePc layer has a relatively high charge transfer resistance (Table 4.3) whereas the MWCNT layer has a relatively low charge transfer resistance therefore it can be assumed that the flow of charge is much slower through the FePc layer than it is through the MWCNT layer. The capacitance of the MWCNT layer is also much greater than the FePc layer indicating its ability to hold charge. The Nyquist plot for the hybrid electrode suggests that there are two distinct time

constants at high frequency (Fig 4.12A). This could be due to FePc and MWCNTs forming two distinct barriers to the diffusion of ions. Impedance data obtained for FePc (Table 4.1) showed that it exhibited a high charge transfer resistance relative to a bare GCE whereas data obtained for MWCNTs (Table 4.2) showed that it had a very low charge transfer resistance relative to a bare GCE. It could then be assumed that the charge transfer resistance of the FePc layer could be lowered through the association of FePc and MWCNTs. The fitted data tends to suggest that the immobilized layer of FePc and MWCNTs is indeed more conductive to the diffusion of ions relative to an immobilized layer of only FePc.

Table 4-3. Fitted data obtained for impedance spectroscopy of bare GCE and FePc:MWCNT-GCE

Parameter	Bare GCE	Parameter	Hybrid
R_s	89.467 Ω (±0.804)	**R_s**	207 Ω (±169)
R_{ct}	5.915 Ω (± 3.3)	**R_{ct} (FePc)**	75.9 Ω (±53.9 mΩ)
W	51.2 µMho (±0.863)	**C (FePc)**	9.12E-06 F (±1.58E-06 F)
Q	6.720 µMho (±3.435)	**R_{ct} (MWCNTs)**	23.3 Ω (±7.8 Ω)
N	0.909 (±0.0004)	**C (MWCNTs)**	126 µF (±0.00011 µF)
T	N/A	**Q**	540 µMho (±0.0005 µMho)
-	-	**R_{ct}**	48.92 Ω (±163 mΩ)
-	-	**W**	0.02 Mho (±0.0006 Mho)

Bode plots for the bare GCE and FePc:MWCNT-GCE (Figure 4.14B) clearly shows that the phase angle throughout the frequency range scanned is less than 90° meaning that there is a current leakage through the FePc:MWCNT layer. The phase shift of the FePc:MWCNT-GCE is much less than that of a bare GCE, FePc-GCE and a MWCNT-GCE. The phase shift for a FePc:MWCNT-modified GCE was much less than 90° which would indicate that the FePc:MWCNT layer is highly permeable to ions from the bulk solution allowing for efficient charge transfer between the redox species and the electrode surface.

The impedance data therefore suggests that the coupling of MWCNTs to FePc is beneficial to the reduction of oxygen. FePc showed a high R_{ct} relative to a bare GCE whereas a MWCNT-modified GCE exhibited a lower R_{ct} relative to both a FePc-modified GCE and a bare GCE. Although FePc exhibits a high R_{ct}, the conductive nature of MWCNTs overcomes this problem and plays a role in the transfer of electrons through the hybrid surface.

4.4 Conclusions

Oxygen reduction at MWCNT-modified electrodes was investigated from pH 2 to pH 8. The reductive potential for oxygen at a MWCNT-modified GCE was shifted by as much as 403 mV (at pH 7) to a more positive potential relative to a bare GCE indicating that MWCNTs were somewhat catalytic towards the ORR. The catalytic behavior was attributed to oxygen-containing functional groups present at edge plane defects present on MWCNTs. This was shown by Banks and Compton (2006). MWCNT-modified electrodes exhibited current responses substantially higher (as high as 21.8 μA) than that of a bare GCE, and comparable to that observed at a FePc-GCE. The increase in current response of the MWCNT-modified electrode was due to the increase in electrode surface area thereby increasing the number of reactive sites. The increase in current response however was only substantial at loading rates greater than 1 mg/ml. Literature has shown MWCNTs to be catalytic towards the reduction of oxygen (Kruusenberg *et al*., 2009).

The current response of the FePc:MWCNT hybrid electrode was greatly increased for the ORR relative to FePc- and MWCNT-modified electrodes. This was attributed to MWCNTs increasing the available surface area of the electrode thereby allowing for greater FePc loading onto the electrode surface. The reduction potential for oxygen obtained from the hybrid electrode showed a large shift towards a more positive potential; the shift in potential was greater than that observed at a FePc-modified electrode indicating that the hybrid electrode was catalytic towards oxygen reduction. This was true at a pH of 2 to 8 except at pH 5, where the reduction potential observed for the hybrid electrode was more negative than that

observed for FePc. This change in reduction potential coincided with a peak in current response. This behavior was not observed for FePc alone, suggesting it was a function of the MWCNTs. Several studies have shown the utilization of MWCNTs as an electrocatalyst support due to the increased surface area they provide (Okunola *et al*., 2008; Wang *et al*., 2008).

Impedance spectroscopy of the modified surfaces further explained the electrochemical behaviour observed for the modified electrodes. MWCNTs are known to be highly conductive (Wildgoose *et al.*, 2006); MWCNT-modified electrodes exhibited much lower resistance to the flow of charge than that seen with a bare GCE whereas FePc exhibited a higher R_{ct} relative a bare GCE. The impedance behaviour of the hybrid electrode showed more complex behavior; there were two distinct time domains present on the electrode surface. Coupling FePc to MWCNTs decreased the charge transfer resistance of the hybrid electrode. Wu and Xu (2007) showed that MWCNT-modified GCEs exhibited lower R_{ct} due to their porous nature therefore using MWCNTs as an electrocatalytic support can decrease the R_{ct} exhibited by the electrocatalyst, thus supporting the notion that MWCNTs aid in lowering the R_{ct} of FePc.

In this chapter, MWCNTs were shown to be catalytic towards the reduction of oxygen. In combination with FePc, which itself was catalytic towards ORR, there was a substantial increase in the reduction current and lowered reduction potential of oxygen at the electrode surface. This behavior was supported by impedance spectroscopy which showed a decrease in the charge transfer resistance of MWCNT-modified electrodes.

5 Chapter 5: The utilization of nanostructrured surfaces in a microbial fuel cell

Power generation of MFCs can be affected by many factors including the type of microorganism used, fuel biomass type and concentration, ionic strength of the system, pH, temperature, and reactor configuration (Liu et al, 2005). Great gains in power production are to be made through the use of superior electrode materials. Pt-based electrodes have been used in several studies as it has been shown to be superior in terms of power production relative to carbon-based electrodes such as graphite and carbon paper (Cheng *et al.*, 2006; Oh and Logan, 2006). Power densities in hydrogen fuel cells, which use Pt-coated electrodes, are orders-of-magnitude larger than those achieved so far in MFCs however the cost of Pt is a stumbling block (Oh et al, 2004). Much research however has gone into developing electrodes using alternative catalysts such as metallophthalocyanines and metalloporphyrins. These catalysts are inexpensive and have shown similar performances to Pt for the reduction of oxygen (Zhao et al, 2005). This chapter examines the effect of modification of carbon paper with FePc and MWCNTs for enhancing the power output of a MFC.

5.1.1 Growth Kinetics of *Enterobacter cloacae*

The bacterium *Enterobacter cloacae* was utilized in these studies. *E.cloacae* is a facultative anaerobe that is known to metabolically produce hydrogen (Kumar and Das, 2001). It was considered to be an ideal candidate for use in a MFC due to its hydrogen producing ability and the fact that it is a facultative anaerobe thereby overcoming the problem of maintaining anaerobic conditions in the anode at all times. A gram stain showed pink rod-shaped bacterial cells which is in line with *E.cloacae*, which is gram-negative and rod-shaped (Appendix 3). Its growth characteristics were investigated to determine the time taken for the bacterium to reach its log growth phase (Fig 5.1).

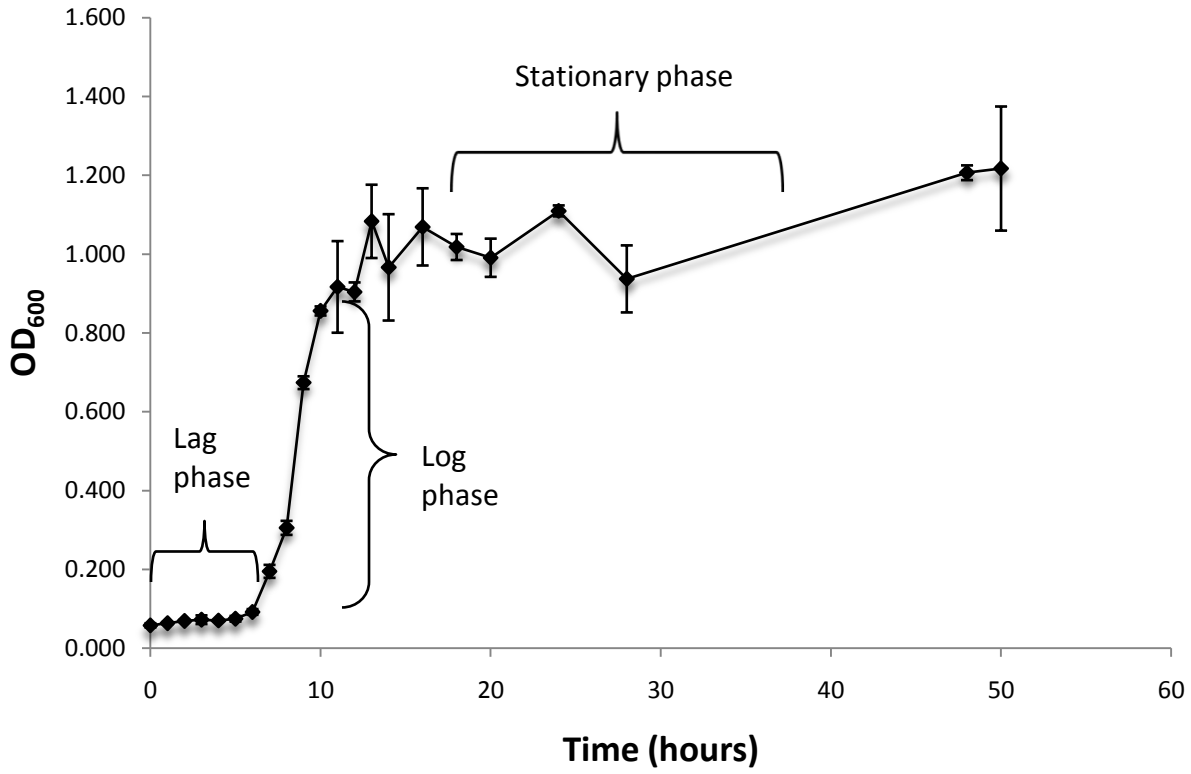

Figure 5-1. Growth curve of Enterobacter cloacae at 30°C in reinforced clostridial medium. Error bars represent mean ± standard deviation. n =3

The first 6 hours of the growth curve (Fig 5.1) represents the lag phase. This occurs because cells have been taken from a stationary phase culture (stored at -20°C in glycerol) in which they would have been starved of essential nutrients and therefore require some time to resynthesize essential cellular components such as enzymes (Madigan and Martinko, 2006). From 7 hours until 13 hours, the bacterial cells are in log phase growth (Fig 5.1). The log phase is the period in which the bacterium is in its optimum metabolic state (Madigan and Martinko, 2006). From 13 hours, the cells are in the stationary phase in which there is no net increase or decrease in cell number (Madigan and Martinko, 2006). The cells however are still metabolically active (Madigan and Martinko, 2006). If given more time, the optical density would decrease as a result of cell death due to nutrient depletion and accumulation of waste (Madigan and Martinko, 2006).

5.1.2 Assessment of modified electrodes in a microbial fuel cell

The power generation of various electrode configurations was investigated in a MFC (Fig 5.2). From preliminary work performed in chapter 3, bulk FePc was considered for use as an electrocatalyst based on its ability to catalyze the reduction of oxygen. MWCNTs, as discussed in Chapter 4, were also shown to enhance the reduction of oxygen. MWCNTs were shown to be catalytic towards oxygen reduction; they enhanced the current generation by increasing the surface area of the electrode. They were therefore chosen as an electrocatalyst support for FePc. The effect that FePc and MWCNTs has on the power generated from a MFC was determined in several configurations as described below (Figure 5.2):

Table 5-1. Summary of electrode modifications used in MFC

	Anode	Cathode
Configuration 1	Bare carbon paper	Bare carbon paper
Configuration 2	Bare carbon paper	FePc
Configuration 3	MWCNTs	FePc
Configuration 4	MWCNTs	Bare carbon paper
Configuration 5	MWCNTs	Hybrid (FePc:MWCNTs)
Configuration 6	Bare carbon paper	Platinum-embedded carbon paper

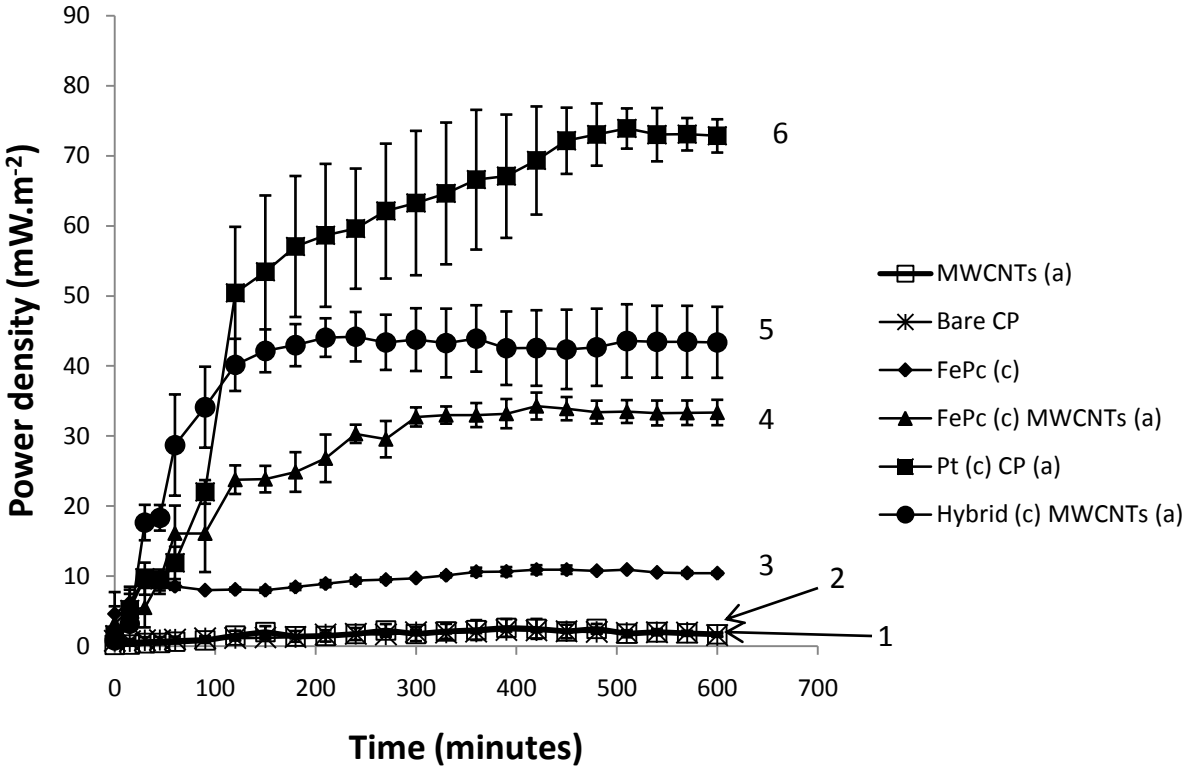

Figure 5-2. Power generation of various modified electrodes in a MFC over a 10 hour period. Error bars show standard deviation from mean. (a) represents the anode and (c) represents the cathode. n = 3.

Platinum-embedded carbon paper gave a peak power density of 73.88 mW/m^2 (Table 5.1). A Platinum-embedded carbon paper electrode used in the cathodic compartment of the MFC generated the highest power density, and was thus used as the result to which other electrodes would be compared to. Carbon paper was chosen as the electrode material for use in the MFC due to the favourable properties of carbon such as the lower cost of the material. Carbon paper electrodes themselves showed minimal power production (2.30 mW/m^2) relative to platinum and the modified electrodes. This then served as the base level of power production with which any improvement shown by the nanostructured electrodes would be compared to. FePc-modified electrodes used at the cathode showed an increase of 374 % in power production relative to bare carbon paper (Fig 5.2). This was expected as the electrochemical data obtained for FePc suggested it was catalytic towards the reduction of oxygen. This is in line with studies

done by Zhao (2005) and Hao Yu *et al.* (2009). This result conforms with the electrochemical data (Chapter 3).

When FePc was used at the cathode and MWCNTs were used at the anode, there was a further increase in the power production of 1390 % relative to bare carbon (Fig 5.2). The use of a hybrid electrode was expected to lead to a large increase in power production as electrochemical data (see Chapter 4) obtained for the hybrid electrode showed that it outperformed all other electrodes for the reduction of oxygen. This could be attributed to two factors. The use of MWCNTs, as earlier discussed, greatly enhances the surface of the electrode allowing for greater loading of FePc. The MWCNTs also improve electron transfer between the catalyst and electrode surface. The combination of these two factors would greatly enhance the performance of the electrode. It was evident from impedance spectroscopy of MWCNT-modified electrodes that the immobilized layer played a role in decreasing the charge transfer resistance of the electrode surface (Chapter 4). The conductive nature of MWCNTs combined with the catalytic nature of FePc therefore display a synergistic relationship.

Although the focus was primarily on the use of modified electrodes at the cathode, the role of MWCNTs was investigated for use in the anodic compartment as they have been shown to be beneficial to power production (Nambiar *et al.*, 2009). This increase in power density was not observed when MWCNTs were used alone at the anode (Fig 5.2). The power density obtained from MWCNT-modified electrodes peaked at 2.83 mW/m^2. This is only marginally better (23% increase) than bare carbon paper however the standard deviation obtained for the MWCNT-modified electrodes was much higher than that of bare carbon paper (Table 5.1). As such, the role of MWCNTs at the anode is thus not clear. MWCNTs have been observed to increase power output in a MFC when immobilized at a carbon electrode (utilizing a platinum-embedded carbon electrode at the cathode), therefore it can be deduced that the absence of a catalyst for oxygen reduction is an important aspect in the overall output. This is supported by the increase in power density when FePc was immobilized at the cathode and MWCNTs were immobilized at the anode relative to only FePc at the cathode (Figure 5.2).

Table 5-2. Summary of power densities obtained for various modified electrodes in MFC. Standard deviation is shown in brackets. n = 3.

MFC	Peak Power Density ($mW.m^{-2}$)	% increase relative to bare carbon paper
Bare Carbon Paper	2.30 (±0.21)	-
Platinum	73.88 (±2.87)	3112%
FePc (cathode)	10.92 (±0.60)	374%
MWCNTs (anode)	2.83 (±1.41)	23%
FePc (C); MWCNTs (A)	34.27 (±1.92)	1390%
Hybrid (C); MWCNTs (A)	44.17 (±3.52)	1820%
Negative control (bare carbon paper without bacteria)	1.01 (±0.108)	-

The maximum power density was calculated for each MFC operated according to the following equation (Logan, 2008):

$$\mathbf{P}_{elec} = \frac{\mathbf{E}^2_{MFC}}{\mathbf{A}_{elec}\mathbf{R}_{ext}}$$

where E is the MFC potential (in volts), A_{elec} is the area of the electrode (in m^2) and R_{ext} is the external resistance (in Ω). The equation normalized the power to the electrode surface area. Since both sides of the electrode were exposed to the electrolyte, the area calculated included the area of both sides added together. A summary of the peak power densities (Table 5.1) shows that use of a platinum electrode at the cathode generated the highest power density. This is an expected result for platinum. Each modification showed an increase in power density relative to bare carbon paper. The best performing modified electrode was the FePc-MWCNT hybrid electrode which, when used in conjunction with MWCNTs at the anode, gave a power density approximate to one-third of the power density of the platinum electrode (Table 5.1).

It can be seen from the results that there is an initial increase in power production over the first three hours that cannot be attributed to bacterial growth (Figure 5.3). Although a log phase bacterial culture was used for inoculation of the anode, this would require some time for the bacteria to acclimatize to the growth medium and begin producing sufficient hydrogen to generate voltage. A MFC without bacteria was run thus as a negative control to examine the power production of the MFC in the absence of bacteria (Fig 5.3).

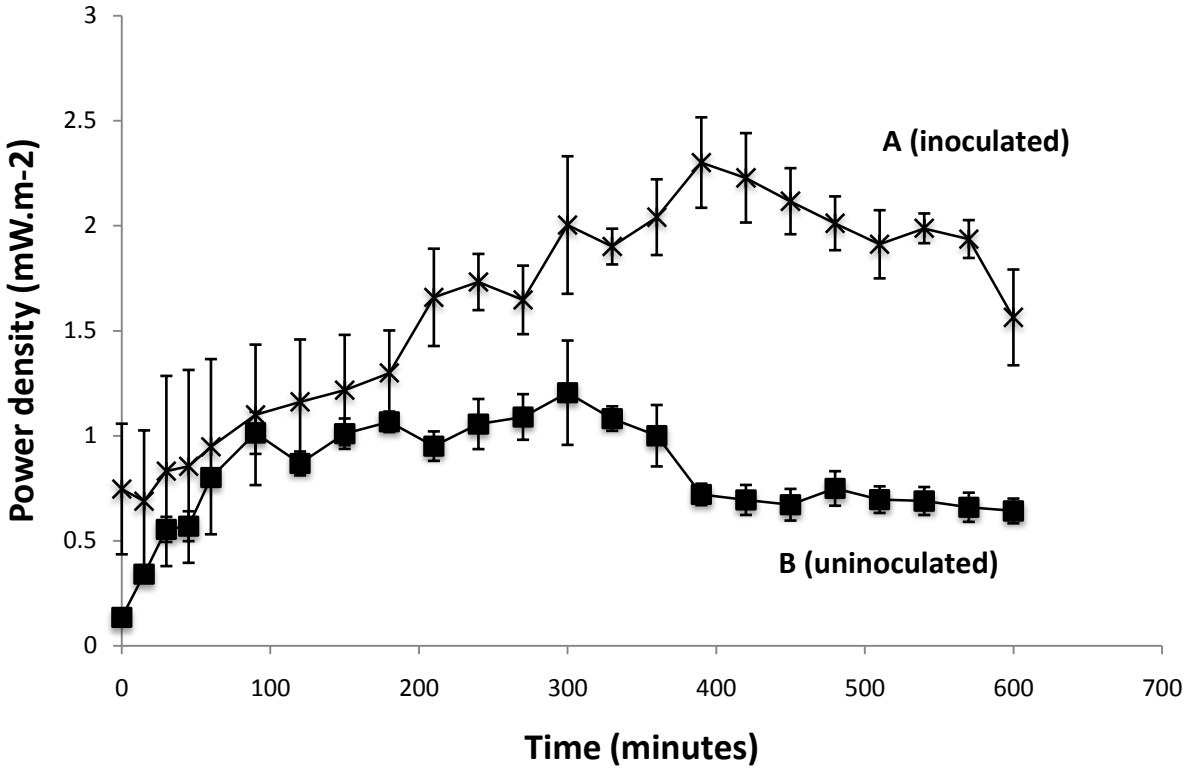

Figure 5-3. Comparison of power generation in a MFC using RCM with and without *E.cloacae*. A) MFC inoculated with *E.cloacae*. B) MFC uninoculated (*E.cloacae* absent). Unmodified carbon paper electrodes were used for both the anode and cathode. Error bars show standard deviation from mean. n = 3

In the presence of *E.cloacae*, there is an initial increase in power density from 0 min to 200 min. An identical increase is seen from 0 min to 200 min for the MFC in which *E.cloacae* is absent (negative control). From 200 min onwards, the power generated by the MFC containing bacteria continues to steadily increase whereas the power generated by the MFC without bacteria begins to level out. From 300 min onwards, the power density of the MFC without bacteria begins decreasing.

This implies that oxidation of components of the medium was responsible for the initial increase in power density observed over the first 200 min. Cysteine (L-cysteine hydrochloride) is often added to growth media as it chemically scavenges dissolved oxygen so that the solution remains anoxic (Logan, 2008). With respect to the negative control (Figure 5.3), the increase in power density from 0 min to approximately 180 min can then be attributed to possible

oxidation of the cysteine. This would supply the system with electrons to generate power as opposed to the bacteria producing hydrogen which would serve as a source of electrons (Figure 5.3).

At a similar time at which the power tails off in the negative control, there is a slight increase in the power produced by the MFC inoculated with bacteria. This indicates that the bacteria have acclimatized and reached a sufficient metabolic level to have an influence on power produced i.e. the bacterium has started synthesizing hydrogen thereby driving the increase in power generation. This seems to be supported when comparing the OD_{600} of the bacteria to the power density produced (Figure 5.4). The bacterial culture requires time to acclimatize to the growth medium and only shows an increase in the OD_{600} (i.e. bacterial growth) from about 2 hours. The initial increase in power could therefore be attributed to the oxygen scavenger present in the growth medium.

Several studies on MFCs have tended to use a minimal salts medium (MSM), as opposed to a defined growth medium such as RCM, to eliminate any potential influence that the medium may have on power production (Logan, 2008). RCM however is a useful growth medium for use in the MFC as it allows for fairly rapid growth of the bacterium relative to MSM in which bacterial growth is slower.

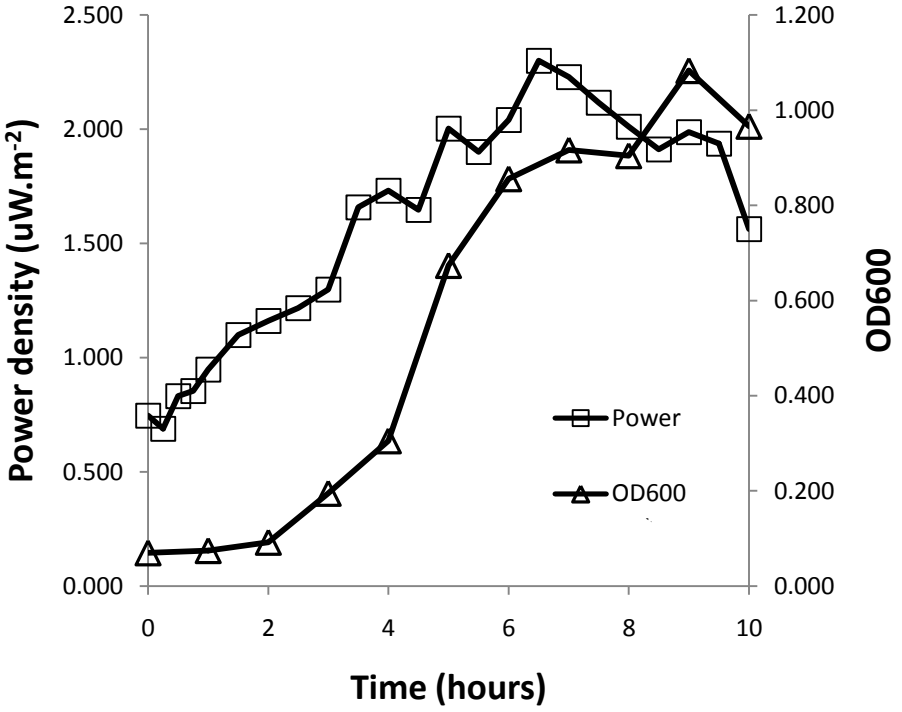

Figure 5-4. Change in power density (left y-axis) of a MFC related to the bacterial growth as measured by the OD600 (right y-axis) of the bacterial culture grown in RCM. The MFC used bare carbon paper electrodes.

5.2 Optimization of microbial fuel cell

5.2.1 Dispersal of Iron phthalocyanine and MWCNTs

Nanostructures, as mentioned in Chapter 1, have a high surface to volume ratio. With this increase in surface area, the attractive force between the aggregates also increases (Vaisman *et al.,* 2006). In the case of MWCNTs, highly entangled nanotubes will result in electrodes with performance which is far below their theoretical potential (Vaisman *et al.*, 2006). The physical association of polymers with carbon nanotube surfaces has been shown to enhance the dispersion of CNTs in both water and organic solvents (Vaisman *et al.*, 2006). The immobilization of the electrocatalyst and support material like MWCNTs onto the electrode surface is critical not only for performance of the electrode but also for the lifespan of the

electrode. Covalent and non-covalent means have been used for attachment and/or immobilization of electrocatalysts and MWCNTs (Vaisman *et al.*, 2006).

Chitosan has been used in biosensors to immobilize metal nanoparticles as well as carbon nanotubes onto electrode surfaces (Casagrande *et al.*, 2008). Chitosan has also been shown to improve the dispersal of MWCNTs in biosensors and fuel cells (Jiang *et al.*, 2009; Nambiar *et al.*, 2009). Not only does it aid dispersal, chitosan also helps to stabilize the immobilized catalytic layer on the electrode surface (Jiang *et al.*, 2009). Nafion™ has been used in biosensors and has shown several benefits as discussed before in chapter 1 (Sun *et al.*, 1999; Wang *et al.*, 2003). It has been used for the dispersal of nanotubes in several studies (Wu and Xu, 2007; Okunola *et al.,* 2008; Prehn *et al.*, 2008). It has also been shown to aid proton transfer (Wu and Xu, 2007) however Maruyama *et al.* (1998) showed that it had no significant effect on the kinetics of O_2 reduction on gold.

Very little literature detailing the use of Triton X-100 in MFCs is available. Triton X-100 is a non-ionic surfactant that has been used in the dispersion of carbon nanotubes (Kruusenberg *et al.*, 2009).

Figure 5.5 shows the effects of using the three aforementioned dispersants. Only Nafion™ showed an increase in power production relative to electrodes without dispersant however taking into the account the error involved, there was no significant improvement ($p < 0.05$). Electrodes prepared with Triton X-100 and chitosan showed power production similar to modified electrodes that had no dispersal agents (Fig 5.5).

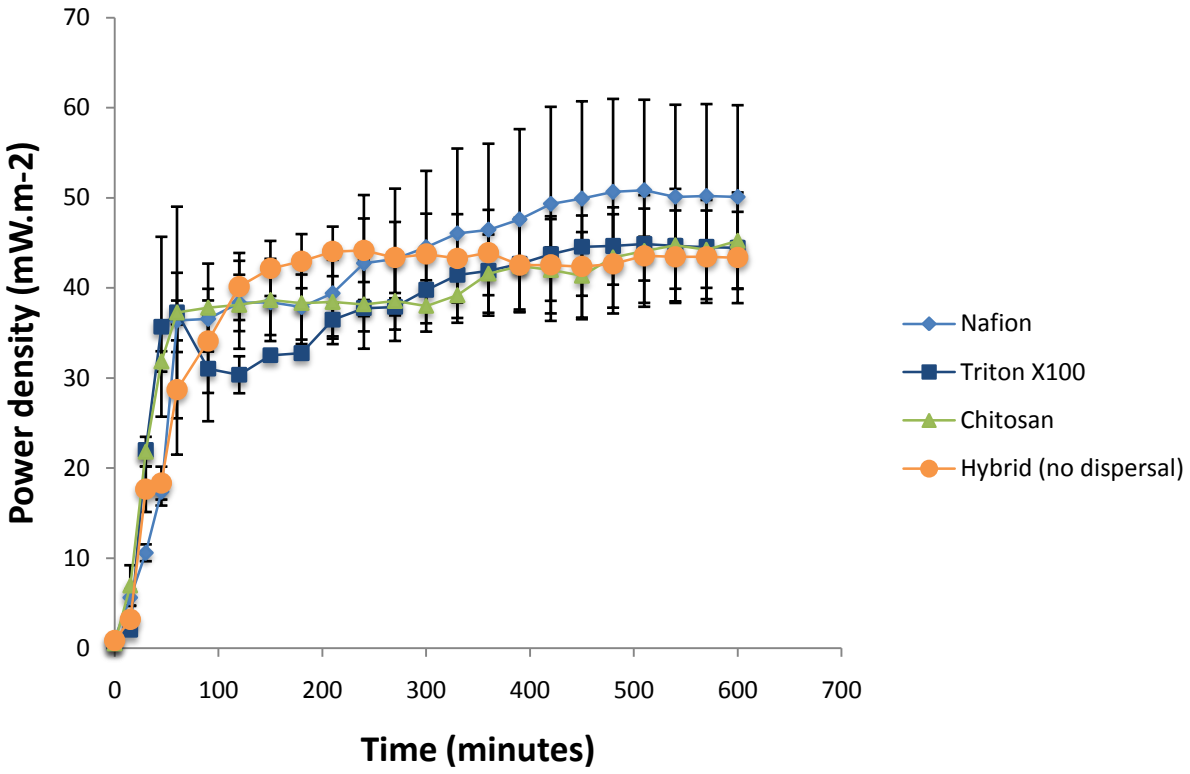

Figure 5-5. Effect of the use of dispersal agents in a MFC with FePc:MWCNTs at the cathode and MWCNTs at the anode dispersed in each of the dispersal agents. Error bars show standard deviation from mean. n = 3

Chitosan consists of amino groups which may carry a positive charge while the CNTs have been acid treated and contain many carboxyl groups that carry a negative charge. The chitosan will likely attract the CNTs electrostatically therefore leading to clumping. This could explain why when chitosan was used, there was no apparent enhancement of the power (Fig 5.5). This could be overcome if non-functionalized CNTs were used as they do not carry a charge. The non-functionalized MWCNTs however would have to be washed in a strong acid such as nitric acid to remove impurities and hence limit the effect of metal nanoparticles towards the electroactivity. Nambiar *et al.*, (2009) showed that chitosan enhanced the dispersal of non-functionalized MWCNTs. Triton X-100 is non-ionic and it should in theory provide improved dispersal of the CNTs relative to chitosan as there would be little attraction between the triton X-100 and the CNTs. There is however very little difference between chitosan and Triton X-100

(Fig 5.5). Of the three surfactants used, only Nafion™ showed an increase in power production, albeit with a high margin of error. Nafion™ consists of a Teflon™ backbone containing ionic sulphonate groups that carry a negative charge. As the CNTs also carry a negative charge, the CNTs would more than likely be well dispersed in Nafion™ due to charge repulsion between the Nafion™ and CNTs. The use of dispersal agents in a MFC for functionalized MWCNTs therefore did not enhance the power produced relative to standard procedures in which MWCNTs are dispersed in DMF. According to Vaisman *et al.* (2006), sonicating the functionalized MWCNTs in an organic solvent such as DMF should lead sufficient dispersal.

5.2.2 Effect of temperature

The effect of temperature on the power generation in the MFC was investigated. The optimum growth temperature for *E.cloacae* is in the range of 30°C – 35°C (Kumar and Das, 2005). At this temperature it would be expected that the bacterium would optimally utilize the necessary components of the growth medium and would therefore be generating more hydrogen than at lower temperatures. The effect of this on the power production of the MFC is evident from Figure 5.6.

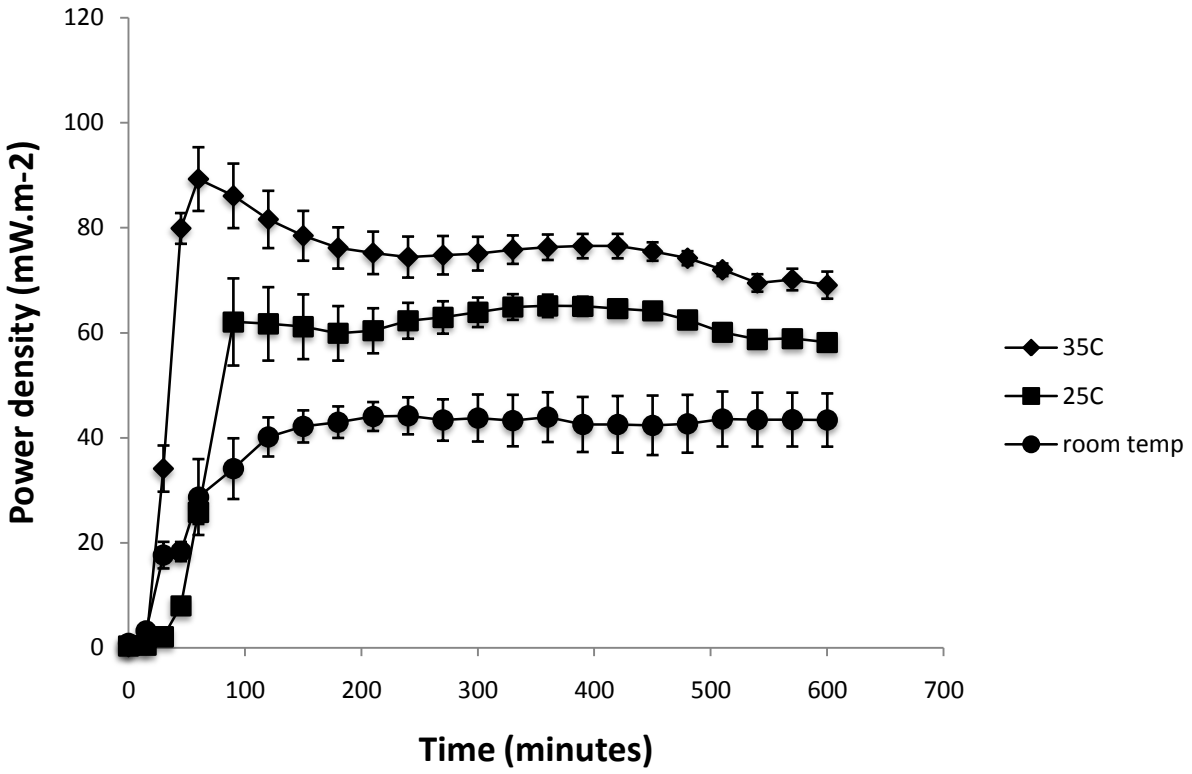

Figure 5-6. Power generation of modified electrodes in a MFC operated at room temperature (20°C) as well as at 25°C and 35°C. FePc:MWCNT modified electrodes were used at the anode while MWCNT-modified electrodes were used at the anode. Error bars show standard deviation. n = 3

Considering the results obtained under steady state conditions (i.e. after 200 min), the peak power production at 35°C is twice as much as that generated at room temperature (Fig 5.5). Liu *et al.* (2005) showed a 9% increase in power production when the temperature was increased from 20°C to 32°C. Even at 25°C, the power production of the MFC resulted in a 32% increase in power production compared to room temperature. Assuming the bacterial cells have access to sufficient substrate, they are expected to grow optimally at 35°C. It was seen in Figure 5.3 that *E.cloacae* only influenced the power production from about 200 min onwards. It is evident that the power density peaks sooner at higher temperatures (Fig 5.6). At 25°C, power production peaks around 90 min while at 35°C it peaks at around 60 min. This could be related to the growth of the bacterium because at higher temperatures (35°C), *E.cloacae* is more metabolically active than at room temperature and it can be assumed that the growth rate would be higher at 35°C. If the growth rate increases with temperature, *E.cloacae* would

acclimatize to the growth medium sooner and would therefore begin producing hydrogen sooner hence the earlier peak in power production. This result however will be influenced by the presence of cysteine as the oxidation of this compound would also increase with increasing temperature.

Optimal growth will allow for optimal hydrogen production which will lead to increased power production in the MFC. Not only will the temperature directly influence the growth of the bacteria, the rate of diffusion within the system will be accelerated. As no agitation of either the anode or cathode occurs, the movement of the substrate to the electrode depends on diffusion. Without this process occurring, the bacterial cells will have difficulty accessing the substrate which can directly influence the level of hydrogen production. The rate of diffusion increases with an increase in temperature (Voet and Voet, 2006).

5.2.3 Effect of stirring

Agitation of the anodic compartment of a MFC through either bubbling through gas or stirring the solution could be important in aiding the movement of substrate through the solution. This would be beneficial to the bacterial cells so that there would be a constant supply of nutrients in close proximity to them. The effect of agitation of the anodic compartment was investigated (Fig 5.7).

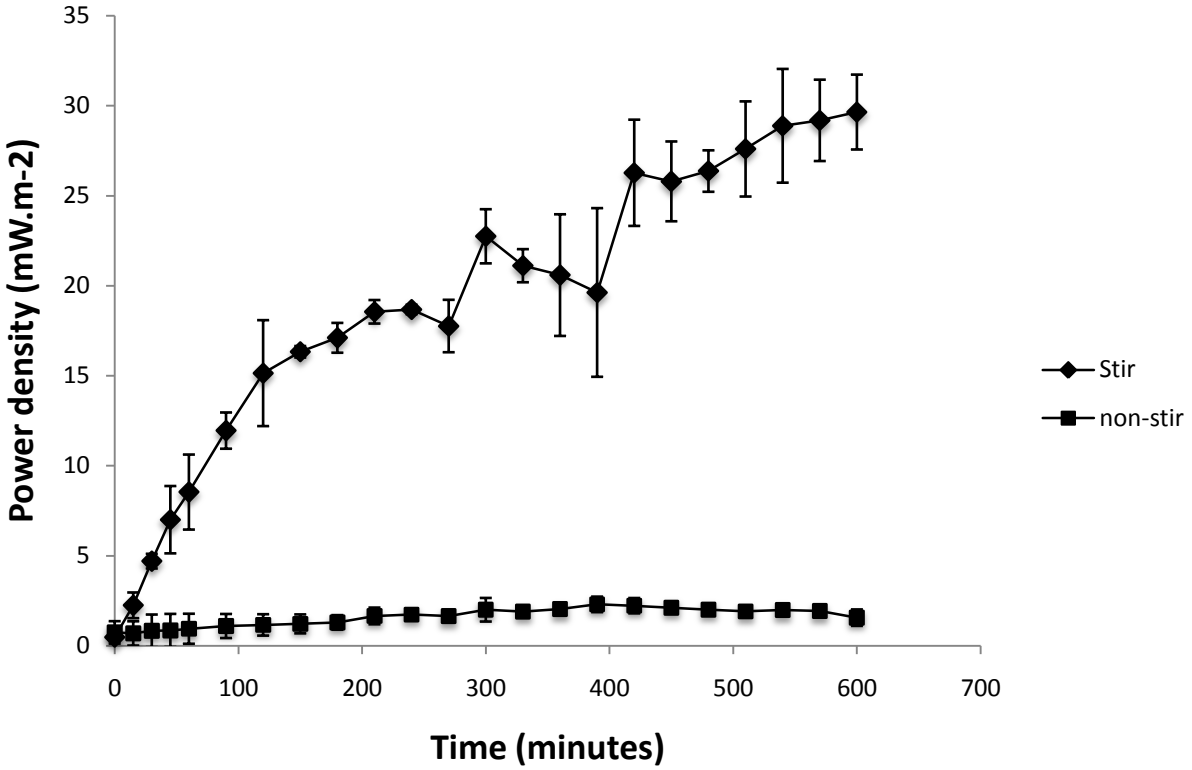

Figure 5-7. Effect of stirring on power generation in a MFC operated for 10 hours. Bare carbon paper electrodes were used at both the anode and cathode. Error bars show standard deviation from mean. n = 3

It was shown clearly that the power production was significantly enhanced through agitation of the anodic compartment (Fig 5.7). The solution was stirred at a constant rate of 100 rpm. Using relatively low speeds would ensure no shearing of the cells would occur. There was a sustantial increase in the power produced by the MFC when the anodic compartment was agitated relative to a MFC in which the anodic compartment was not agitated. As mentioned earlier, this increase could be attributed to enhanced mass transport of the substrate through the solution. Agitation of the solution would also allow the movement of the bacterial cells through the solution. It was evident visually from the MFC that was not agitated, that the bacterial cells quickly settled to the bottom of the anodic compartment. It would be beneficial for the bacterial cells to be in direct contact with the electrode; however the time in which the MFC was operated was insufficient to allow for biofilm formation. By agitating the solution, it allowed the bacterial cells to more readily come into contact with the electrode surface and the

substrate. Agitation of the cathode would need to be explored as well as there is potential for further increases in power density as the agitation would enhance the diffusion of oxygen in solution.

5.2.4 Effect of Ionic strength

The ionic strength of the electrolyte (growth medium in this case) used in a MFC plays a role in its performance as the presence of more dissolved salts and hence higher ion concentration leads to a greater solution conductivity (Liu *et al.*, 2005). The ionic strength (IS) of the medium affects solution conductivity, and the IS has been shown to affect power generation by Liu *et al.* (2005). The IS of the growth medium can be altered through the addition of NaCl. High levels of NaCl are possibly detrimental to the growth of the bacteria therefore relatively low levels (100 mM, 200 mM, and 300 mM) were tested. The IS of growth medium was adjusted by adding NaCl into the solution. Unmodified electrodes were used in this study.

Figure 5.8 shows the effect that the increase of the IS of the anodic compartment had on power density. The power produced by the MFC progressively increased as the concentration of NaCl and hence the IS of the solution increased (Fig 5.8).

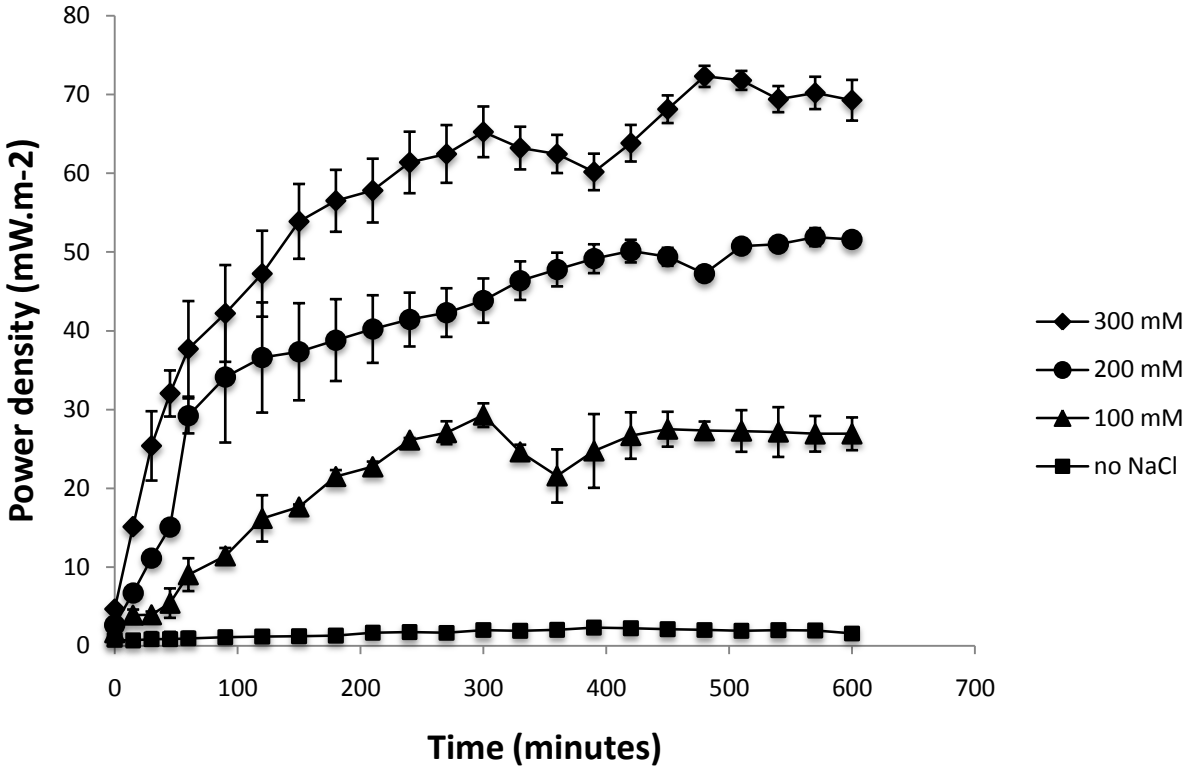

Figure 5-8. Effect of ionic strength on power generation in a MFC operated over 10 hours. Bare carbon paper electrodes were used at both the anode and cathode. Error bars show standard deviation from mean. n = 3

There was an increase in the power production of approximately 146% when the IS of the growth medium in the anode was increased from 100 mM to 300 mM. The IS is measured as the NaCl concentration and is not the total IS of the medium. Liu *et al.* (2005) showed an approximate 60% increase in power production when increasing the IS of the growth medium, through the addition of NaCl, from 100 mM to 300 mM. The MFC in these studies was operated with bare carbon paper, whereas Liu *et al.* (2005) used Pt-embedded carbon paper electrodes for their study which would account partly for the 60% increase compared to the increases seen in this study.

An ion gradient is expected to be established between the anodic compartment and cathodic compartment once NaCl is added. This is attributed to the fact that no NaCl was added to the cathode therefore it would have a low IS relative to the anode. This gradient would drive the

diffusion of cations to the cathode which is essential to the power production of the fuel cell. An increase in the movement of cations, particularly H^+ ions, would lead to the increase in the reduction of oxygen in the cathodic compartment. Liu *et al.* (2005) also suggested that the increase in IS leads to a decrease in internal resistance. A decrease in the internal resistance of the MFC would lead to greater power production due to the lower resistance to the flow of electrons within the system.

The concentrations used appeared to have no affect on the growth of the bacteria as the power produced increased steadily with the increase in NaCl concentration. The increase however could be attributed mainly to the change in IS rather than an increase in the metabolic activity of the bacterium. NaCl is generally not known to enhance growth of bacterium, but it can lead to a decrease in the growth rate if present in high concentrations. Liu *et al.* (2005) showed that at concentrations of 400 mM and greater, NaCl became toxic to the bacteria.

Table 5-3. Summary of power densities obtained after optimization of MFC. Standard deviation is shown in brackets. n = 3

Optimization of MFC	Peak Power Density ($mW.m^{-2}$)	% increase relative to bare carbon paper
Dispersal using - Chitosan	44.74 (±6.24)	1845%
- Triton X100	44.88 (±0.79)	1851%
- Nafion™	50.19 (±10.20)	2082%
Temp – 35°C	86.06 (±6.14)	3641%
- 25°C	65.11 (±2.14)	2730%
Stirring (bare carbon paper)	29.649 (±2.07)	1189%
Ionic strength – 300 mM	72.28 (±1.34)	3042%
- 200 mM	51.57 (±1.14)	2142%
- 100 mM	29.27 (±1.503)	1172%

In summary, temperature, agitation, and ionic strength all play a role in the power generation of the MFC. The effect of all three parameters operating together in a MFC was investigated. The power output was compared to a MFC operated with a Pt-embedded carbon paper electrode at the cathode and a MFC utilizing a hybrid FePc:MWCNT electrode at the cathode and a MWCNT electrode at the anode in the absence of stirring, temperature increase and IS

increase. After optimization of the MFC with regards to the aforementioned parameters, the power production was greatly enhanced (Fig 5.8).

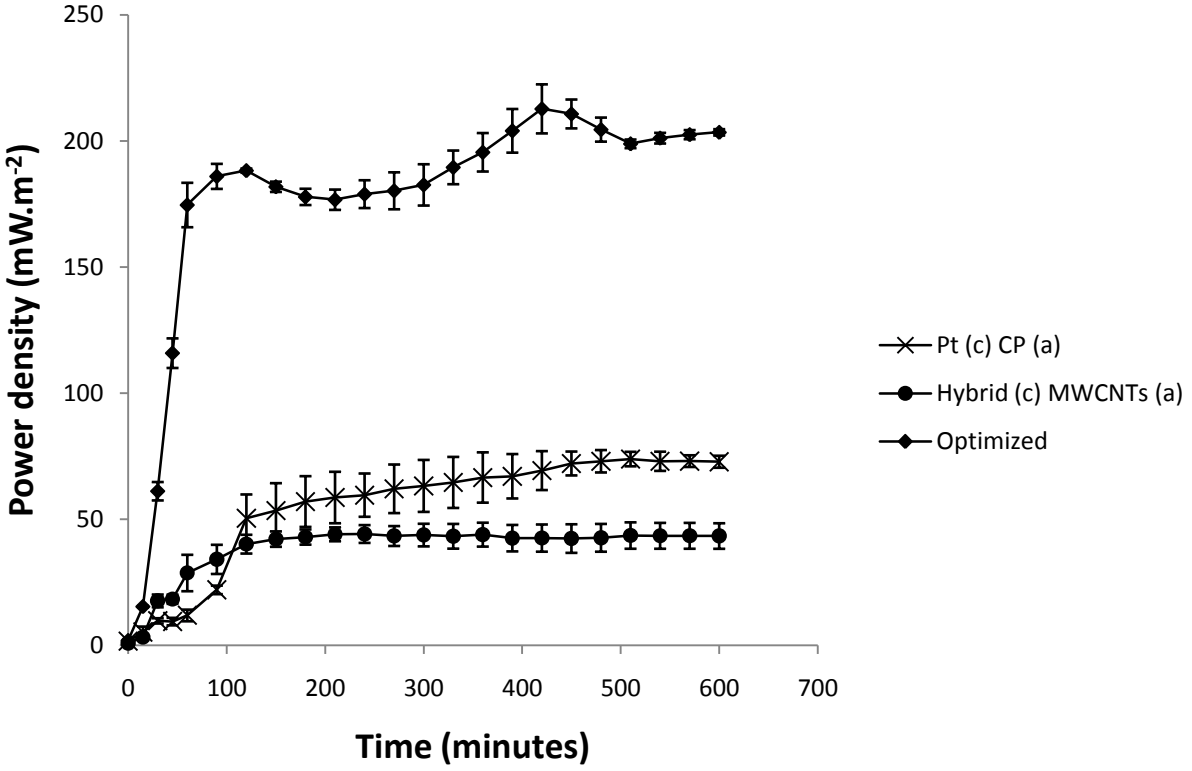

Figure 5-9. Power generation in an optimized MFC (where a hybrid electrode was used at the cathode, MWCNTs were used at the anode; NaCl conc. 200 mM, agitated at 100 rpm, 35°C). Error bars show standard deviation from mean. n = 3

The power production of the modified electrodes without optimized parameters was lower than that obtained from using platinum electrodes; however upon optimization the peak power density increased substantially (Figure 5.8). The peak power density when using platinum electrodes in the MFC was 73.8 mW/cm^2 whereas the peak power density for the modified electrodes in the MFC was 212.72 mW/m^2 after optimization (44.17 mW/m^{-2} before optimization). This represents a 190% increase over platinum and an approximately 380% increase over an unoptimized MFC using the same modified electrodes.

5.3 Conclusions

In an H-type MFC utilizing the bacterium *E.cloacae*, platinum embedded carbon paper electrodes generated a maximum power density of 73.88 $mW.m^{-2}$ whereas bare carbon paper electrodes generated a maximum power density of 2.30 $mW.m^{-2}$. FePc-modified electrodes showed an improvement over bare carbon paper, with a power density 5 times higher than that of bare carbon paper (10.92 $mW.m^{-2}$ vs. 2.30 $mW.m^{-2}$). Further increases were seen from FePc-modified electrodes when FePc was coupled to MWCNTs. The results suggested the presence of an oxygen reduction catalyst was crucial to increasing the power density.

MWCNTs are known to aggregate therefore various dispersal agents were investigated for use for the modification of the electrodes so that aggregation could be overcome. The power densities obtained for modified electrodes in which the dispersal agents were used shows no increase over electrodes in which no dispersal agent had been used.

Operating temperature, agitation, and ionic strength of the MFC were identified as areas for improvement on the basis of previous studies performed on the optimization of MFCs. All MFC work had been done at room temperature however the bacterium used, *E.cloacae*, grows optimally at higher temperatures. It was shown that power densities obtained from the MFC increased with increasing temperature from 20°C (44.17 $mW.m^{-2}$) to 35°C (86.06 $mW.m^{-2}$).

Agitation of the solution would overcome mass transfer limitations within the anode and allow for greater nutrient flow through the solution allowing the bacterial cells to be in close contact with their substrate. The power density obtained from an MFC in which the anodic compartment had been agitated (29.86 $mW.m^{-2}$) was significantly higher than that of a MFC in which the anodic compartment had not been agitated (2.30 $mW.m^{-2}$). Cheng *et al.* (2006) showed that a continuous flow of nutrients across the anode increased the power production relative to having no flow over the anode.

An increase in the ionic strength of the bacterial growth medium in the anodic compartment was seen to increase the power density obtained from the MFC. The IS of the anode was increased using NaCl at concentrations of 100 mM, 200 mM and 300 mM. The power density obtained in an MFC with no added NaCl was 2.30 $mW.m^{-2}$ whereas on addition of NaCl, the power density rose substantially with a peak at 300 mM NaCl of 72.28 $mW.m^{-2}$. Liu *et al*. (2005) showed similar increases in power density of a MFC through addition of NaCl.

Optimization of the MFC, using nanostructure-modified electrodes, generated 212.7 $mW.m^{-2}$ which represents a 118% increase relative to a MFC utilizing Pt-embedded carbon electrodes while an MFC utilizing nanostructure-modified electrodes that had not been optimized generated 43.6 $mW.m^{-2}$. A power density of 212 $mW.m^{-2}$ compares favourably with previous studies of MFCs. Min *et al.* (2005) used swine wastewater as a feedstock in a single-chambered and two-chambered MFC and utilizing Pt-embedded carbon electrodes, obtained power densities of 261 $mW.m^{-2}$ from a single-chambered MFC and 45 $mW.m^{-2}$ from a two-chambered MFC. Other studies using Pt-embedded carbon electrodes have yielded power densities of up to 1500 $mW.m^{-2}$, however most studies have used wastewater as feedstock as well as a microbial consortium (as opposed to a single bacterial species) which is known to yield higher power densities (Logan and Regan, 2006).

In this chapter, FePc displayed its ability as an ORR catalyst for use in MFCs. Coupling FePc to MWCNTs have been shown to be beneficial for use in modification of electrode surfaces, with the nanostructured surfaces generating power densities comparable to platinum-based electrodes in an identical MFC set-up. With more work to be done with regards to the MFC design and operation, there are several more gains in power densities to be made.

6 Chapter 6: Overall conclusions and Future recommendations

6.1 Conclusions

This study examined the utilization of iron phthalocyanine as an electrocatalyst for the reduction of oxygen in the cathodic compartment of a MFC as well as using acid functionalized multi-walled carbon nanotubes as an electrocatalyst support. The aim of the study was to enhance the ORR using nanostructured surfaces comprising FePc and MWCNTs to modify electrodes that would be used to increase the power density obtained from a laboratory scale H-type MFC.

The UV/Vis spectrum of nano FePc exhibited a sharper Q and B bands, relative to bulk FePc, a result of improved dispersal of nano FePc in CTAB. The Raman spectrum of nano FePc exhibited subtle differences in peak intensities and shifts in wavelengths of particular peaks, particularly the band representing C-H bonding, relative to the bulk FePc. An electrochemical analysis of bulk and nano FePc using CV showed that both forms of FePc were catalytic towards the reduction of oxygen. A bare GCE showed a peak reduction current at pH 8 of 2.606 µA (±0.005) at a potential of -680 mV (±0.004), bulk FePc gave a peak reduction current at pH 8 of 15.50 µA (±3.9) at a potential of -108 mV (±0.004), while nano FePc gave a peak reduction current at pH 8 of 19.747 µA (±0.942) at a potential of -51 mV (±0.041).

Both nano and bulk FePc showed increased current response and reductive potential shifts relative to a bare GCE however there was no significant difference between either form of FePc. There was no linear trend observed for ORR across a pH range for both modified and unmodified surfaces. A similar result was observed by Zhang and Yang (2007) for ORR at a bare GCE whereby no linear trend was observed. Impedance spectroscopy showed that bulk FePc-modified surfaces exhibited a higher charge transfer resistance relative to a bare GCE which was attributed to the bulky ring system of FePc. FePc-GCE also showed less capacitive ability than the bare GCE, which would be due to passivation of the electrode surface due to the immobilization of FePc.

The electrochemical analysis of MWCNTs showed that MWCNTs were catalytic towards the reduction of oxygen. Oxygen reduction at MWCNT-GCEs gave a maximum reductive current response at pH 8 of 13.770 µA (±0.747) at a potential of -509 mV (±0.019). The increased current response seen from the MWCNT-GCE was attributed to the increased surface area afforded by the immobilized NTs whereas the catalytic behavior of the NTs was due to the edge plane sites of the MWCNTs as well as oxygen-containing functional groups present at these edge plane sites. Impedance of MWCNTs showed that they had a lower resistance to the flow of charge relative to a bare GCE, confirming that they were conductive as mentioned in literature.

Electrochemical analysis of hybrid FePc:MWCNT electrodes showed a peak reductive current for oxygen at pH 5 of 24.71 µA (±0.132) at a potential of -84 mV (±0.002). The increased electrode surface area afforded by the immobilized MWCNTs allowed for greater FePc loading hence the increased current response. Impedance spectroscopy of a MWCNT-GCE showed that the immobilized layer of MWCNTs was conductive to the flow of charge. The deposited layer of MWCNTs also increased the capacitance of the electrode relative to a bare GCE. The hybrid GCE exhibited more complex behavior. It was apparent that the immobilized FePc and MWCNTs each exhibited resistance to the flow of charge however the overall R_{ct} was lowered relative to FePc alone which could be attributed to the conductive nature of the MWCNTs. A summary of the modified surfaces show the enhanced catalytic behavior of the electrode relative to an unmodified surface (Table 6.1). The hybrid surface showed the greatest increase in current response relative to all other surfaces.

Table 6-1. Summary of Current and Potential responses of modified surfaces

Electrode surface	Maximum Reduction Current (µA)	Reduction Potential (mV)
Bare GCE	2.66 (pH 8)	-680 (pH 8)
FePc-GCE	15.5 (pH 8)	-108 (pH 8)
MWCNT-GCE	13.7 (pH 8)	-333 (pH 8)
Hybrid-GCE	24.7 (pH 5)	-84 (pH 5)

FePc and MWCNTs were utilized in the modification of carbon paper electrodes for use in a MFC. The power density obtained from bare carbon paper electrodes was used as the minimum baseline while the power density obtained from platinum-embedded carbon paper was used as the standard with which to compare other analyses to. The modified electrode with which the highest power density was obtained was from a combination of using a hybrid (FePc:MWCNT) electrode at the cathode and using a MWCNT-modified electrode at the cathode. This particular configuration generated a power density of 44.17 $mW.m^{-2}$ (±3.52) relative to platinum electrodes which generated 73.88 $mW.m^{-2}$ (±2.87) while bare carbon paper electrodes generated 2.30 $mW.m^{-2}$ (±0.21). To aid dispersal, and hence increase the power density, of FePc and MWCNT on the electrode surface, chitosan, Nafion™, and triton X-100 were investigated for their ability to improve dispersion. None of the dispersal agents showed any significant improvement in the power densities generated.

The MFC was operated at three different temperatures, namely room temperature (20°C), 25°C and 35°C, to ascertain the affect of temperature. It was found that the power density generated at 35°C was much higher than at the lower temperatures. The power density obtained was 86.06 $mW.m^{-2}$ (±6.14) as opposed to 44.17 $mW.m^{-2}$ (±3.52) at room temperature. The increase was concluded to be a result of increased metabolic activity of the bacterium used, *E.claocae*, as its optimal growth temperature is 35°C.

An increase in the IS of the anode through the addition of NaCl was found to enhance the power density generated using bare carbon paper electrodes with a peak power density of 72.28 (±1.34) $mW.m^{-2}$ using 300 mM NaCl as opposed to 2.30 $mW.m^{-2}$ (±0.21) in which no NaCl was added. The increase was attributed to the increase of the ion gradient between the anode and cathode; this led to an increase in the diffusion of ions to the cathode. The effect of agitating the anodic compartment through stirring was investigated. There was a sharp increase in the power density generated, as opposed to when no agitation occurred. The peak power density when agitation was used reached 26.649 $mW.m^{-2}$ (±2.07) as opposed to 2.30 $mW.m^{-2}$ (±0.21) in which no stirring occurred. The increase seen was concluded to be a result of

improved mass transport within the system. Although the energy input to achieve these gains was high, the result demonstrated the potential increases in power densities that may be achieved through agitation of the system. If an alternative, less energy demanding means of agitation can be utilized, the net energy balance would be more favourable.

Through optimizing the aforementioned parameters, the maximum power density obtained from the MFC using the nanostructure modified electrodes peaked at 212.72 $mW.m^{-2}$. This was a significant increase in power generation relative to bare carbon paper electrodes; it also represented a significant increase in power generation relative to platinum-based electrodes.

This thesis clearly showed the catalytic nature of FePc and MWCNTs towards the reduction of oxygen, offering an alternative to using platinum. Nano FePc, for the first time, was utilized as a ORR catalyst. No significant improvement was offered by nano FePc relative to bulk FePc though. As seen in previous studies (Agboola *et al*., 2008), the incorporation of MWCNTs as a catalyst support led to greater improvement in the current response for the reduction of oxygen. All modified surfaces exhibited similar behavior towards ORR in that no apparent linear trend was observed for current and potential responses. The analysis of the modified surfaces in an *Enterobacter cloacae* MFC further confirmed the results obtained through electrochemical analysis. A hybrid electrode configuration was most suited for use in a MFC, as hybrid surfaces exhibited higher power densities relative to other modified surfaces. There has been little work done on using MWCNT-based hybrid surfaces in MFCs; however improvements seen in chemical fuel cells through the use of hybrid surfaces can be applied to MFCs. The power density obtained from the MFC in this study however was relatively low and until the power density is increased substantially, there is no real world application as yet. This thesis has shown however firstly the potential of using FePc and MWCNTs as a catalyst and support respectively and secondly the improvements in power density that can be attained through optimization of the operating parameters of a MFC.

6.2 Future Recommendations

Physical adsorption of FePc and MWCNTs onto carbon-based electrodes is a simple hassle-free approach to immobilization however it may not be the most suitable means of immobilization for long term use of the electrodes. There are several other methods of immobilization of FePc and MWCNTs that can be explored. Covalent attachment to the electrode surface may be possible. A variety of functional groups may be added to FePc and MWCNTs, which in turn may be used in covalent attachment to the electrode. Entrapment of FePc and MWCNTs in conductive polymers offers a viable solution. Robust immobilization strategies will be essential in MFCs in which agitation of either the anode or cathode is used.

There are further gains to be made in the power density obtained from MFCs. Using a wastewater stream as a feedstock can potentially enhance power generation as wastewater can serve as a rich source of nutrients. There is however a particular benefit of remediation of wastewater coupled to power generation. Wastewater can be remediated by MFCs as shown by several studies (Min *et al.*, 2005; Fen *et al.*, 2008; Mohan *et al.*, 2008). The utilization of a microbial consortium as opposed to pure bacterial strains can also lead to enhanced power generation particularly when a wastewater feedstock is being used as a microbial consortium, potentially consisting of varied aerobic and anaerobic species, which will be able to use up most of the nutrients within the feedstock and will adapt more easily to changes in growth conditions.

The architecture of the fuel cell is often seen as a limiting factor in terms of power generation. To ensure optimal operating conditions there needs to be a continual supply of nutrients to the microbes present, and transport of ions to the electrodes from the bacteria is essential. To overcome these problems, a continual flow of medium through the fuel cell is particularly desirable. This could however be energetically taxing on the system as pumps require electricity. A gravity-fed pump could alleviate this concern. Other considerations based around the design of the fuel cell include electrode spacing and exposed electrode surface area. The spacing of electrode has been shown to affect power generation (Cheng *et al.*, 2006). An H-type

fuel cell configuration, although ideal for lab-scale testing, is flawed in design in that the electrodes are generally spaced far apart. Using a more compact design to remove the distance between the electrodes created by the glass bridge would be ideal. Several designs have been investigated such as single-chambered MFCs (Min et al., 2005) and stacked MFCs (Ref).To increase the exposed electrode surface area, a different electrode configuration could be investigated. Either a stacked electrode configuration or use of a mesh-like electrode design should be investigated.

The power density obtained from MFCs is still too low and until the power density is increased substantially, there is no real world application. MFCs however can generate high enough voltage (close to 350 mV) to be used for another important application. A bioelectrochemically assisted microbial reactor (BEAMR) is essentially a modified fuel in which a voltage is applied to the cell in order to produce hydrogen ("biohydrogen") (Ditzig *et al.*, 2007). Typically the voltage required ranges from 200 mV to 700 mV. The set-up for the BEAMR is essentially the same as that of a MFC, and therefore any gains made for MFCs could also be applied to the BEAMR. The BEAMR can also utilize a wastewater stream. Theoretically the voltage generated from the MFC is enough to be used for hydrogen generation from the BEAMR. Ideally, a MFC powered by a wastewater stream would generate sufficient voltage to apply to a BEAMR which in turn would generate biohydrogen.

7 References

Agboola, B.O., Mocheko, A., Pillay, J. and Ozoemena, K.I. (2008). Nanostructured cobalt phthalocyanine single-walled carbon nanotube platform: electron transport and electrocatalytic activity on epinephrine. Journal of Porphyrins and Phthalocyanines, **12:** 1289-1299.

Antolini, E. (2008). Review Carbon supports for low-temperature fuel cell catalysts. Applied Catalysis B: Environmental, **88**: 1-24.

Baker, R., Wilkinson, D.P. and Zhang, J. (2008). Electrocatalytic activity and stability of substituted iron phthalocyanines towards oxygen reduction evaluated at different temperatures. Electrochimica Acta, **53**: 6906–6919.

Baker, R., Wilkinson, D.P. and Zhang, J. (2009). Facile synthesis, spectroscopy and electrochemical activity of two substituted iron phthalocyanines as oxygen reduction catalysts in an acidic environment. Electrochimica Acta, **54**: 3098–3102.

Banks, C.E. and Compton, R.G. (2005). Exploring the electrocatalytic sites of carbon nanotubes for NADH detection: an edge plane pyrolytic graphite electrode study. The Analyst, **130**: 1232-1239.

Baranton, S., Coutanceau, C, J.-M. L´eger, J-M., Roux, C., and Capron, P. (2005). Alternative cathodes based on iron phthalocyanine catalysts for mini- or micro-DMFC working at room temperature. Electrochimica Acta, **51:** 517–525.

Bard, A.J. and Faulkner, L.R. (1980). Electrochemical methods: fundamentals and applications. Chapter 6 Potential sweep methods. Chapter 14 Electroactive layers and modified electrodes, by A.J. and Faulkner, L.R. Bard, 226-243 and 580-589, New York, USA: John Wiley.

Batchelor-McAuley, C., Wildgoose, G.G., Compton, R.G., Shao, L., Green, M.L.H. (2008). Copper oxide nanoparticle impurities are responsible for the electroanalytical detection of glucose seen using multiwalled carbon nanotubes. Sensors and Actuators B, **132**: 356–360.

Bayo, K., Ouedraogo,G.V., Terzian, G. and Benlian, D. (1990). Uv-visible and IR spectra of iron(II) phthalocyanine polymer complexes linked by bis-pyridinato ligands. Polyhedron, **9**: 1087-1090.

Beck, F. (1977). The redox mechanism of the chelate-catalyzed oxygen cathode. Journal of Applied Electrochemistry, **40**: 239-245.

Biffinger, J.C., Pietron, J., Ray, R., Little, B. and Ringeisen, B.R. (2007). A biofilm enhanced miniature microbial fuel cell using *Shewanella oneidensis* DSP10 and oxygen reduction cathodes. Biosensors and Bioelectronics, **22**: 1672–1679.

Boone, B.E., Gichuhi, A. and Shannon, C. (1999). Resonance Raman spectroscopy as a probe of electrosynthesized materials: principles and selected results. Analytica Chimica Acta, **397**: 43-51.

Bullen, R.A., Arnot, T.C., Lakeman, J.B, and Walsh, F.C. (2006). Biofuel cells and their development. Biosensors and Bioelectronics, **21**: 2015-2045.

Casagrande, T., Lawson, G., Li, H., Wei, J., Adronov, A. and Zhitomirsky, I. (2008). Electrodeposition of composite materials containing functionalized carbon nanotubes. Materials Chemistry and Physics, **111:** 42–49.

Ceyhan, T., Altındal, A., Erbil, M.K. and Bekarog˘lu, O. (2006). Synthesis, characterization, conduction and gas sensing properties of novel multinuclear metallo phthalocyanines (Zn, Co) with alkylthio substituents. Polyhedron, **25**: 737–746.

Cheng, S., Liu, H., and Logan, B.E. (2006). Increased Power Generation in a Continuous Flow MFC with Advective Flow through the Porous Anode and Reduced Electrode Spacing. Environmental Science Technology, **40**: 2426-2432.

Coster, H.G.L., Chilcott, T.C. and Coster, A.C.F (1996). Impedance spectroscopy of interfaces, membranes and ultrastructures. Bioelectrochemistry and Bioenergetics, **40**: 79-98.

Curtiss, P.S., Dreicer, M. and Rabl, A. (1996). Environmental Impacts and Costs of Nuclear and Fossil Fuel cycles. WREC.

Davis, F. and Higson, S.P.J. (2007). Biofuel cells – Recent advances and applications. Biosensors and Bioelectronics, **22**: 1224-1235.

De Wael, K., Westbroek, P., Bultinck, P., Depla, D., Van den Abeele, P., Adriaens, A. and Temmerman, E. (2005). Study of the deposition and Raman and XPS characterization of a metal ion tetrasulphonated phthalocyanine layer at gold surfaces: density functional theory calculations to model the vibrational spectra. Electrochemistry Communications **7**: 87–96.

Ditzig, J., Liu, H. and Logan, B.E. (2007). Production of hydrogen from domesticwastewater using a bioelectrochemically assisted microbial reactor (BEAMR). International Journal of Hydrogen Energy, **32**: 2296 – 2304.

Du, Z., Li, H. and Gu, T. (2007). Research review paper A state of the art review on microbial fuel cells: A promising technology for wastewater treatment and bioenergy. Biotechnology Advances, **25** (2007) 464–482.

Duarte, J.C., Luza, R.C.S., Damosa, F.S., Tanakab, A.A. and Kubota, L.T. (2008). A highly sensitive amperometric sensor for oxygen based on iron(II) tetrasulfonated phthalocyanine and iron(III) tetra-(*N*-methyl-pyridyl)-porphyrin multilayers. Analytica Chimica acta, **612:** 29–36.

El Hourch, A. and Belcadi, S. (1992). Electrocatalytic reduction of oxygen at iron phthalocyanine modified polymer electrodes. Journal of Electroanalytical Chemistry, **339**: 1-12.

Emmenegger, Ch., Mauron, Ph., Sudan, P., Wenger, P., Hermann, V., Gallay, R. and Züttel, A. (2003). Investigation of electrochemical double-layer (ECDL) capacitors electrodes based on carbon nanotubes and activated carbon materials. Journal of Power Sources, **124**: 321-329.

Feng, Y., Wang, X., Logan, B.E. and Lee, H. (2008). Brewery wastewater treatment using air-cathode microbial fuel cells. Applied Microbiology Biotechnology, **78**: 873-880.

Fogel, R., Mashazi, P., Nyokong, T. and Limson, J. (2007). Critical Assessement of the Quartz Crystal Microbalance with Dissipation as an analytical tool for Biosensor development and Fundemental Studies: Metallophthalocyanine-Glucose oxidase biocomposite sensors. Biosensors and Bioelectronics, **23:** 95-101.

Glaister, B.J., Mudd, G.M. (2010). The environmental costs of platinum–PGM mining and sustainability: Is the glass half-full or half-empty? Minerals Engineering **23**: 438–450.

Gong, K., Yang, Y., Zhang. M., Su, L., Xiong, S. and Mao, L. (2005). Electrochemistry and electroanalytical applications of carbon nanotubes: review. Analytical Sciences, **21**: 1383-1393.

Gouadec, G. and Colomban, P. (2007). Raman Spectroscopy of nanomaterials: How spectra relate to disorder, particle size and mechanical properties. Progress in Crystal Growth and Characterization of Materials, **53:** 1-56.

Guo, D-J. and Li, H-L. (2006). Electrocatalytic oxidation of methanol on Pt modified SWCNTs. Journal of Power Sources, **160**: 44-49.

Hacker, V., Wallnofer, E., Baumgartner, H., Schaffer, T., Besenhard, J.O., Schrottner, H. and Schmied, M. (2005). Carbon nanofiber-based active layers for fuel cell cathodes – preparation and characterization. Electrochemistry Communications, **7:** 377–382.

Hao Yu, E., Cheng, S., Logan, B.E. and Scott, K. (2009). Electrochemical reduction of oxygen with iron phthalocyanine in neutral media. Journal of Applied Electrochemistry, **39**: 705–711.

Hao Yu, E.,Cheng, S., Scott, K. and Logan, B.E. (2007). Microbial fuel cell performance with non-Pt cathode catalysts. Journal of Power Sources, **171:** 275–281.

Harnisch, F., Savastenko, N.A., Zhao, F., Steffen, H., Brüser, V. and Schröder, U. (2009). Comparative study on the performance of pyrolyzed and plasma-treated iron(II) phthalocyanine-based catalysts for oxygen reduction in pH neutral electrolyte solutions. Journal of Power Sources, **193**: 86–92.

Hoel, M. and Kverndokk, S. (1996). Depletion of fossil fuels and the impacts of global warming. Resource and Energy Economics, **18**: 115-136.

Hu, C.G., Feng, B., Xi, Y., Zhang, Z.W. and Wang, N. (2007). Modification of carbon nanotubes and their electrochemical detection. Diamond & Related Materials, **16**: 1988–1991.

Janczuk, B., Gonzalez-Martin, M.L., Bruque, J.M., Dorado-Calazanz, C. and Moreno Del Pozo, J. (1995). The Relationship between the Interfacial Free Energy and the Free Energy of Micellization of Triton X-100 and Sodium Dodecyl Sulfonate. Journal of Colloid and Interface Science, **176**: 352-357.

Jiang, H-J., Zhao, Y., yang, H., and Akins, D.L. (2009). Synthesis and electrochemical properties of single-walled carbon nanotube–gold nanoparticle composites. Materials Chemistry and Physics, **114**: 879–883.

Kakade, B.A., and Pillai, V.K. (2008). An efficient route towards the covalent functionalization of single walled carbon nanotubes. Applied Surface Science, **254**: 4936-4943.

Kim, J., Jia, H., and Wang, P. (2006). Challenges in biocatalysis for enzyme-based biofuel cells. Biotechnology Advances, **24**: 296-308.

Kissinger, P.T. and Heinemann, W.R. (1996). Laboratory techniques in electroanalytical chemistry 2nd Edition, by P.T. and Heinemann, W.R. Kissinger, 11-48, 52-60, 293-305, 443-466. New York, USA: Marcel Dekker Inc.

Kruusenberg, I., Alexeyeva, N., and Tammeveski , K. (2009). The pH-dependence of oxygen reduction on multi-walled carbon nanotube modified glassy carbon electrodes. Carbon, **47**: 651–658.

Kumar, N. and Das, D. (2001). Continuous hydrogen production by immobilized *Enterobacter cloacae* IIT-BT 08 using lignocellulosic materials as solid matrices. Enzyme and Microbial Technology, **29:** 280–287.

Kunadian, I., Andrews, R., Pinar Menguc, M. and Qian, D. (2009). Thermoelectric power generation using doped MWCNTs. Carbon, **47**: 589-601.

Lever, A.B.P. (1999). The Phthalocyanines – Molecules of Enduring value; a Two-dimensional Analysis of Redox Potentials. Journal of Porphyrins and Phthalocyanines, **3**: 488-499.

Leznoff, C.C. and Lever, A.B.P. (1993). Phthalocyanines: properties and applications Volume 3. Chapter 1: The redox chemistry of metallophthalocyanines in solution, by Lever, A.B.P., Milaeva, E.R. and Speier, G., pg26-48. New Yord, USA: VCH Publishers Inc.

Li, B., Kawakami, T. and Hiramatsu, M. (2004). Surfactant effects on optical absorption spectra of iron phthalocyanine nanoparticles in water. Materials Research Bulletin, **39**: 1265–1269.

Li, J. and Zhang, Y. (2006). Cutting of multi walled carbon nanotubes. Applied Surface Science, **252**: 2944-2948.

Li, Y., Shi, X. and Hao, J. (2006). Electrochemical behavior of glassy carbon electrodes modified by multi-walled carbon nanotube/surfactant films in a buffer solution and an ionic liquid. Carbon, **44**: 2664-2670.

Li, Y., Wang, P., Li, F., Huang, X., Wang, L. and Lin, X. (2008). Covalent immobilization of single-walled carbon nanotubes and single-stranded deoxyribonucleic acid nanocomposites on glassy carbon electrode: Preparation, characterization, and applications. Talanta, **77**: 833-838.

Liu, H., Songa, C., Zhang, L., Zhang, J., Wang, H., and Wilkinson, D.P. (2006). Review: A review of anode catalysis in the direct methanol fuel cell. Journal of Power Sources, **155**: 95–110.

Logan, B.E. (2008). Microbial Fuel Cells. Chapter 1: Introduction. 1-11. Chapter 4: Power Generation. 44-61. John Wiley and Sons, New Jersey.

Logan, B.E. and Regan, J.M. (2006). Microbial challenges and harnessing the metabolic activity bacteria can provide energy for a variety of applications, once technical and cost obstacles are overcome. Environmental Science and Technology, **40**: 5172-5180.

Lu, Y., and Reddy, R.G. (2007). The electrochemical behavior of cobalt phthalocyanine/platinum as methanol-resistant oxygen-reduction electrocatalysts for DMFC. Electrochimica Acta, **52:** 2562–2569.

Madigan, M.T., Martinko, J.M. and Parker, J. (2004). Brock Biology of Microorganisms 11th edition. Chapter 6: Microbial Growth, by M.T., Martinko, J.M. and Parker, J. Madigan, 140-144. New Jersey, USA: Prentice Hall international editions.

Maldonado, S. and Stevenson, K.J. (2004). Direct Preparation of Carbon Nanofiber Electrodes via Pyrolysis of Iron(II) Phthalocyanine: Electrocatalytic Aspects for Oxygen Reduction. Journal of Physical Chemistry B, **108:** 11375-11383.

Maldonado, S., Morin, S. and Stevenson, K.J. (2006). Electrochemical oxidation of catecholamines and catechols at carbon nanotube electrodes. Analyst, **131**: 262–267.

Mamuru, S.A. and Ozoemena, K.I (2009). Impedimetric and electrocatalytic properties of nanostructured iron(II) phthalocyanine at pyrolytic graphite electrode. Materials Chemistry and Physics, **114:** 113–119.

Manoharan, R., Wang, Y. and Feld, M.S. (1996). Histochemical analysis of biological tissues using Raman spectroscopy (review). Spectrochemica Acta Part A, **52:** 215-249.

Mansfeld, F. (1990). Electrochemical Impedance Spectroscopy (EIS) as a new tool for investigating methods of corrosion protection. Electrochemica Acta, **35**: 1533-1544.
Maruyama, J. and Abe, I. (2002). Cathodic oxygen reduction at the interface between Nafion™ and electrochemically oxidized glassy carbon surfaces. Journal of Electroanalytical Chemistry **527**: 65- 70.

Maruyama, J., Inaba, M., and Ogumi, Z. (1998). Rotating ring-disk electrode study on the cathodic oxygen reduction at Nafion®-coated gold electrodes. Journal of Electroanalytical Chemistry, **458**: 175–182.

Mashazi, P.N., Westbroek, P., Ozoemena, K.I. and Nyokong, T. (2007). Surface chemistry and electrocatalytic behaviour of tetra-carboxy substituted iron, cobalt and manganese phthalocyanine monolayers on gold electrode. Electrochimica Acta, **53**: 1858–1869.

Matemadombo, F. and Nyokong, T. (2007). Characterization of self-assembled monolayers of iron and cobalt octaalkylthio substituted phthalocyanines and their use in nitrite electrocatalytic oxidation. Electrochimica Acta, **52**: 6856–6864.

Matemadombo, F., Durmus, M., Chamunorwa Togo, C.A., Limson, J.L. and Nyokong, T. (2009). Characterization of manganese tetraarylthiosubstituted phthalocyanines self-assembled monolayers. Electrochimica Acta, **54**: 5557–5565.

Matemadombo, F., Westbroek, P., and Nyokong, T. (2007). Electroanalysis of thiocyanate using a novel glassy carbon electrode modified by aryl radicals and cobalt tetracarboxy phthalocyanine. Electrochimica Acta**, 53**: 480-486.

Matson, R.J. and Carasso, M. (1999). Sustainability, energy technologies, and ethics. Renewable Energy, **16:** 1200-1203.

Melendres, C.A. (1980). Mossbauer and Raman Spectra of Carbon-Supported Iron Phthalocyanine. Journal of Physical Chemistry, **84**: 1936-1939.

Min, B., and Angelidaki, I. (2008). Innovative microbial fuel cell for electricity production from anaerobic reactors. Journal of Power Sources, **180**: 641–647.

Min, B., Kim, J.R., Oh, S.E., Regan, J.M. and Logan, B.E. (2005). Electricity generation from swine wastewater using microbial fuel cells. Water Research, **39**: 4961–4968.

Nambiar, S., Togo, C.A. and Limson., J.L (2009). Application of multi-walled carbon nanotubes to enhance anodic performance of an *Enterobacter cloacae*-based fuel cell. African Journal of Biotechnology, **8**: 6927-6932.

Oh, S., Min, B. and Logan, B.E. (2004). Cathode performance as a factor in electricity generation in Microbial fuel cells. Environmental Science Technology, **38**: 4900-4904.

Oh, S. and Logan, B.E. (2005). Hydrogen and electricity production from a food processing wastewater using fermentation and microbial fuel cell technologies. Water Research, **39**: 4673–4682.

Okunola, A., Kowalewska, B., Bron, M., Kulesza, P.J. and Schuhmann, W. (2008). Electrocatalytic reduction of oxygen at electropolymerized films of metalloporphyrins deposited onto multi-walled carbon nanotubes, Electrochimica Acta, **54**: 1954-1960.

Parra, V., Hernandoa, T., Rodrıguez-Mendeza, M.L. and de Saja, J.A. (2004). Electrochemical sensor array made from *bis*phthalocyanine modified carbon paste electrodes for discrimination of red wines. Electrochimica Acta, **49:** 5177–5185.

Pillay, J. and Ozoemena, K.I. (2009). Layer-by-layer self-assembled nanostructured phthalocyaninato iron(II)/SWCNT-poly(*m*-aminobenzenesulfonic acid) hybrid system on gold surface: Electron transfer dynamics and amplification of H_2O_2 response. Electrochimica Acta, **54**: 5053-5059.

Prehn, K., Warburg, A., Schilling, T., Bron, M. and Schulte, K. (2008). Towards nitrogen-containing CNTs for fuel cell electrodes. Composites Science and Technology, **69**: 1570-1579.

Qiao, Y., Ming Li, C., Bao, S-J., and Bao, Q-L. (2007). Carbon nanotube/polyaniline composite as anode material for microbial fuel cells. Journal of Power Sources, **170**: 79-84.

Ragoisha, G.A. and Bondarenko, A.S. (2005). Potentiodynamic electrochemical impedance spectroscopy. Electrochimica Acta, **50**: 1553–1563.

Rao, S.M. and Xing, Y. (2008). Simulation of nanostructured electrodes for polymer electrolyte membrane fuel cells. Journal of Power Sources, **185**: 1094–1100.

Ravindra, K., Bencs, L. and Van Grieken, R. (2004). Review: Platinum group elements in the environment and their health risk. The Science of the Total Environment, **318**: 1–43.

Rout, U.K., Akimoto, K., Sano, F., Oda, J., Homma, T. and Tomoda, T. (2008). Impact assessment of the increase in fossil fuel prices on the global energy system, with and without CO2 concentration stabilization. Energy Policy, **36**: 3477– 3484.

Salimi, A., Noorbakhsh, A. and Ghadermarz, M. (2005). Direct electrochemistry and electrocatalytic activity of catalase incorporated onto multiwall carbon nanotubes-modified glassy carbon electrode. Analytical Biochemistry, **344**: 16–24.

Schilling, T., and Bron, M. (2008). Oxygen reduction at Fe–N-modified multi-walled carbon nanotubes in acidic electrolyte. Electrochimica Acta, **53:** 5379–5385.

Shahrokhian, S., Ghalkhani, M. and Amini, M.K. (2009). Application of carbon-paste electrode modified with iron phthalocyanine for voltammetric determination of epinephrine in the presence of ascorbic acid and uric acid. Sensors and Actuators B, **137**: 669–675.

Silva, J.F., Griveau, S., Richard, C, Zagal, J.H., and Bediou, F. (2007). Glassy carbon electrodes modified with single walled carbon nanotubes and cobalt phthalocyanine and nickel tetrasulfonated phthalocyanine: Highly stable new hybrids with enhanced electrocatalytic performances. Electrochemistry Communications, **9:** 1629-1634.

Šljukić, B., Banks, B. and Compton, R.G. (2005). An Overview of the Electrochemical Reduction of Oxygen at Carbon-Based Modified Electrodes. Journal of the Iranian Chemical Society, **2:** 1-25.

Stolarczyk, K., Nazaruk E., Rogalski, J. and Bilewicz, R. (2008) Nanostructured carbon electrodes for laccase-catalyzed oxygen reduction without added mediators. Electrochimica Acta, **53**: 3983–3990.

Streeter, I., Wildgoose, G.G., Shao, L., and Compton, R.G. (2008). Cyclic voltammetry on electrode surfaces covered with porous layers: An analysis of electron transfer kinetics at single-walled carbon nanotube modified electrodes. Sensors and Actuators B, **133**: 462–466.

Subramanian, N.P., Li, X., Nallathambi, V., Kumaraguru, S.P., Colon-Mercado, H., Wu, G., Lee, J-w. and Popov, B.N. (2009). Nitrogen-modified carbon-based catalysts for oxygen reduction reaction in polymer electrolyte membrane fuel cells. Journal of Power Sources, **188**: 38-44.

Sun, G-Q., Wang, J-T., Gupta, S., and Savinell, R.F. (2001). Iron (III) tetramethoxyphenylporphyrin (FeTMPP-Cl) as electrocatalyst for oxygen reduction in direct methanol fuel cells. Journal of Applied Electrochemistry, **31**: 1025-1031.

Sun, J., Hu, Y-y., Bi, Z. and Cao, Y-q. (2009). Simultaneous decolorization of azo dye and bioelectricity generation using a microfiltration membrane air-cathode single-chamber microbial fuel cell. Bioresource Technology, **100**: 3185–3192.

Sun, W., Xue, J., Chen, J., Mao, L., Jin, L., Yamamoto, K., Tao, S. and Jin, J. (1999). Measurement of dioxygen by electrocatalytic reduction on microelectrodes modified with Nafion and methyl viologen. Talanta, **49**: 345–356.

Tan, K.T., Lee, K.T., and Mohamed, A.R. (2008). Role of energy policy in renewable energy accomplishment: The case of second-generation bioethanol. Energy Policy, **36**: 3360– 3365.

Tantang, H., Ong, J.Y., Loh, C.L., Dong, X., Chen, P., Chen, Y., Hu, X., Tan, L.P. and Li, L-J (2009). Letter to the Editor: Using oxidation to increase the electrical conductivity of carbon nanotube electrodes. Carbon, **47**: 1867-1870.

Tau, P. and Nyokong, T. (2007). Electrocatalytic oxidation of nitrite by tetra-substituted oxotitanium(IV) phthalocyanines adsorbed or polymerised on glassy carbon electrode. Journal of Electroanalytical Chemistry, **611**:10–18.

Taylor, R.J. and Humffray, A.A. (1975). Electrochemical studies on glassy carbon electrodes iii. oxygen reduction in solutions of low ph (ph<10). Journal of Electroanalytical Chemistry, **64**: 85—94.

Vaisman, L., Wagner, H.D. and Marom, G. (2006). The role of surfactants in dispersion of carbon nanotubes. Advances in Colloid and Interface Science, **128–130**: 37–46.

van der Brink, F., Visscher, W. and Barendecht, E. (1984). Electrocatalysis of cathodic oxygen reduction by metal phthalocyanines Part IV Iron phthalocyanine as eletrocatalyst: Mechanism. Journal of Electroanalytical Chemistry, **175**: 279-289

Van der putten, A., Elzing, A., Visscher, W. and Barendrecht, E. (1987). Redox potential and electrocatalysis of O_2 reduction on transition metal chelates. Journal of Electroanalytical Chemistry, **221:** 95-104.

Venkata Mohan, S., Mohanakrishna, G., Srikanth, S., and Sarma, P.N. (2008). Harnessing of bioelectricity in microbial fuel cell (MFC) employing aerated cathode through anaerobic treatment of chemical wastewater using selectively enriched hydrogen producing mixed consortia. Fuel, **87**: 2667–2676

Wang, J. (1994). Analytical Chemistry. Chapter 1: Fundamental concepts, Chapter 2: Study of electrode reactions and interfacial properties, by J. Wang, 1-42. New Yord, USA: Wiley-VCH.

Wang, X-M., Hua, J-M., Zhang, J-Q, and Cao, C-N. (2008). Characterization of surface fouling of Ti/IrO2 electrodes in 4-chlorophenol aqueous solutions by electrochemical impedance spectroscopy. Electrochimica Acta, **53**: 3386–3394

Wang, Z., Zhang, Q., Kuehner, D., Xu, X., Ivaska, A. and Niu, L. (2008). The synthesis of ionic-liquid-functionalized multiwalled carbon nanotubes decorated with highly dispersed Au nanoparticles and their use in oxygen reduction by electrocatalysis. Carbon, **46**: 1687-1692

Wartewig, S. and Neubert, R.H.H. (2005). Pharmaceutical applications of Mid-IR and Raman spectroscopy. Advanced Drug Delivery Reviews, **57**: 1144– 1170

Watanabe, K. (2008). Recent Developments in Microbial Fuel Cell Technologies for Sustainable. Bioenergy Journal of Bioscience and Bioengineering, **106**: 528-536

Wen, Q., Wa, Y., Cao, D., Zhao, L. and Sun, Q. (2009). Electricity generation and modeling of microbial fuel cell from continuous beer brewery wastewater. Bioresource Technology, **100**: 4171–4175

Wen, Y., Ye, J-S., Zhang, W-D., Sheu, F-W., Xu, G.Q. (2007). Electrocatalytic oxidation of methanol on a platinum modified carbon nanotube electrode. Microchim Acta

Wildgoose, G.G., Banks, C.E., Leventis, H.C., and Compton, R.G. (2006). Review: Chemically Modified Carbon Nanotubes for Use in Electroanalysis. Microchimica Acta, **152:** 187–214

Wu, G. and Xu, B-q. (2007). Carbon nanotube supported Pt electrodes for methanol oxidation: A comparison between multi- and single-walled carbon nanotubes. Journal of Power Sources, **174**: 148–158

Xiao, L., Wildgoose, G.G, and Compton, R.G. (2009). Exploring the origins of the apparent "electrocatalysis" observed at C60 film-modified electrodes. Sensors and Actuators B, **138**: 524–531

Yang, H-H. and McCreery, R.L. (2000). Elucidation of the Mechanism of Dioxygen Reduction on Metal-Free Carbon Electrodes. Journal of The Electrochemical Society, **147**: (9) 3420-3428.

Yi, H., Wu, L-Q., Bentley, W.E., Ghodessi, R., Rubloff, G.W., Culver, J.N. and Payne, G.F. (2005). Biofabrication with Chitosan. Biomacromolecules, **6**: 2881-2894.

Yilmaz, I., Arslan, S., Guney, S., Becerik, I. (2007). Synthesis, electro-spectroelectrochemical characterization and electrocatalytic behavior towards dioxygen reduction of a new water-soluble cobalt phthalocyanine containing naphthoxy-4-sulfonic acid sodium salt. Electrochimica Acta, **52**: 6611–6621

Yin, H-s., Zhou, Y-l and Ai, S-y (2009). Preparation and characteristic of cobalt phthalocyanine modified carbon paste electrode for bisphenol A detection. Journal of Electroanalytical Chemistry, **626:** 80–88

Zanguina, A., Bayo-Bangoura, M., Bayo, K. and Ouedraogo, G.V. (2002). IR and UV-visible spectra of Iron(ii) phthalocyanine complexes with phosphine or phosphate. Bulletin Chemical Society of Ethiopia, **16**: 73-79

Zecca, A. and Chiari, L. (2010). Viewpoint Fossil-fuel constraints on global warming. Energy Policy, **38**: 1–3

Zhang, G. and Yang, F. (2007). Electrocatalytic reduction of dioygen at glassy carbon electrodes modified with polypyrrole/anthraquinonedisulphonate composite film in various pH solutions. Electrochemica Acta, **52**: 6595-6603.

Zhao, F., Harnisch, F., Schroder, U., Scholz, F., Bogdanoff, P., and Herrmann, I. (2005). Application of pyrolysed iron (II) phthlocyanine and CoTMPP based oxygen reduction catalysts as cathode materials in microbial fuel cells. Electrochemistry Communications, **7**: 1405-1410.

Zheng, J-S, Wang, M-X., Zhang, X-S., Wu, Y-X., Li, P., Zhou, X-G. and Yuan, W.K. (2008). Platinum/carbon nanofiber nanocomposite synthesized by electrophoretic deposition as electrocatalyst for oxygen reduction. Journal of Power Sources, **175:** 211–216

Zhou, H., Lin, Y., Yu, P., Su, L. and Mao, L. (2009). Doping polyaniline with pristine carbon nanotubes into electroactive nanocomposite in neutral and alkaline media. Electrochemistry Communications,

Zhou, M., Guo, L., Hou, Y., and Peng, X. (2008). Immobilization of Nafion-ordered mesoporous carbon on a glassy carbon electrode: Application to the detection of epinephrine. Electrochimica Acta, **53**: 4176–4184

Internet Reference 1: www.ren21.net. Accessed 03/03/2009

Internet Reference 2: www.tc.umn.edu Accessed 17/03/2009
Internet Reference 3: www.pburch.net Accessed 03/03/2009

Internet Reference 4: www-ibmc.u-strasbrg.fr Accessed 24/08/2009

8 Appendix I:

The slope of the Tafel plot (β) can be used to extract kinetic parameters of the electrochemical redox reaction, particularly the number of electrons involved in the rate limiting step of the redox reaction (n_a) and the transfer coefficient (α) which is a measure of the symmetry of the energy barrier between oxygen and its reduced form. The product of $n_a.\alpha$ can also be obtained from the Tafel slope by the following equation:

$$\beta = 2.303 \frac{R\,T}{\alpha n_a\,F} \qquad \text{(equation 2)}$$

Where β represents the Tafel slope, R the Molar gas constant, T the temperature, n_a the number of electrons involved in the rate limiting step, α the transfer coefficient and F the Faraday constant (Bagotski, 2006). For an irreversible diffusion controlled system, the Tafel slope may be determined from the shift in peak oxidation potential upon increasing scan rate (Figure 1). Phosphate buffer was selected for the Tafel analysis.

A

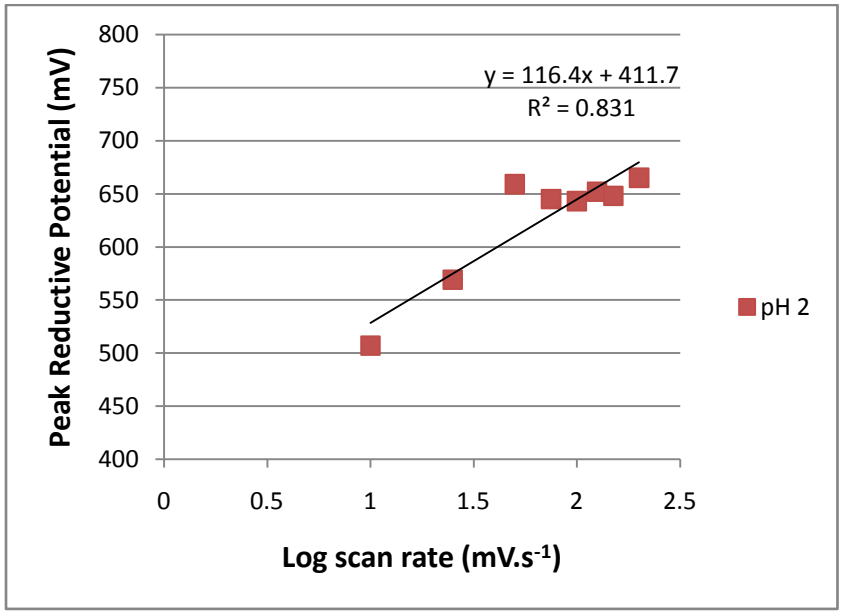

B

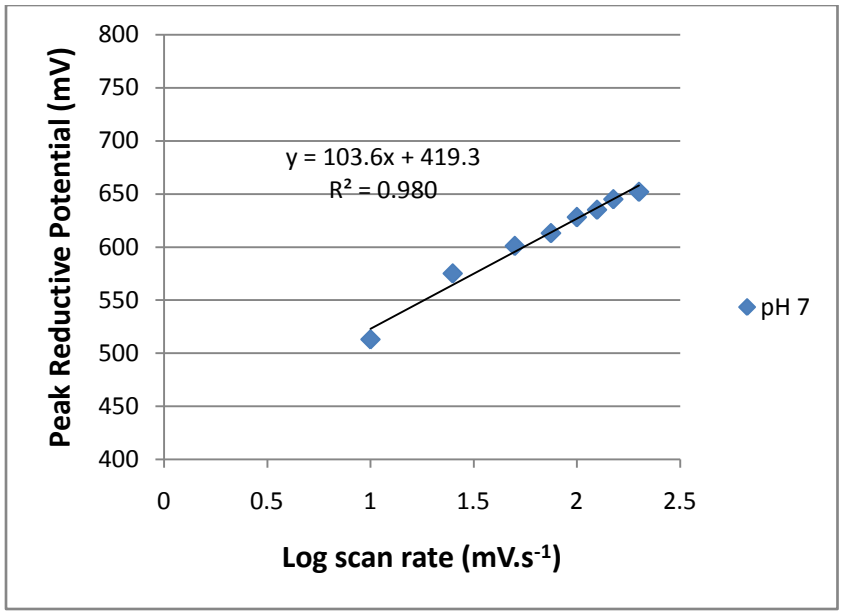

Figure 1: Peak reductive potential for the reduction of oxygen at a bare GC as a function of the log of increasing scan rate (10 mV, 25 mV, 50 mV, 75 mV, 100 mV, 125 mV, 150 mV, 200 mV). A) pH 2; B) pH 7. Analysis was done in 0.1 M sodium phosphate buffer.

The linear correlation between the shift in peak potential and the logarithmic of scan rate follows the relation:

$$Ep = \frac{\beta}{2} \log v + constant \quad \text{(equation 3)}$$

Where Ep represents the peak anodic potential (V), v represents the scan rate (V/s) and β represents the Tafel slope (Majidi, et. al, 2006). From the slope of the plot of peak reductive potential vs. log scan rate, the Tafel slope (β) can be determined. Using equation 2, the value of $\alpha\, n_a$ can then be calculated using the Tafel slope calculated from equation 3.

The linear relation of peak current magnitude and square root of scan rate for the reduction of oxygen follows the Randles-Sevcik equation for a diffusion controlled irreversible redox reaction shown as (Bard, 1980):

$$Ip = 2.98 \times 10^5 \, n_t (\alpha \, n_a)^{1/2} \, A \, D^{1/2} \, C \, v^{1/2} \text{ (equation 4)}$$

Where I_p represents the peak current, n the total number of electrons transferred, α the transfer coefficient , n_a the number of electrons transferred during the rate limiting step, A the electrode surface area, D the diffusion coefficient (1.94 x 10^{-5} cm^2s^{-1}), C the concentration of oxygen (3 x 10^{-7} $mol.cm^{-3}$) and v the scan rate. The $n_a\alpha$ was calculated from Equation 2. The increase in peak reduction current with increasing scan rate is consistent with diffusion controlled mass transport of oxygen to the electrode surface (Figure 2). D is equal to the diffusion coefficient for oxygen in phosphate buffer.

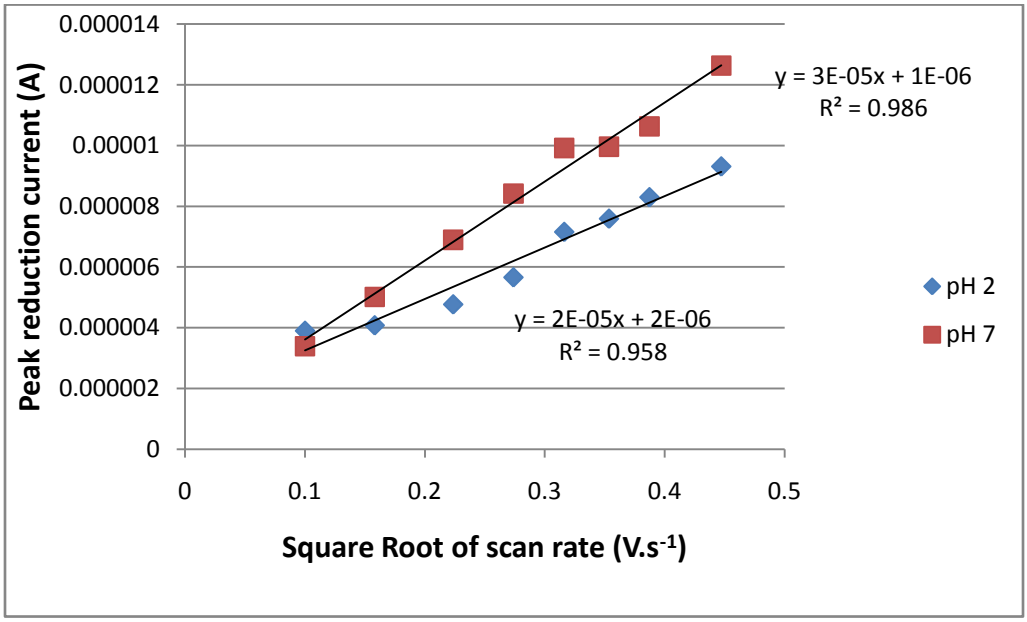

Figure 2: Peak reductive current for the reduction of oxygen at a bare GC as a function of the square root of increasing scan rate (0.010 V, 0.025 V, 0.050 V, 0.075 V, 0.100 V, 0.125 V, 0.150 V, 0.200 V). Analysis was done in 0.1 M sodium phosphate buffer.

Using equation 4, the number of electrons (n) involved in the reduction of oxygen can be calculated for pH 2 and pH 7.

9 Appendix II:

Ferricyanide redox species undergo a fast outer sphere one electron transfer reaction almost irrespective of the electrode material present and as a result is extensively used in literature for electrode characterisation (Eldin and Abdel-Hady, 2008). For outer sphere electron transfer, ferricyanide does not interact strongly with the electrode surface allowing for redox reactions to occur at a distance of at least a solvent layer from the electrode. This prevents electrode fouling as the concentration of ferricyanide ions at the electrode surface is essentially the same as in the bulk electrolyte solution. The electrochemical reduction of the ferricyanide ion to ferrocyanide is represented as:

$$Fe^{III}(CN)_6^{3-} + e^- \rightarrow Fe^{II}(CN)_6^{4-}$$

For a bare GCE, an anodic peak potential of 0.32 V during the forward scan followed by a cathodic peak potential of 0.231 V during the return scan was observed for the ferricyanide redox system at a scan rate of 100 $mV.s^{-1}$ (Figure 1A). The peak to peak separation in potential of 59 mV is indicative of a fully reversible process present for the redox reaction of ferricyanide. For a MWCNT-GCE, an anodic peak potential of 0.313 V during the forward scan followed by a cathodic peak potential of 0.239 V during the return scan was observed for the ferricyanide redox system at a scan rate of 100 $mV.s^{-1}$ (Figure 1B). The peak to peak separation in potential of 58 mV is indicative of a fully reversible process present for the redox reaction of ferricyanide.

A

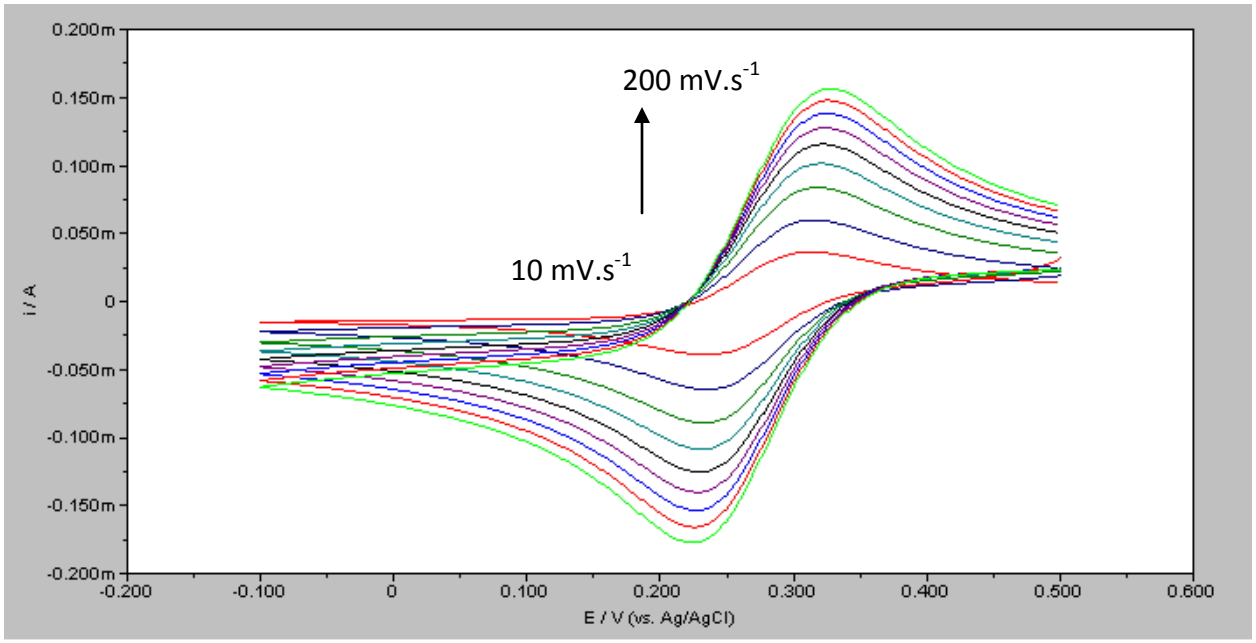

B

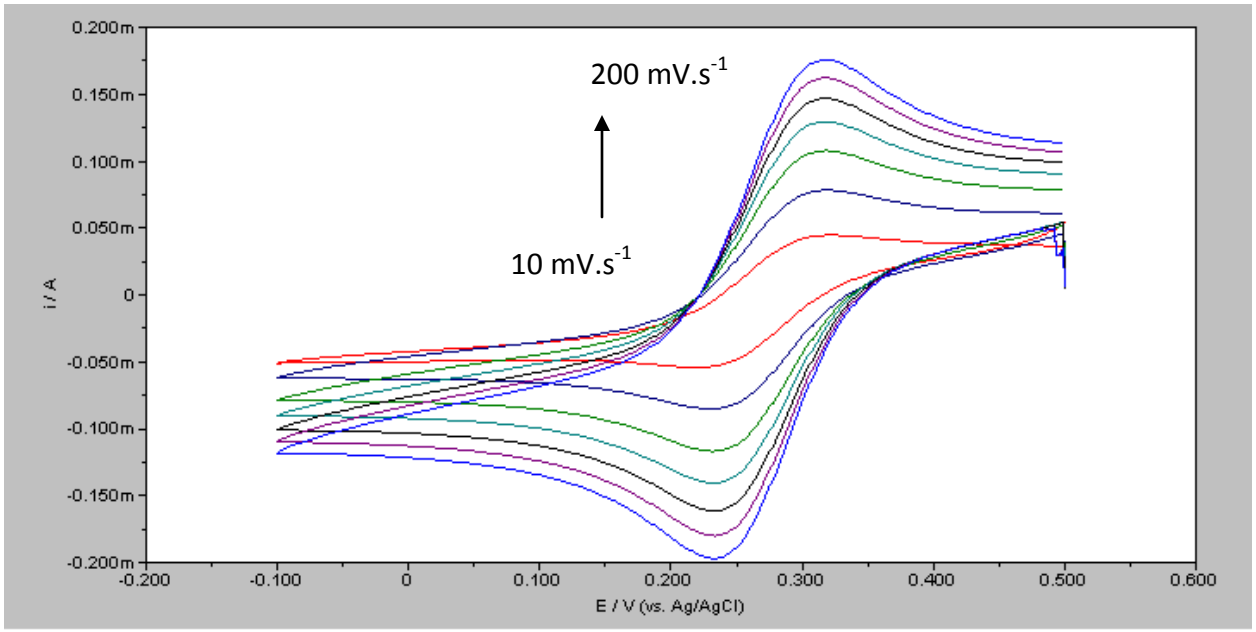

Figure 1: Cyclic voltammograms of 5 mM ferricyanide/ferrocyanide in 1 M potassium chloride at a bare GCE (A) and a MWCNT-modified GCE (B) with increasing scan rate (10 mV, 25 mV, 50 mV, 75 mV, 100 mV, 125 mV, 150 mV, 200 mV).

Figure 2 represents the linear correlation of peak oxidation current and square root of scan rate indicating a diffusion controlled redox process for the ferricyanide couple.

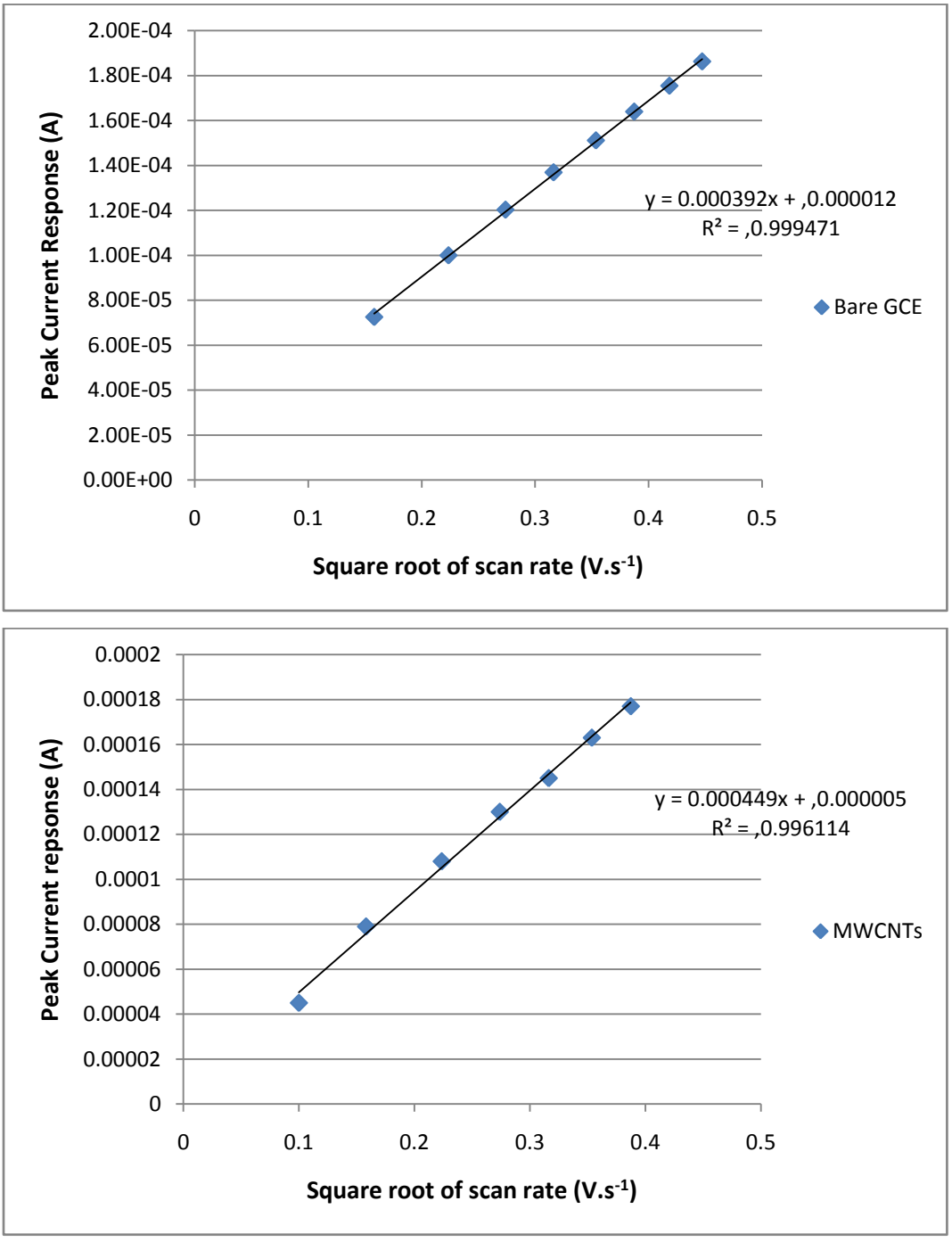

Figure 2: Peak oxidative current for the reduction of ferricyanide/ferrocyanide at a bare GCE (A) and MWCNT-GCE (B) as a function of the square root of increasing scan rate (10 mV, 25 mV, 50 mV, 75 mV, 100 mV, 125 mV, 150 mV, 200 mV). Analysis was done in 1 M potassium chloride

For a diffusion controlled reversible system, the peak current magnitude is defined by the Randles-Sevcik equation:

$$Ip = 2.69 \times 10^5 \, n^{3/2} \, A \, D^{1/2} \, C \, v^{1/2} \quad \text{(equation 1)}$$

Where I_p represents the peak current, n the total number of electrons transferred, A the electrode area, D the diffusion coefficient, C the concentration of ferricyanide and v the scan rate. According to Konopka and McDuffie, the diffusion coefficient for 5 x 10^{-6} mol.cm^{-3} potassium ferricyanide in 1 M potassium chloride is approximated as 7.26 ± 0.11 x 10^{-6} cm^2/s.

Calculation of the slope for the linear plot of peak oxidation current vs. the square root of scan rate (Figure 2) allowed for the determination of effective surface area for the bare GCE as 0.10 cm^2 and for a MWCNT-GCE, a value of 0.12 cm^2 was calculated.

10 Appendix III:

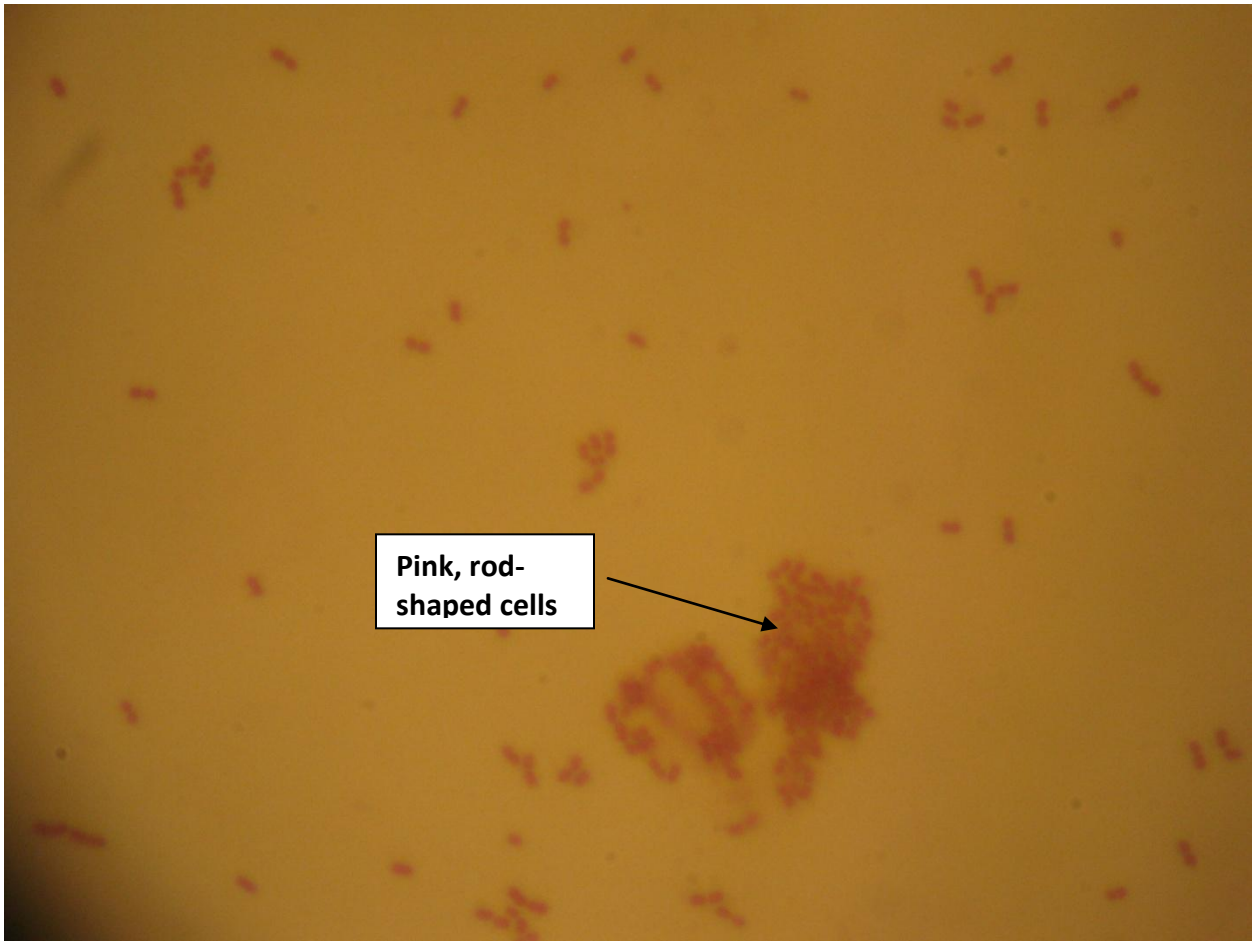

Figure 1: Gram stain of a log phase culture of *Enterobacter cloacae*. Magnification 400x